

POLITECNICO DI TORINO

Department of Electronics and Telecommunications Engineering

**Electronic Engineering
Master Degree Course**

Master Degree Thesis

Bluetooth Low-Energy Sensor Node For Gas Monitoring



Supervisor

Prof. Simone Corbellini

Co-supervisor

Prof. Marco Parvis

Candidate

Carlo Milan

July 2018

Contents

Acronyms	7
1 Introduction	9
2 System overview	11
2.1 Gas sensing device	11
2.2 Surrounding network description	12
Back-end layer	13
Bridge layer	13
Front-end layer	14
3 Gas sensing technologies	17
3.1 Catalytic detection of combustible gasses	17
3.2 Thermal conductivity gas sensors	18
3.3 Optical gas detection	18
3.4 Metal-oxide (MOX) gas sensors	18
3.5 Amperometric electrochemical gas sensors	19
4 Electrochemical amperometric gas sensors	21
4.1 Structure	21
4.1.1 Gas Membrane [1]	22
4.1.2 Electrodes [1]	22
4.1.3 Electrolyte	23
4.2 Commercial sensors	23
4.2.1 Temperature dependence	23
4.2.2 Humidity effects	24
4.2.3 Long term stability and lifetime	24
5 Electrochemical amperometric gas sensors comparison	25
5.1 Sensor comparison	25
5.2 Selected sensors	27
5.2.1 Cross sensitivity	28
5.2.2 Humidity effect	28
5.2.3 Temperature effect	28
Baseline current dependence	29
Sensitivity dependence	30

6	Conditioning circuit	33
6.1	Theory	33
6.1.1	Three terminal sensors	33
6.1.2	Two terminal sensors	35
6.1.3	Output filtering	36
	First order filter	37
	Second order filter	38
6.2	Design	39
6.2.1	Components choice	41
	OP-AMP	41
	DAC	42
	Output channels	43
	Output reference	45
	ADC	46
	Temperature and relative humidity sensor	48
6.2.2	Output filtering	48
6.2.3	Complete circuit schematic	51
6.2.4	Output equation with linear temperature compensation	52
 7	 Control unit	 57
7.1	Micro-controller description	57
7.2	Development environment	57
	Demo board [2]	59
	Software Tools	60
7.3	Developed libraries	61
7.3.1	AD7799 Library	62
	Register level	62
	Funciton level	64
	High level	67
7.3.2	AD7799 Functioning	69
7.4	Firmware	73
7.4.1	Alarms and warings	73
7.4.2	Firmware description	74
	Measurement phase	75
	Transmission packet building	76
	Size of the data	76
	Transmission strategy	77
	Data transmission	78
	Data reception	79
	Data packet composition	80
	Free-to-air transmission	80
	Serialized transmission	81
	De-serialization	82
	Measurements storing	83

8	Experimental results	85
8.1	Power consumption	85
8.2	Output noise	88
8.3	Power supply rejection	91
8.4	Temperature effect	91
8.5	Humidity effect	99
9	Conclusions	101
A	Electrochemical amperometric gas sensor theory	107
A.0.1	Working Principle	107

Acronyms

CO carbon monoxide. 22, 26

Cl₂ chlorine. 110

H₂S sulfuric acid. 26, 27, 40, 41, 85, 101, 110

NO nitrogen oxide. 112

NO₂ nitrogen dioxide. 26, 27, 40, 41, 81, 101, 110

O₃ ozone. 110

SO₂ sulfur dioxide. 26, 27, 40, 41, 48, 51, 70, 81, 85, 89, 90, 92–94, 96, 99, 101, 112

ACGIH American Conference of Governmental Industrial Hygienists. 73

AD Advertising Data. 79

CE Counter Electrode. 19, 22, 33–36, 40, 42, 110, 112

CNT carbon nanotubes. 22

EC electrochemical. 24, 33

Ethanol Ethanol. 112

GCC GNU Cross-Compiler. 60

IDLH Immediately Dangerous to Life or Health. 74, 81

KCL Kirchhoff current law. 33

MOX Metal-oxide. 3, 18, 19

PSRR Power Supply Rejection Ratio. 47

PTFE polytetrafluoroethylene. 22

RE Reference Electrode. 19, 22, 33–36, 40–42, 112

RH relative humidity. 24, 26

STEL Short Term Exposure Limit. 74, 81

TLV Threshold Limit Value. 73

TPB three-phase boundary. 21, 22

TWA Time Weighted Average. 73, 81

VOC Volatile Organic Compounds. 19

WE Working Electrode. 19, 21, 22, 25–27, 33–35, 41, 54, 99, 110–112

Chapter 1

Introduction

The capability of measuring the concentration of gaseous analytes is of interest in different areas, from industrial safety to environmental monitoring. A wide variety of gasses is present in the atmosphere, produced both by industrial and natural processes. Their constant monitoring helps to prevent and analyze the effects on people, on the natural environment and on materials.

The constant presence of polluting agents in urban areas promotes the interest in monitoring the indoor air quality inside workplaces, homes and public areas. For example, carbon monoxide and nitrogen oxides, generated in hydrocarbons combustion processes, are widely present in metropolitan locations. Moreover, several industrial processes imply the production of toxic gasses. In such cases a continuous monitoring of the factory environment is mandatory in order to prevent harmful situations. For example, the hydrogen sulfide, an extremely dangerous agent, is a waste product for the food industry, coke production, leather tanning industry and many others.

The effects of toxic gasses on humans and animals are both of long and short term. Most of them directly involve the respiratory tract, eyesight and the neural system. Also plants and crops are negatively affected by such gasses causing land degradation. Moreover, their effect is also visible on monuments and buildings.

The purpose of this work is to design a measurement system capable of performing environmental monitoring of a wide variety of gas in indoor locations where a cabled network would be of difficult installation and a constant maintenance not possible. In particular, the system should be included into an existing wireless environmental monitoring sensor network, developed during past years at Polytechnic of Turin, whose nodes are capable to operate for several years without attendance. This wireless network is currently composed by battery powered Bluetooth nodes that can measure temperature and humidity and that are designed to work in conditions where neither a continuous power source nor a continuous Internet connection are present. These features require the use of a low power architecture capable of both wirelessly transmitting and storing all the produced data into an internal memory. The gas sensor node should therefore be able as well to operate as data-logger and as wireless Bluetooth low-energy node.

The wide variety of aeriform polluting agents encourages the development of a system capable of detecting as many different gaseous analytes as possible, where their

concentration can be dangerous with a prolonged exposure.

The work started with the investigation of the available gas sensing technologies suitable for the development of the system. The characteristics of each sensor, for each considered type of gas, has been compared analyzing the impact on the system's performances. After this preliminary step, the work focused on the design of a measurement system capable of functioning with all the selected sensors, making particular attention to the power consumption of every component present in it, to comply with the severe power requirements. During the design an appropriate microcontroller optimized for Bluetooth low-energy transmission has been chosen and the firmware has been developed to correctly control all the components and take measurements from the sensor. Subsequently the Bluetooth wireless transmission has been addressed taking particular care to the radio power consumption. A complete prototype of the designed measurement system has been realized and the circuit characteristics compliance with the proposed specifications has been validated. The system verification procedure started with power consumption measurements to verify the possibility of powering the system with a small sized battery. After these initial tests the electronics of the node has been metrologically characterized, into a climatic chamber, employing one of the selected gas sensors. The obtained results confirmed the expected electronic performance and reliability under the test conditions.

Chapter 2

System overview

2.1 Gas sensing device

The device design object of this thesis aims to monitor the concentration of different gaseous analytes in indoor ambient where cabled networks and constant monitoring are not available. These requirements, as already anticipated in the introductory part, brings to implement this system as a long life battery powered wireless sensor that has the capability to internally store all the measurements for its entire life and also transmit them to a receiver. The long life specification has been decided to be of one year to comply the lack of local monitoring. This denote the low power architecture that has to characterize the system and therefore the design procedure, without overlooking the aim of monitoring a wide variety of gas, that would allow the employment of the system in different areas, where different aeriform analytes are present.

All the proposed objectives are listed below

- measure the concentration of different gaseous analytes
- battery powered device
- low power consumption that guarantee a lifetime of one year
- capability of store the measurements for its entire life
- capability of wireless transmitting the measurements

The system architecture that aims to comply all the requirements listed above needs to include

- a gas sensor with the relative conditioning circuit to sense the gas concentration
- a battery that powers the system
- a memory that stores all the measurements during its entire life
- a wireless radio to transmit the measurements
- a micro-controller that manages the functioning

The proposed architecture is shown in the block diagram of Figure 2.1.

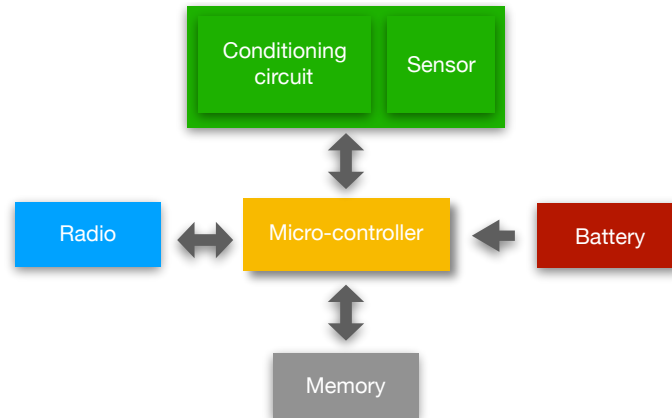


Figure 2.1: System architecture block diagram

Gas sensor and conditioning circuit Is the part of the system capable of sensing the target gas. It has to be designed with in mind low power consumption added to the capability of host different sensors sensitive to a wide variety of gaseous analytes.

Battery It power the system for its entire life. It has to be characterized by a small volume and weight.

Memory It has to store all the measurements taken for the entire life of the device.

Wireless radio It transmits the measurements. It has to be compatible with the network of which the device is part of and at the same time be able to transmit all the produced data maintaining a low power consumption.

Micro-controller It has to be capable of managing the whole system. The choice of this part of the system has to carefully be made considering the low power consumption requirement and the presence of all the required peripherals to correctly manage the system. In addition it has to support Bluetooth communication.

The device which requirements have been just described has to be inserted into an existing wireless monitoring network already developed in past years at Polytechnic of Turin, that is described in the next section.

2.2 Surrounding network description

The gas sensing system developed in this work has to be included into an existing wireless environmental sensor network that actually is equipped with temperature and humidity sensors.

The existing infrastructure, shown in Figure 2.2, is a cloud based environmental monitoring system [3, 4]. The aim of the project is to measure and store on the cloud the ambient temperature and relative humidity for more than one year without

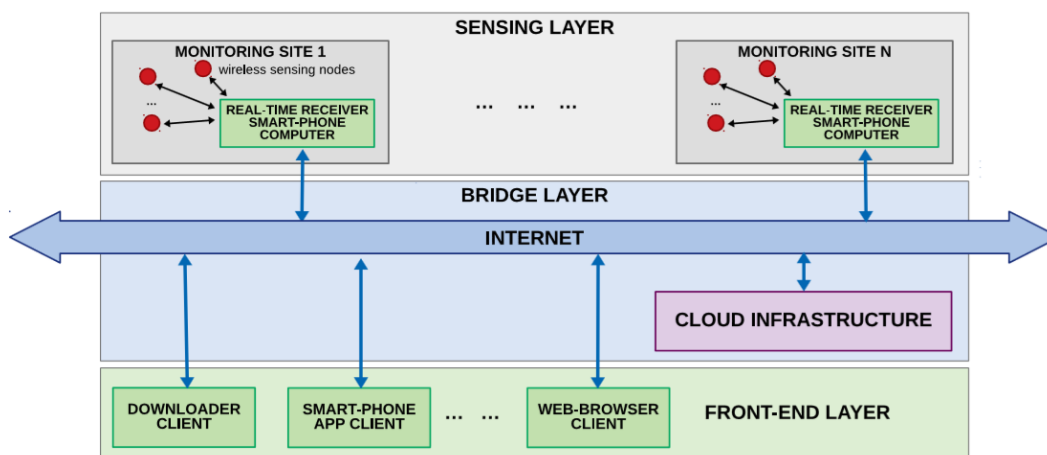


Figure 2.2: Existing network infrastructure

human intervention. Providing also the capability to work without the presence of a continuous power supply and Internet connection. Overall, the system is a three layer structure composed by a back-end, a bridge and a front-end layer. The back-end layer is composed by the peripheral sensing nodes. The bridge layer has the role of collecting the measurements from the sensor nodes and transmit them to the cloud by mean of an Internet connection. In the front end layer the collected data are presented and, if necessary, post-processed to provide useful information to the reader.

Back-end layer

The back-end layer is constituted by small wireless battery powered sensor nodes that can be placed around the monitored location up to a 10 m from the receiver. They have the role of sensing the physical quantity of interest and transmit them to the receiver. The long-life requirement, of one year, implies a very low power design. In fact, the communication with the receiver, takes place by mean of the Bluetooth LE technology that is capable to maintain the power consumption of the wireless section of the sensor under $20 \mu A$ during sleep. In addition, the data post processing, when necessary, is not carried out by the node but committed to the other layers of the infrastructure. Another important aspect to underline is the system capacity to continue working without an Internet connection or even when a central receiver is not available. To cope with this aspect every node is equipped with a storage memory commensurate to the maximum number of data produced by the sensor in its entire life. In this way, even if the node never transmits to the bridge layer, it can be directly accessed by a user in the same physical location that can download all the data once.

Bridge layer

The bridge layer collects the measurements from all the sensor present in its wireless transmission range and send them to the cloud through an Internet connection. It



Figure 2.3: Screen shot of a wireless receiver’s graphical panel

consists of a device that, from the back-end layer point of view, is the central node of the Bluetooth network that receive all the data sent by the peripheral sensing nodes. It also has to be equipped with a Wi-Fi or Ethernet module to access the cloud through an Internet connection. The operations listed above implies that the device designated for this role cannot be battery powered, or at least needs a periodic access to the mains. However the network architecture consisting of multiple wireless sensing node and a single receiver greatly relaxes the constraints connected to the presence of a continuous power source.

Front-end layer

The front-end layer is the part of the system accessible by users and administrators. Here the gathered data are presented and eventually post-processed. The administrators also have the possibility to re-configure sensor parameters. Three different user interfaces are available:

- A local visualization on personal computer of users that are in the same physical location of the receiver. Through this kind of user interface is possible to read, visualize graphically the measurements and configure the sensors.
- The receiver’s graphical control panel, accessible through smart-phones by administrators locally or through the Internet. This interface permits to check the status and measurements of the sensor and reconfigure it.
- A web page, that avoid the installation of any software, authorized to query a cloud DSP unit capable of processing the measurements.

An example screen shot of temperature and relative humidity monitoring is shown in Figure 2.3.

As previously said the purpose of the this work is to provide to the system the capability to make a long-term indoor gas concentration monitoring.

The new nodes should be lined up with the actual system. Therefore they should be battery powered devices that transmit the measurements through Bluetooth LE. They should reach a lifetime of one year, at least, and maintain dimensions similar to the existing nodes. This requirements reflects on the choice of the sensing technology that should be done making particular attention to its power requirements and dimensions. In addition the variety of gas to measure should be considered to develop a system useful in different situations and contexts.

Chapter 3

Gas sensing technologies

Different gas sensing mechanisms have been analyzed and a brief overview [5] is present below.

3.1 Catalytic detection of combustible gasses

Catalytic gas sensors are able to detect combustible gasses as hydrogen, methane and butane. Their working principle consists of igniting the target gas and measure the temperature of the combustion to detect its concentration. Usually the ignition temperature of those gasses is elevated, for this reason this kind of sensors employ catalytic materials, for the target combustible gas, to lower the ignition temperature. Metal oxides are mainly used in such sensors to catalyze the combustion of flammable gases. The early versions of those kind of sensors employed a platinum wire functioning both as heater, in order to provoke the reaction, and as temperature meter. The sensing element is constituted by small grains that forms a porous structure, called *pellistor*, in which the gas penetrates, increasing the sensitivity. The sensors are constituted by a Wheatstone bridge with a gas sensing element, a reference element and two fixed resistors. The gas detection unbalances the Wheatstone bridge permitting to detect the resistance variation of the sensing element provoked by the temperature increase. The presence of an heating element inside those sensors leads to an high power consumption. In recent years the micromachined fabrication of this kind of sensors [6] brought to a reduction of the dissipated power. In addition, pulsed excitation methods experimented for this kind of sensors [7] further provided a power dissipation reduction. For the measurement system developed in this work the power requirement of commercial catalytic sensors is still too elevated. For example the CDH3 methane sensor from Alpha Sense has an average power consumption of $\sim 190\text{ mW}$ and the MP-7217 methane sensor, from SGX Sensortech, requires a current of 39 mA at 2.9 V that has to be maintained for at least its whole response time of 12 s .

3.2 Thermal conductivity gas sensors

Thermal conductivity gas sensors measure are based on the thermal absorption of heat from a heating element to the target gas. For this reason only gasses with a thermal conductivity higher than the air can be measured in this way such as hydrogen and methane. Again in this case the presence of a heating elements is an obstacle to the employment of this technique in this low-power system. The VQ5467TS ammonia sensor, from SGX Sensortech, is the least power consuming of its series but require a current of 40 *mA* at 3 *V* with a ~ 20 *s* response time. The least power consuming sensor of this type that has been found is the PTC-01P from Pematron, sensible to CO_2 , CH_4 and H_2 , that has a typical power consumption of 5 *mW*.

3.3 Optical gas detection

This gas detection technique is based on the optical adsorption, emission or scattering of light, at a specific wavelength, when comes in contact with specific structures that interacts with the gas. In general, such kind of sensors consist of three parts, a light emitting element, a light detector and a structure that reacting with the target gas changes its optical properties.

The research on this methods is very intense. It started with the detection of flammable gasses, like hydrogen [8], and continues with the aim of expanding the detectable types of gasses [9, 10, 11, 12], reducing the power consumption for the employment in wireless systems [13, 14] and miniaturization [15]. Nevertheless the promising results of those techniques it is still difficult to find commercial sensors able to detect a wide variety of analytes. In fact only CO_2 , CO , hydrocarbons and ammonia can actually be sensed using sensors available on the market. Moreover, those available sensors are still characterized by a higher power consumption respect to that permitted by to be developed. For example the NDIR sensors IRM-AT and IRC-AT sensible to methane and CO_2 respectively, from Alpha sense, require a current of 60 *mA* at a minimum operating voltage of 2 *V* with a response time of 40 *s*. The IR11 series sensible to CO_2 from SGX Sensortech has almost the same power requirements, as with the IR12, 13 and 14 series sensible to hydrocarbons and acetylene.

3.4 Metal-oxide (MOX) gas sensors

Metal-oxide gas sensors are often called conductometric gas sensor because their electrical equivalent consists of a variable resistance R , usually made of tin dioxide. In clean air the electrons inside the material are attracted by the oxygen molecules present on its surface. The target gas, when present, reacts with the adsorbed oxygen resulting in the release of the previously attracted electrons which therefore take part to the current conduction, provoking an increase of the current inside the resistance. However, the conductance variation is appreciable only at a specific temperature. In fact, inside those sensor a resistive heating element is present called

heating resistance R_H , which has the role of increase the temperature of the sensible part of the sensor in order to reach the highest sensitivity. Once again, the presence of an heating element inside the sensor represents an high power dissipation source. Nevertheless, the miniaturization of this kind of sensors decrease their power dissipation towards tens of milli-Watts. For example the CCS801 for Volatile Organic Compounds (VOC), from AMS reports, an average power consumption of 0.9 mW in pulsed mode. An aspect not favourable to this sensing technology, according to the actual presence of commercial sensors, is the small variety of gas analytes that can be sensed. But an important aspect in favour of MOX sensors is their low price respect to the others, being in the order of units of dollars.

3.5 Amperometric electrochemical gas sensors

This kind of sensors generate a current proportional to the concentration of the gaseous analyte to which they are exposed, for this reason they are referred as amperometric gas sensors. Their working principle is analogous to a fuel cell, in fact they are also called *micro fuel cells*. They are constituted by two electrodes, called Working Electrode (WE) and Counter Electrode (CE), immersed in an electrolyte. Sometimes a third Reference Electrode (RE) is added to provide additional stability to the sensor. The target gas reacts with the WE generating a current that can be either positive or negative. If the target gas is a reducing species the electrons flows outside the sensors through the WE, if the analyte is an oxidizing species the electrons flow in the opposite direction. To permit a correct operation of the sensor, an equal and opposite amount of electrons has to be provided to the CE. Moreover some sensors require that a bias voltage is applied between the WE and the RE, if present. If only two electrodes are available the bias has to be applied between the WE and the CE. The maximum current generated by the WE, and that has to be provided to the CE, ranges from hundreds to tens of micro-ampere. This electrical current magnitude results in a very low power dissipation in the order of tens of μW at maximum. This aspect make this kind of sensing technology feasible for the application under investigation. Moreover different kind of gases can be detected using this technology. For example the SPEC sensor company produces amperometric sensors for gasses like NH_3 , SO_2 , NO_2 , CO , O_2 and O_3 .

This short analysis already suggest that the amperometric detection can be employed to develop the new sensing nodes thanks to its low power consumption and wide variety of gas types detectable. Among the other sensing technologies the MOX sensors stands out thanks to the sensors low price and dimensions. However with MOX sensors is necessary to implement operating techniques that further reduces their power consumption. In conclusion it has been decided to use amperometric gas sensors for the advantages explained above.

Chapter 4

Electrochemical amperometric gas sensors

4.1 Structure

Most sensors have a vertical structure as shown in Figure 4.1. The gas diffuses into the sensor through a capillary diffusion hole and reaches the sensor chamber. An hydrophobic membrane divides the WE and the chamber. The function of this first part of the sensor is the selection and the regulation of the quantity of chemical elements that comes in contact with the WE. The capillary barrier and the sensor chamber regulate this quantity by regulating the capillary diameter, the volume of the chamber and the hydrophobic membrane pore size. The membrane has also the function of filtering out unwanted particles and to prevent the electrolyte evaporation. This part of the sensor, together with the WE and the electrolyte is called three-phase boundary (TPB) (interface between the gas, the electrode and the electrolyte) [1]. It constitutes a fundamental sensing section, for which the area is a crucial aspect, being the place where the analyte first reaction takes place. In some cases also an additional external filter is used to better prevent unwanted substances to pollute the sensor chamber, as dust.

Indeed by an appropriate selection of this elements sensor selectivity, sensitivity and operating life can be improved.

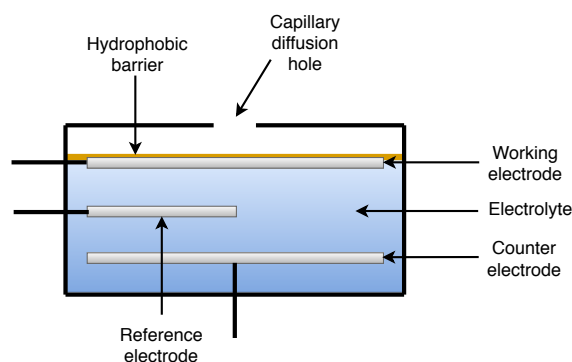


Figure 4.1: Electrochemical sensor structure

4.1.1 Gas Membrane [1]

The gas membrane can be made of different materials, both polymeric and inorganic. The factors that determines the choice of this component are several and include the permeability to the target gas, the electrolyte leakage prevention, the manufacturability, the thickness and its durability. Being part of the TPB, most of times, this membranes are tightly related with the WE fabrication. Are either used to coat the WE or, in modern fabrication processes, to act as deposition layer for the WE electrode material . Common chosen materials are thin solid Theflon films or microporous Theflon film for which the first example were prepared by Niedrach and Alford in 1965 for fuel cells [16] . Sawyer et al. in 1958, investigating different membrane materials, achieved the best performance using polyethylene instead of saran and natural rubber [17]. Also hydrophobic porous materials, such as prous polytetrafluoroethylene (PTFE), are suitable for gas sensing, especially when coated with metals. To increase the area of the TPB, PTFE membranes with an nanocomposite material of carbon nanotubes (CNT) and PTFE have been investigated [18]. The area enlargement is due to the high surface of carbon nanotubes that togther with the PTFE layer forms an "hair morphology" surface. Catalyst are then electrochemically deposited over this structure forming an high-sensitivity TPB.

4.1.2 Electrodes [1]

Working Electrode and Counter Electrode are usually made of noble metals, such as platinum or gold because they offer several advantages, from structural to chemical properties. First of all they make a definite interface with the electrolyte and they are porous enough to allow an adequate diffusion of the target gas inside them. From the chemical point of view they act as catalysts for the reaction with gaseous element of interest. In sensor where a bias potential is required they contribute to extend the lifetime of the system because they are less subject to corrosion respect to not-noble metals. One of the first gas diffusion electrodes was developed by Niedrach [16]. It was a sintered Teflon-Pt catalyst covered with a porous Teflon film, acting as a filter. It was successfully tested hydrogen-oxygen and hydrogen-air fuel cells. Contemporary gas diffusion electrodes derive from the Niedrach one. These electrodes are the result of a mixture of Teflon and powder of metal catalyst deposited on a metal wire screen or on a totally hydrophobic porous Teflon film. This fabrication process results in highly interlocked matrices of pores, electrolyte channels, electrons conducting paths and electrocatalytic surfaces. This kind of diffusion electrode built together with the sensor membrane forms an highly efficient TPB leading to sufficient high currents and sensitivity making it feasible for sensing species with a poor and slow electroactivity, such as the oxidation of hydrocarbons and *CO* [19, 20, 21, 22, 23, 24, 25, 26].

The Reference Electrode usually has a slightly different composition. It has to maintain a stable potential with the WE and be as much as possible insensitive to temperature, pressure and relative humidity variations. Differently from other two electrodes it is not a site of chemical reactions, therefore the porosity of the material is not requested. *Ag/AgCl* or *Pt/air* reference electrode are usually used.

4.1.3 Electrolyte

Most of gas sensors are equipped with aqueous electrolytes. Acid or halide-halate for acidic gas [27]. They are a limit for the sensor operating life because of they evaporation, that is even accelerated in case of high temperatures or low relative humidity. Starting from the middle 1970 non aqueous solid polymer electrolytes have been investigated [28, 29, 30, 31, 32, 33, 34, 35, 36].

Schenider in 1978 described one of the first solid electrolyte sensors for chlorine detection [35]. It was more reliable than other chlorine sensor which electrodes, selective to chlorine, usually dissolved in liquid electrolytes. Similarly Venkatasetty described the invention of a solid electrolyte carbon monoxide sensor [32]. Solid polymer electrolytes at the beginning were plastic sheet of specific polymeric material that when saturated with water became ionic conductors. Nafion is an example of such material having a good proton conductivity, high permeability and chemical stability. In fact Nafion permits the passage of cations and blocks anions being useful in a wide variety of sensor where hydrogen ions passage is required, as the hydrogen cations resulting from the oxidation of carbon monoxide. Nafion exhibits also resistance to acids and strong oxidants, has an high structural stability and good thermal stability, but it freezes at low temperatures.

4.2 Commercial sensors

In this section the most important characteristics of commercial electrochemical gas sensors are addressed. Temperature and relative humidity effects, long term stability and lifetime of sensors are included.

4.2.1 Temperature dependence

As previously anticipated in the theory section, this kind of sensors are affected by temperature. In general, temperature dependence can be summarized into two principal effects, the baseline current dependence and the sensitivity dependence. Assuming that the sensor is characterized by a linear current-gas concentration relation, those two effect can be seen as an offset modification for the baseline current dependence and a span change for the sensitivity dependence. More in detail, the baseline current is the current that the sensor generates when gas is not present. As temperature increases above 0 °C also the baseline current does. It is important to notice that the baseline current increase, most of times, is appreciable above 20 °C. The majority of sensors datasheets indicate a recommended temperature range within which the sensors maintains its specified characteristics. Out of this range the sensor is not guaranteed to work and also may report permanent damages. The recommended range is usually not narrower than $-20\text{ °C} \div +40\text{ °C}$. This operating temperature limit can derive from the electrolyte composition, especially if aqueous, thus subject to evaporation, or to other components freezing or melting.

4.2.2 Humidity effects

Differently from the temperature dependence, the relative humidity (RH) affects sensors reading in a more complex way. Overall the relative humidity effects on EC sensors can be divided into short-term and long-term effects, caused respectively by operation under a critical RH value for a short period of time or for a long period. Can be considered short-term effects daily changes in humidity. These causes a reversible sensitivity change. Long-term effects are those that lasts for more than one/two weeks, and, unlike the others, can cause an irreversible change of sensitivity. In general, for each sensor that detects a specific analyte, the response is different. Loss of sensitivity, for sensors that use an aqueous electrolyte, is common under prolonged operation under a given RH_{min} limit, due to electrolyte evaporation. In the opposite case, for sensors that involve water in their chemical processes, when the RH is over a given RH_{max} limit, the water permeation inside the sensor can cause an increase of reaction kinetics involving H_2O , resulting in a sensitivity increase. In addition, for some sensors, another aspect to discuss is the dynamic response to abrupt RH changes. To this situations, they reacts generating current spikes. In fact, in the case of rapid increase in the ambient relative humidity, happening in the order of seconds, the sensor generates a positive current spike, returning to a constant signal within some seconds. The spike is negative for decreasing RH. For this reason it is important to wait for the sensor stabilization before reading its output current if such a situation is detected.

4.2.3 Long term stability and lifetime

All EC sensors, even if they always operate inside the recommended environmental conditions, are subject to a sensitivity degradation, caused by the chemical activity of the sensor, that obviously cannot last forever. Electrodes oxidation, the always present electrolyte evaporation and other degradation processes of some part of the sensor contribute to the constant sensitivity loss. A typical value for a wide variety of sensors is within 2 % degradation of the signal per month. This means 24 % for one year, being problematic for the accuracy of the application, considering also that bad environmental condition can even worsen this value.

All the issues listed above also affects the sensor lifetime. For example, when the electrolyte is almost totally evaporated or when the sensor membrane is no longer able to filter unwanted elements, the system is no longer able to detect the analyte of interest. Common lifetime specifications are of 1 or 2 years. Modern designs can reach even 5 years of life.

Chapter 5

Electrochemical amperometric gas sensors comparison

5.1 Sensor comparison

The application subject of this work requires amperometric gas sensors with specific characteristics. In the previous chapter some of the critical aspects that characterize this kind of sensor were discussed. They are sensor particularly sensitive to temperature and relative humidity variations. As stated in some sensor data-sheets, the temperature effect is compensable, contrarily to the relative humidity dependence that has a complex influence on the sensor current. One of the most critical aspect in the choice of a feasible sensor for this specific application is the lifetime. The majority of the sensors have a maximum lifetime of one year. A one year life is required in this case but it would be better to have some headroom. Moreover a sensible long term drift effect is usually present. For example some sensors presents a long term drift of 2 % *per month*, resulting in a total drift of 24 % at the and of their life (of one year). Therefore this aspect has to carefully be taken into account during the sensor choice process.

The majority of this sensor are fabricated with noble metals and complex processes. This directly imply an elevated cost. In fact their price usually range from 10 to 100 dollars, making them the most expensive part inside the system.

As discussed in the theoretical section, the sensitivity of this kind of sensors is directly proportional to the WE surface area. In addition the total quantity of electrolyte that a sensor contains affects both the sensitivity and its lifetime. These two facts imply that, in general, sensors with a big WE surface area and with an adequate reservoir of ectrolyte will show better sensitivity and longer lifespan. Those two characteristics directly influence the total volume of the sensor. In fact the majority of commercial sensor have a big volume compared to the parts that usually constitutes the surrounding conditioning circuit. By the way, in recent years, more advanced fabrication techniques have brought to the markets smaller sensor with an increased lifetime. In the specific case of the application object of this work the dimension of the sensor has to be taken into account in order to comply the specification of small size. All in all, the most weighted parameters that have been considered during the choice are the lifetime, the price and the dimensions of the

sensor. Of course those were not the only determining factors, also other more general parameters, listed next, were considered.

The comparison has been made considering sensors for the same target gas, in order to better compare their characteristics. The sensors taken into exam for this comparison are produced by [SPEC Sensors](#), [SGX Sensortech](#), Euro gasman and Alpha sense .The considered characteristics are:

	Units
• Range	<i>ppm</i>
• Sensitivity	<i>nA/ppm</i>
• Sensitivity error	<i>nA/ppm</i> and % of nominal sensitivity
• Resolution	<i>ppm</i>
• Long term drift	% per year
• Recommended temperature	°C
• Recommended RH	%
• Lifetime	years
• Total volume of the sensor	<i>mm³</i>
• Price	euro

The comparison is organized in multiple tables, one for each type of gas, shown at the end of the chapter. The considered gaseous analytes are CO , H_2S , NO_2 and SO_2 . From the comparison tables it can be noticed that all the considered sensors can withstand to almost the same temperature and relative humidity range and, most of the times, sensors with higher maximum current have a shorter lifetime.

The maximum current i_{WEMAX} is calculated multiplying for each sensor its range and its nominal sensitivity, giving a suggestion on the current capability of the sensor. For example, for the H_2S table, can be seen that all the SGX sensors have almost all the same i_{WEMAX} despite having different ranges, that directly translates in the difference of sensitivity. It can be noticed that in this case a lower sensitivity if the i_{WEMAX} is almost equal imply a bigger sensitivity error E_s . However this reasoning is applicable on sensor that are built using the same technological processes and can bring to wrong considerations if applied on sensors of which the constructive details are not clear. In fact, from the comparison tables can be noticed that SPEC sensors have the least maximum current, but are characterized by a better resolution respect to all the others. In addition they show a better response time and more than doubled lifetime than all other sensors. Another advantage that characterize SPEC sensors is the lower size respect to others since they have almost the same surface area, but a lower thickness of 4 *mm* at maximum against the 20 *mm* of almost all other sensors. Finally they resulted to be the least expensive sensors. For the application object of this work, as already explained in the introductory part, the lifetime and the size of the sensing node are crucial. SPEC sensors stands out above all the others considering this two characteristics. Furthermore, all other sensors are much more expensive, having an average price of around 50 \$ against the 15 \$ for the sensors produced by SPEC. This considerations brings to choose the sensors produced by SPEC.

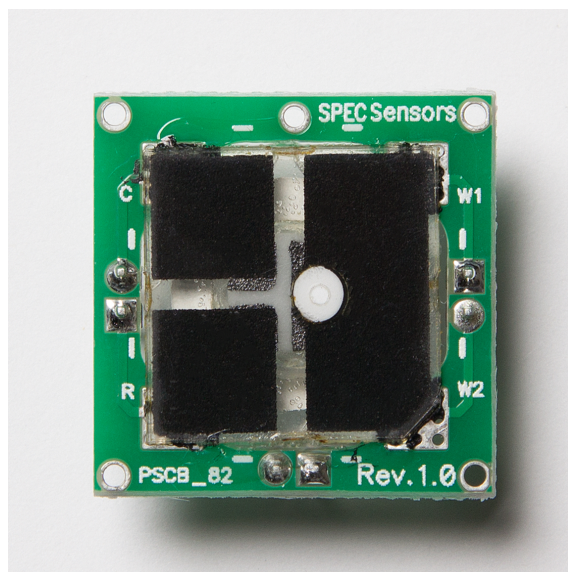


Figure 5.1: A SPEC amperometric electrochemical gas sensor

Target gas	Sensor name	S_{calib} [nA/ppm]
H_2S	3SP H2S 50 Package 110-303	297.15
SO_2	3SP SO2 20 P Package 110-601	37.25
NO_2	3SP NO2 5F P Package 110-507	-28.37

Table 5.1

5.2 Selected sensors

The sensors comparison brought to chose SPEC sensors to develop the application, shown in Figure 5.1. During this choice, the most weighted parameters were the lifetime, the price and the size. According to these three values, SPEC sensors resulted to be the preferred choice for some target analytes: H_2S , SO_2 , NO_2 . The chosen gas sensors are listed in Table 5.1.

They are three electrode sensors. They all have a lifetime longer than all other commercial sensors and in some cases shorter response time. Their sensitivity error may seem bigger than other sensors but they are singularly calibrated before selling and the calibrated sensitivity value S_{calib} is provided for each sensor. A long term drift value is not specified in the datasheet but it may lie inside the repeatability term that is 3 % of reading for all sensors. According to that the uncertainty on S_{calib} is of 3 % as well. In Table 5.1 the value of S_{calib} for each sensor is given. For the SO_2 sensor a negative sensitivity is reported because the sensor current exits from the WE, instead of entering as in the other sensors.

As all other amperometric gas sensors, also those chosen for this application are affected by temperature and humidity variations, as well as they show cross-sensitivity to other gaseous analytes. All these aspects are addressed below more in detail

	Sensor>>	CO	H2S	O3; -200mV	O3; 0mV	NO2	SO2	EtOH	NO
Gas	ppm tested	ppm Measured							
Carbon Monoxide	400	400.0	1.1	<0.05	<0.05	<0.1	7.3	251.4	4.0
Hydrogen Sulfide	25	<1	25.0	-5.8	-12.5	-5.8	142.3	63.2	78.6
Ozone	5	<1	-0.9	5.0	5.0	5.0	-3.3	<5	-1.8
Nitrogen Dioxide	10	<1	-2.0	10.0	5.0	10.0	1.4	<5	0.8
Sulfur Dioxide	20	<1	1.7	0.1	tbd	<0.1	20.0	11.6	11.0
Ethanol	200	5.4	-1.9	2.3	tbd	2.3	-1.8	200.0	-1.0
NO	50	26.1	1.2	0.2	tbd	0.2	90.5	54.5	50.0

Figure 5.2: Cross-sensitivity table taken from SPEC Application Notes

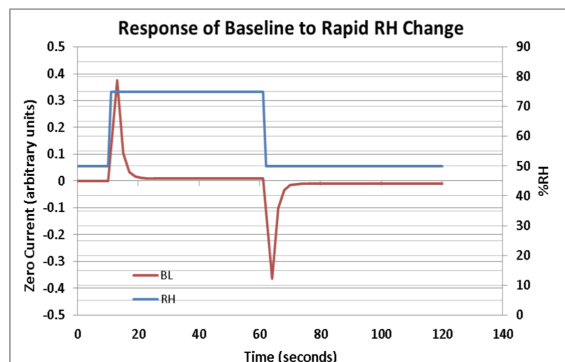


Figure 5.3: Humidity transient response in time domain taken from SPEC Application Notes

5.2.1 Cross sensitivity

All the amperometric gas sensor shows cross-sensitivity effects to gas analytes different to the target. The table provided by the company is reported in Figure 5.2. It shows, for each sensor type, the measured part-per-million when exposed to a given concentration of each analyte.

5.2.2 Humidity effect

A relative humidity fast variation rather than a steady state effect have a transient impact on the sensor's output current. On the contrary, if the sensor operates from several days in an humidity condition outside its specified range, that vary from sensor to sensor, can experience a *permanant* loss of sensitivity. The motivations that brings to this permanent effect were already addressed in the section 4.2.2 of Chapter 4. Regarding fast humidity variations, as can be seen from the Figure 5.3, taken from the Applications Notes of the company, when the humidity suddenly increases for the output current experience a positive spike. The current spike is negative if the humidity decreases. The height of the spike is not given but it is stated that the current recovers from this effect within some seconds returning back to a value within 10 *ppb* of that before the humidity variation.

5.2.3 Temperature effect

SPEC sensors are specified for continuous operation in the $-20\text{ }^{\circ}\text{C} \div 40\text{ }^{\circ}\text{C}$ range and intermittent operation in the $-30\text{ }^{\circ}\text{C} \div 50\text{ }^{\circ}\text{C}$. The ambient temperature variation

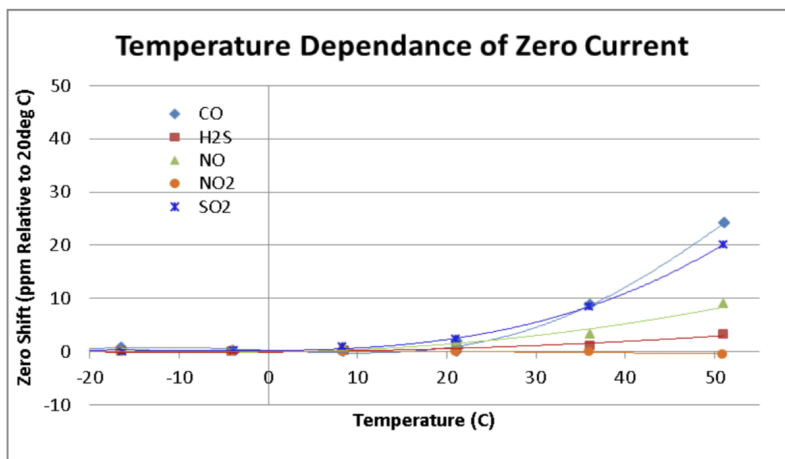


Figure 5.4: Baseline current dependence graph of different sensors taken from SPEC Application Notes

has two distinct effects on the output current of these sensors, generated by different chemical mechanisms. The first considered effect involves the *baseline current* of the sensor, i.e. its output current at zero gas concentration. The second type of temperature dependence affects the sensitivity.

Baseline current dependence

In general, the baseline current has a positive temperature coefficient, different for each gas type sensor. The company, in one of its Application Notes, gives an overview of the typical baseline current temperature dependence for each type of gas, shown in Figure 5.4. From the graph, it can be noticed that the different baseline temperature coefficients among the shown sensors. In addition, it has to be underlined that those curves, for each gas, represent a *typical* dependence, result of an averaging process of measures made with a certain number of sensors. Thus, for achieving the best accuracy, a temperature calibration of the final product is needed, in order to precisely measure the temperature coefficient of the purchased sensor.

The company suggests a linear correction of this effect, providing the equations reported below

$$i_{WE_{zero}}(T) = i_{WE_{zero}}(T_0) + [TC_{zero} \cdot (T - T_0)] \quad (5.2.1)$$

$$i_{WE_{comp}}(T) = i_{WE}(T) - i_{WE_{zero}}(T) \quad (5.2.2)$$

where

- T is the temperature at which the measurement is performed
- T_0 is the reference temperature (i.e. the temperature at which the calibration is made)
- TC_{zero} is the temperature coefficient of the baseline current in $\frac{A}{C}$

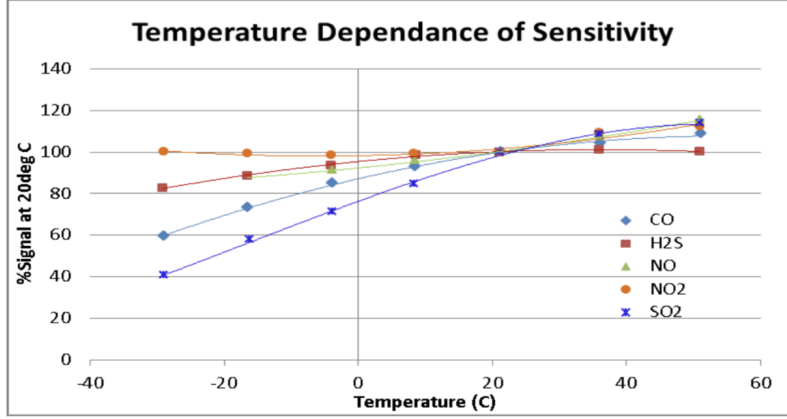


Figure 5.5: Sensitivity temperature dependence graph of different sensors taken from SPEC Application Notes

- $i_{WE_{zero}}(T_0)$ is the baseline current at the reference temperature T_0
- $i_{WE_{zero}}(T)$ is the baseline current at the temperature T
- $i_{WE}(T)$ is the current at temperature T
- $i_{WE_{comp}}(T)$ is the compensated value of the current at temperature T

Therefore to operate this linear correction is necessary to obtain the value of TC_{zero} .

Sensitivity dependence

The ambient temperature also affects the sensitivity of each sensor. As for the baseline current dependence the company provides a general overview of the typical sensitivity dependence characteristics for each gas sensor type, shown in Figure 5.5. Where the same averaging process of different sensor for each gas have been operated. Thus, a calibration of the final product is needed also for the effect on sensitivity. The company provides a linear compensation equation, reported below

$$G = \frac{i_{WE_{comp}}(T)}{S_{calib}} \cdot [1 + TC_{span}(T - T_0)] \quad (5.2.3)$$

where

- G is the gas concentration in *ppm*
- TC_{span} is the temperature coefficient of the sensitivity S_{calib}
- S_{calib} is the calibrated sensitivity of the sensor

In the final applications those effects can not be neglected and a way to implement a compensations system has to be employed. In this case it has been decided to use a temperature sensor that both has to be capable to provide the necessary informations to apply the compensation function and has to detect harmful environmental conditions for the sensor that would result in inconsistent readings, as described before in the temperature and humidity effects.

Brand	Gas	Range		S [nA/ppm]		Res [ppm]	LTD [%/y]	t_s [s]	V_{bias} [mV]	$i_{WE_{MAX}}$ [μA]	HR [%]		T [°C]		Life [y]	Dim. [mm]
		Min	Max	Slope	E_s [%]						Min	Max	Min	Max		
SPEC	H2S	0	50	212	41	0,005	N.S.	15	0	10,6	0	100	-30	55	5	20x20x3
SGX	H2S	0	50	1700	23,5	0,1	20	40	0	85	15	90	-40	50	1	31x31x20
SGX	H2S	0	100	800	25	0,1	24	35	0	80	15	90	-20	50	2	20X20X20.9
SGX	H2S	0	100	700	35,7	N.S.	15	30	0	70	15	90	-30	50	2	20x20x20
SGX	H2S	0	1000	90	44,4	1	24	45	0	90	15	90	-20	50	2	20x20x20

Brand	Gas	Range		S [nA/ppm]		Res [ppm]	LTD [%/y]	t_s [s]	V_{bias} [mV]	$i_{WE_{MAX}}$ [μA]	HR [%]		T [°C]		Life [y]	Dim. [mm]
		Min	Max	Slope	E_s [%]						Min	Max	Min	Max		
SGX	CO	0	1000	100	20	0,5	5	30	0	100	15	90	-30	50	2	31x31x20
SGX	CO	0	500	70	21,4	1	24	30	0	35	15	90	-20	50	2	20x20x20
SGX	CO	0	500	80	37,5	1	10	30	0	40	15	90	-30	50	2	20x20x20
SGX	CO	0	1000	70	35,7	N.S.	20	N.S.	0	70	10	95	-30	50	2	20X20X20
SPEC	CO	0	1000	4,75	57,9	0,1	0	15	0	4,75	0	95	-30	55	5	20x20x3.8
SGX	CO	0	2000	28	35,7	10	24	35	0	56	15	90	-20	50	2	20x20x20

Brand	Gas	Range		S [nA/ppm]		Res [ppm]	LTD [%/y]	t_s [s]	V_{bias} [mV]	$i_{WE_{MAX}}$ [μA]	HR [%]		T [°C]		Life [y]	Dim. [mm]
		Min	Max	Slope	E_s [%]						Min	Max	Min	Max		
α_{SENSE}	SO2	0	100	375	26,7	0,0075	15	40	N.S.	37,5	15	90	-30	50	2	32-3X32-3X16-5
α_{SENSE}	SO2	0	50	400	20	0,0225	15	20	N.S.	20	15	90	-30	50	2	20-2X20-2X20-8
Euro g.	SO2	0	20	500	20	0,1	24	45	0	10	15	90	-20	40	1	20X20X20
Euro g.	SO2	0	20	340	29,4	0,2	24	70	0	6.8	15	90	-20	50	1	32X32X20.3
Euro g.	SO2	0	2000	20	40	5	24	60	0	40	15	90	-20	50	2	20X20X20
Euro g.	SO2	0	2000	23	47,8	5	24	70	0	46	15	90	-20	50	2	32X32X20.3
SGX	SO2	0	20	500	20	0,1	24	45	0	10	15	90	-20	40	1	20X20X20
SGX	SO2	0	2000	20	40	5	24	60	0	40	15	90	-20	50	1	20X20X20
SPEC	SO2	0	20	25	40	0,02	N.S.	15	200	0,5	0	100	-30	50	5	20x20x4

Brand	Gas	Range		S [nA/ppm]		Res [ppm]	LTD [%/y]	t_s [s]	V_{bias} [mV]	$i_{WE_{MAX}}$ [μA]	HR [%]		T [°C]		Life [y]	Dim. [mm]
		Min	Max	Slope	E_s [%]						Min	Max	Min	Max		
SPEC	NO2	0	5	-30	-33,3	0,02	N.S.	15	-25	-0,15	0	100	-40	50	5	20x20x3
SPEC	NO2	0	20	-40	-37,5	0,02	N.S.	300	-200	-0,8	0	100	-40	50	5	20X20X3
SGX	NO2	0	20	600	25	0,1	24	30	0	12	15	90	-20	50	1	20-2X20-2X20-9

Chapter 6

Conditioning circuit

6.1 Theory

There are different kinds of conditioning circuit that can be used for EC gas sensors. Here will be discussed only sensors that operates at a fixed bias potential, in a *potentiostatic* configuration. Therefore the conditioning circuit must include a biasing section to bias the sensor and a current measuring section to read the analyte concentration.

It should be remembered that the bias voltage of this kind of sensors must be held constant for their entire lifetime. Any given modification to its value reflects in a modification of its nominal sensitivity that may take several hours to re-establish once the bias voltage is brought back to its nominal value. This suggest that maintaining a constant bias, without interruption, for the whole operating life of the sensor, it is the best choice in order to avoid any possible damage and maintains the sensor ready for a read operation.

Every amperometric gas sensors require also a load resistance R_L in series with the WE whose suggested value is usually 10Ω , but may vary from sensor to sensor according to the specifications . Its value is a balance between response time of the sensor and the noise power of the current generated by the sensor I_{WE} .

Different kind of conditioning circuits, for two and three electrode sensors, are proposed in the sections below with their advantages and drawbacks.

6.1.1 Three terminal sensors

Three terminals sensors, in addition to the WE and CE, have a Reference Electrode (RE) which role is to stabilize the potential at the WE. For this reason the biasing circuit of this kind of sensors is a little more complex than two terminal versions. As in two terminal sensors, the WE is the terminal from which the current signal is read, while an equal and opposite amount of current should be provided to the CE terminal to allow the sensor to work properly. No current, instead, has to flow inside the RE. Precisely, the currents at the three terminals of the sensor, applying the KCL, follows the relation:

$$I_{WE} = I_{CE} + I_{RE} \quad (6.1.1)$$

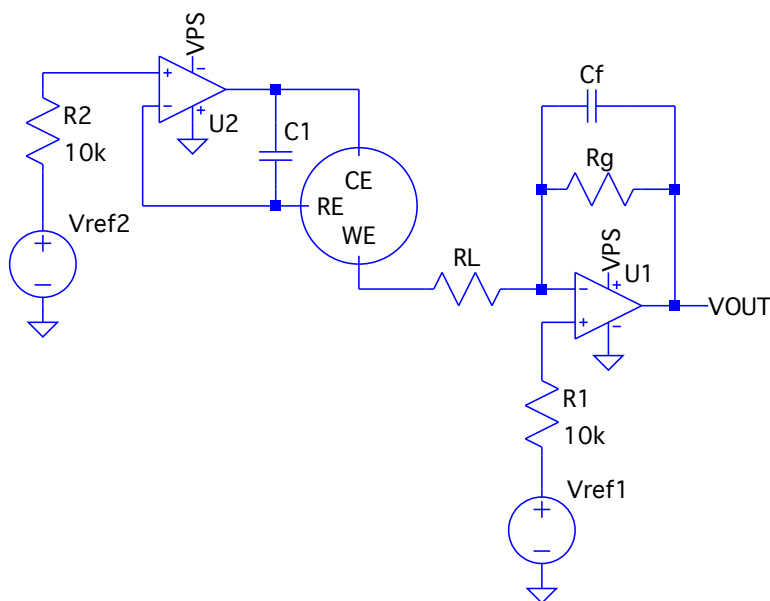


Figure 6.1: First potentiostatic conditioning circuit for amperometric gas sensors

The current flowing in the RE should virtually be zero, in order to maintain its potential as much stable as possible. In fact, the bias potential V_{bias} , specific for the sensor, has to be applied between the WE and the RE terminals.

The first and widely used potentiostatic conditioning circuit capable to cope with all this aspects is shown in figure 6.1. The current generated at the WE is amplified by the trans-impedance stage provided by the operational amplifier U1, that also fixes the potential of the WE to the value V_{ref1} . U2, instead, provides the right amount of current to the CE by observing the potential at the RE, in order to maintain its value equal to V_{ref2} . In this way

$$V_{bias} = V_{WE} - V_{CE} = V_{ref1} - V_{ref2} \quad (6.1.2)$$

The choice of the two reference voltages not only depends on the bias voltage of the sensor. In fact, sometimes, is necessary to provide a common mode reference voltage V_{comm} to the circuit, if a bipolar supply voltage is not available. The reason is that, during the sensor operation, for sensor that has a **positive** I_{WE} **entering** in the WE, thus a negative I_{CE} entering the CE, the potential of the CE is forced below the RE. For this reason is necessary to measure the maximum $V_{RE} - V_{CE}$ difference and increase V_{comm} by a bigger or equal amount in order to give some headroom to the op-amp U2. For example, using a unipolar supply voltage, even if we use a sensor that has null bias voltage $V_{bias} = 0$, we can not set $V_{comm} = 0$, because in that case the output of U2, being not able to reach negative potentials, will not drive the CE below the RE potential. Increasing V_{comm} would permit to U2 to correctly provide the right amount of current to the CE setting its potential below the RE. For sensors that has a **negative** I_{WE} entering the WE the situation

is mirrored. Namely, the V_{comm} can not be setted at the same potential of the power supply but needs to be slightly lower respect to that, because, in this case, the CE potential tends to a bigger value than the RE potential.

The trans-impedance stage permits high amplification factors, using a gain resistance R_g in the order of mega-ohms. In fact, the WE current is directly multiplied by R_g in the V_o equation

$$V_o = R_g \cdot i_{we} \quad (6.1.3)$$

The value of R_g depends on V_{ref1} , on the full-scale voltage reference V_{FS} and on the maximum current generated by the sensor $I_{WE_{MAX}}$. When the maximum current is generated by the sensor the output voltage reaches V_{FS}

$$V_o|_{I_{WE_{MAX}}} = V_{FS} = V_{ref1} + R_g \cdot I_{WE_{MAX}} \quad (6.1.4)$$

so R_g is calculated using

$$R_g = \frac{V_{FS} - V_{ref1}}{I_{WE_{MAX}}} \quad (6.1.5)$$

The load resistance R_L in series with the sensor may affect its bias voltage by $\Delta V_{bias} = I_{WE} \cdot R_L$, but do not disturb the output voltage, because the OP-AMP U_1 , in trans-impedance configuration, reacts to maintain its negative terminal at V_{ref1} . Though, the sources of error in V_o comes directly from the offset voltage V_{offU1} of U_1 that directly affects the output voltage. Also its bias current I_{bU1} may contribute in some cases, although its effect most of times is negligible. For this reason, if an high output accuracy is required, it is preferable for U_1 to have a low noise offset voltage. In addition, rail to rail input and output operational amplifiers may be useful if, beyond precision, if a wide range is required.

To sum up, this potentiostatic circuit is capable of having a flexible bias voltage and permits high trans-impedance gains, therefore is suitable for different kinds of amperometric gas sensors, with the appropriate selection of V_{ref1} , V_{ref2} and R_g

6.1.2 Two terminal sensors

In two terminal sensors the bias voltage is applied directly between the WE and CE and the same, but opposite, current has to be provided to the CE.

In this case the load resistance of the sensor, R_L , can be used to both bias the sensor and generate a potential difference proportional to I_{WE} , as shown in the circuit of Figure 6.2. Where

$$V_o = I_{WE} \cdot R_L \cdot \left(1 + \frac{R_2}{R_1}\right) \quad (6.1.6)$$

In this case, attention should be paid to the maximum variation of potential across R_L , because it is also the bias voltage applied to the sensor, and its stability directly affects the sensor stability and sensitivity.

Using this circuit high amplification factors are not possible, due to its intrinsic nature (i.e. a ratio of resistances in the V_o equation and a possibly low value of R_L). The great advantage of this circuit is that the sensor is always maintained

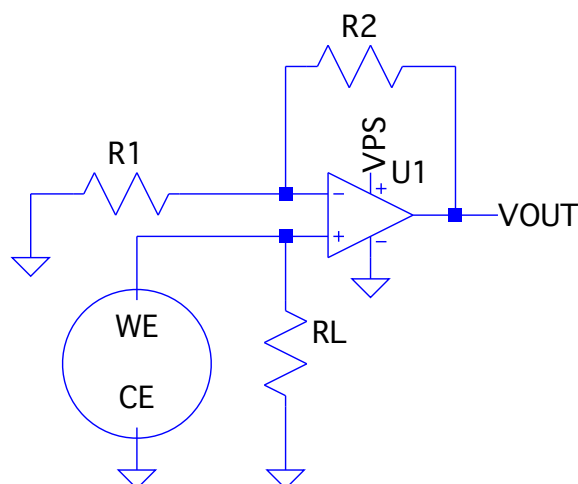


Figure 6.2: Self-biasing configuration for two electrodes gas sensors

biased without the use of any external circuit. Therefore the conditioning system can be designed to consume power only during the reading phase for low power applications.

In addition, for two terminal sensors, the same conditioning circuit described before for three terminal sensors, can be used shorting the CE and RE terminals, as shown in Figure 6.3.

6.1.3 Output filtering

In order to correctly choose the filtering part of the conditioning circuit is necessary to know the response time of the sensor and that required by the application. The response time of amperometric gas sensors is usually slow, in the order of seconds at least. It depends on different characteristics and constructive details of the sensor. The response time is increased by the increment of the load resistance R_L , acting as an RC circuit with the internal capacitance of the sensor, that is usually very big, in the order of milli-Farads. For this reason, to maintain a fast sensor response, R_L should be kept as low as possible. In some cases one may notice that increasing the value of R_L the sensor's noise decreases. This is true only for the noise above a certain frequency, while the noise at very low frequency, under $1Hz$, is not influenced by R_L [37]. Thus, reduce the noise increasing R_L is not so efficient because for that frequency band is more efficient an electronic filtering, that, moreover, does not influence directly the sensor. The electronic output filtering can be of I or II order, both are described below.

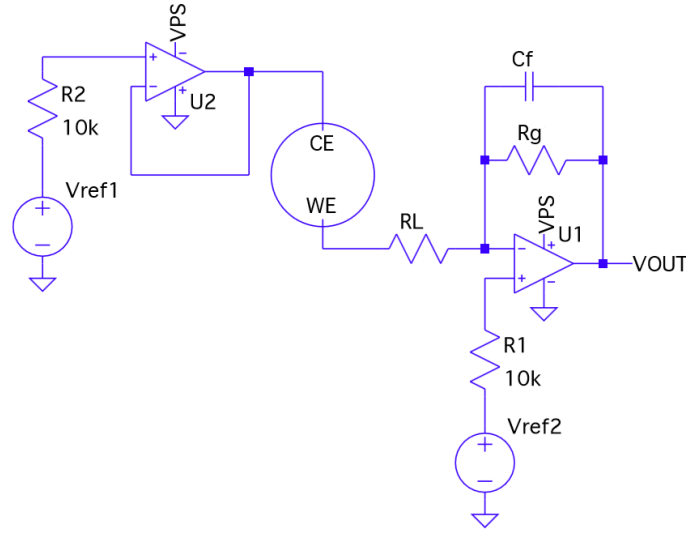


Figure 6.3: Three electrode sensor conditioning adapted for two electrodes sensors

First order filter

First order electronic filtering can be achieved by adding a capacitance, C_f in parallel to the feedback resistance of the trans-impedance stage, R_g , as shown in Figure 6.1. The value of the capacitor C_f is chosen respect to the previously known value of the gain resistance R_g and the preferred pole frequency, that is:

$$f_p = \frac{1}{2\pi R_g C_f} \quad (6.1.7)$$

The transfer function of the trans-impedance stage, without considering the frequency behaviour of the OP-AMP, is

$$H_I(s) = Z_f(s) = \frac{R_g}{1 + sR_g C_f} \quad (6.1.8)$$

that in the frequency domain leads to

$$H_I(j2\pi f) = Z_f(j2\pi f) = \frac{R_g}{1 + j2\pi f} = \frac{R_g}{1 + j\frac{f}{f_p}} \quad (6.1.9)$$

where f_p is the pole frequency defined above and Z_f denote the feedback impedance of the trans-impedance stage.

Supposing an equivalent white noise current source at the input of the trans-impedance stage $i_{n_{input}}$, the output noise $e_{n_{output}}$ integrated over an infinite bandwidth is

$$\begin{aligned}
 e_{n_{output}} &= i_{n_{input}} \int_0^{\infty} |H_I(j2\pi f)| df \\
 &= i_{n_{input}} \int_0^{\infty} \sqrt{\left(\frac{R_g}{1 + j\frac{f}{f_p}}\right)^2} df = \\
 &= i_{n_{input}} R_g^2 \sqrt{\int_0^{\infty} \frac{1}{1 + \left(\frac{f}{f_p}\right)^2} df} \\
 &= i_{n_{input}} R_g^2 \sqrt{[f_p \arctan\left(\frac{f}{f_p}\right)]_0^{\infty}} = \\
 &= i_{n_{input}} R_g^2 \sqrt{f_p \frac{\pi}{2}}
 \end{aligned}$$

In order to make a precise calculation of $e_{n_{output}}$, the equivalent input noise $i_{n_{input}}$ is not to be considered white. In fact $i_{n_{input}}$ has to take into account the noise generated by the OP-AMP and every component placed at its inputs, the sensor included. The OP-AMP, most of times, generates a frequency dependent noise that, particularly at low frequencies, is a $1/f$ noise difficult to eliminate either with a first or second order filter. Among the other noise sources is worth to mention the circuit responsible of generating the reference voltage V_{ref1} , applied at the positive terminal of the OP-AMP that constitutes the trans-impedance stage, namely U_1 .

Second order filter

The second order filter, shown in Figure 6.4, provides an additional filtering capability adding a pole respect to the first order filter to the transfer function, that becomes

$$H_{II}(s) = \frac{R_g}{1 + sR_g C_f} \cdot \frac{1}{1 + sR_{LP} C_{LP}} \quad (6.1.10)$$

that in frequency domain leads to

$$H_{II}(j2\pi f) = \frac{R_g}{(1 + j\frac{f}{f_{p1}})(1 + j\frac{f}{f_{p2}})} \quad (6.1.11)$$

where the two poles frequencies are

$$f_{p1} = \frac{1}{2\pi R_g C_f}, f_{p2} = \frac{1}{2\pi R_{LP} C_{LP}} \quad (6.1.12)$$

The calculation procedure for the first pole frequency has already been addresses. The second pole frequency calculation has two degrees of freedom, therefore is necessary to decide the value of the filtering frequency and either the value of the capacitance or the resistance. The capacitance maximum value can be limited by the availability of the component and by its geometrical dimensions. Also the resistance has not to be too large in order to avoid generating additional noise, that

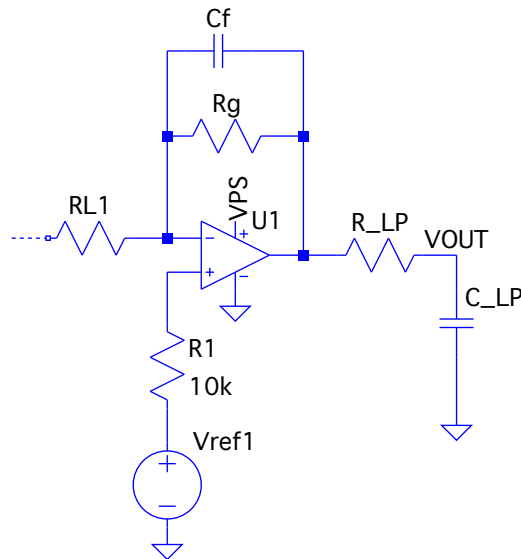


Figure 6.4: Trans-impedance stage with second a order filter

is proportional to its value. If the two poles are at the same frequency the second order filter reduce the output noise power by $\sim 10\%$.

6.2 Design

The purpose of the work is to realize a battery alimeted gas detection system of long durability. The portability constraint implies a very low power approach to the system design. Moreover the system has to be capable of working with different sensors that, for example, have different currents capabilities and bias voltages. Furthermore, the temperature and humidity dependence of the sensor current needs to be compensated, requiring the presence of a relative humidity and temperature sensor.

For the conditioning section it has been decided to use the circuit shown in Figure 6.5, analogous to the previously shown circuit of Figure 6.1.

The circuit has to be capable of working with different amperometric gas sensors, in order to provide the possibility to change the target analyte. Due to the fact that different sensors can have different bias voltages the circuit should be able to modify the value of the two voltage references, V_{ref1} and V_{ref2} . Moreover, also the value of the common mode voltage can change from sensor to sensor, requiring flexibility in that sense too. In addition this flexible system, due to the fact that has to be operative during the whole system life, should ensure a very low power consumption,

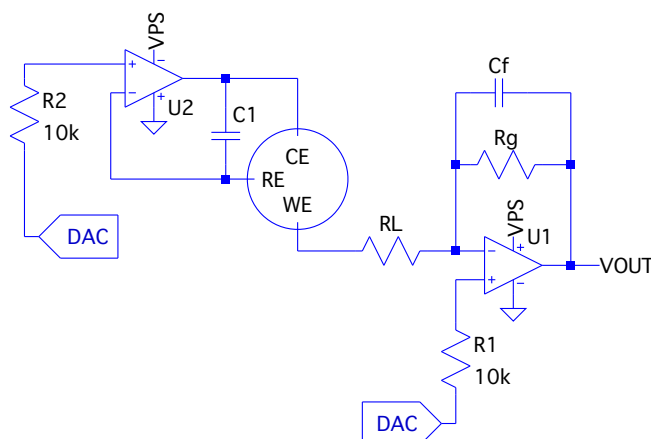


Figure 6.5: Caption

Target gas	Sensor name	Range [ppm]	Res. [ppb]	S_{calib} [nA/ppm]	V_{bias} [mV]
H_2S	3SP H2S 50 Package 110-303	50	5	297.15	0
SO_2	3SP SO2 20 P Package 110-601	20	20	37.25	200
NO_2	3SP NO2 5F P Package 110-507	5	20	-28.37	-25

Table 6.1

requiring a maximum current for functioning in the order of tens of μA . To cope with the necessities explained above it has been chosen to bias the sensors and select the common mode voltage of the circuit at once with two DAC. This ensures the maximum flexibility and a power consumption under the system's constraints.

In order to correctly choose the components of the conditioning circuit a pre-analysis of the worst case based on the chosen sensors characteristics, listed in Table 6.1, it is necessary. However, those values are not enough to calculate the gain of the trans-impedance stage, Eq 6.1.5. The minimum power supply voltage, the voltage references values and the measurement range has to be chosen or decided to complete the calculations.

To calculate the values of the reference voltages it is needed to measure the maximum voltage swing between the RE and the CE, in order to choose a correct value for V_{comm} . This can be done by choosing a temporary value for R_g to permit to the system to work correctly and then measure the $V_{RE \rightarrow CE}$. This value can be measured also in absence of target gas because, even if it is expected to change when the reactions inside the electrochemical cell are more intense, the variation is within a few mV due to the small amount of current, dozen of micro-ampere, that flows into the CE at maximum. Then the V_{comm} value is chosen giving some headroom. For all the sensors 1 V has been chosen for V_{comm} , except for the NO_2 sensor for which

Target gas	Sensor name	R_g	$\Delta V_{o_{min}}$
H_2S	3SP H2S 50 Package 110-303	100 $k\Omega$	150 μV
SO_2	3SP SO2 20 P Package 110-601	1.5 $M\Omega$	1.12 mV
NO_2	3SP NO2 5F P Package 110-507	10 $M\Omega$	5.6 mV

Table 6.2

1.7 V has been chosen.

This finally would permit to obtain V_{ref_1} and V_{ref_2} through the equations

$$V_{ref_1} = V_{comm} + V_{bias}, V_{ref_2} = V_{comm} \quad (6.2.1)$$

where $V_{bias} = V_{WE \rightarrow RE}$, therefore positive if measured from the WE to the RE. The full-scale voltage reference in this case is determined by the minimum value of the power supply voltage, being that the system is battery alimented. For this application $V_{FS} = 2.5$ V is considered for the early steps of the system design, as the components choice.

The last value useful in this preliminary analysis is the target ppm range of the system. This choice can be done by considering the target application of the system, where it is going to be employed and other factors such as the target resolution. Some information can be retrieved considering, for each target gas, the concentration value and its the exposition time harmful for human beings. For now the maximum range is considered for each sensor (i.e. the value reported in Table 6.1).

Now the equation 6.1.5 can be used to calculate R_g , that defines the gain of the trans-impedance stage, therefore directly determines the minimum output voltage variation on the basis of the resolution of each sensor. For example the $\Delta V_{o_{min}}$ for a sensor with resolution of 1 *ppb* is $R_g \cdot S_{calib} \cdot 0.001$ *ppm*. Those values are listed in the table 6.2.

The values of $\Delta V_{o_{min}}$ gives a target resolution to the whole system. Between all the considered sensors, the minimum is $\Delta V_{o_{min}} \simeq 150$ μV of the H_2S sensor that represent the worst which the whole system design considers.

Starting from this point the OP-AMP and the DAC have been chosen.

6.2.1 Components choice

OP-AMP

The portable nature of the system implies that both the operational amplifiers , U_1 and U_2 , has been chosen with a particular attention to their power consumption in conjunction with the capability to function at a minimum voltage lower than the V_{FS} calculated before.

The OP-AMP that forms the trans-impedance stage, U_1 , needs to be characterized by an high-precision and rail-to-rail input and output. The high precision specification derives from the fact that its input offset voltage together with the equivalent input noise source, directly affects the output voltage. The rail-to-rail input and output guarantee that V_o is capable to cover its whole dynamic (i.e. 0 to V_{FS}) in all the operating conditions, especially when the supply voltage of the battery drops

due to its discharge.

U_2 has the role to supply with an adequate current the CE of the sensor while maintaining the RE electrode at a given potential. Nevertheless the V_{bias} of the sensor needs to be as much as stable as possible but it can tolerate an offset steady state error of a few millivolts, relaxing the specifications on the precision of U_2 and of the DA converter.

It has been decided to use a dual channel operational amplifier from Texas Instruments, the TLV8812. It is characterized by very low quiescent current consumption of less than 500 nA per channel. It supports a supply voltage as low as 1.7 V and provides a rail-to-rail output. The major contribution to the output error, as already said, is represented by its offset voltage. In the datasheet, the maximum offset voltage indicated is $V_{off} = \pm 550 \mu V$. It is bigger than the minimum $\Delta V_{o_{min}} \simeq 150 \mu V$ calculated above, but lower than the other two, representing a good compromise between low power consumption and output error.

A more detailed analysis of the systematic contribution to the offset error, in the worst case, is present below. A temperature of 40 ° and a power supply V_{PS} variation of 0.5 V are considered.

The systematic contribution to the output error, mostly determined by V_{off} , is expressed by the equation

$$\Delta V_{off_{systematic}} = V_{off_{MAX}} + TC_{off}(40 \text{ }^\circ\text{C} - 25 \text{ }^\circ\text{C}) + V_{off_{PSRR}} \cdot \Delta V_{PS} \quad (6.2.2)$$

where

- $TC_{off} = 1 \mu V/^\circ\text{C}$
- $V_{off_{PSRR}} = 60 \mu V/V$

therefore

$$\Delta_{off_{systematic}} = 550 + 20 + 30 = \pm 600 \mu V \quad (6.2.3)$$

The random contribution to the output noise at a frequency below 10 Hz was already given, but a precise noise analysis that takes into account all the components is done at the end of the chapter.

DAC

In the choice process of a digital-to-analog converter responsible for generating the reference voltages, V_{ref1} and V_{ref2} , is fundamental the power consumption rather than precision because it must continuously operate for the entire life of the system, being a significant contribute to the power budget. Moreover its driving capability and speed are not critical requirements due to the low magnitude of its output current and due to the fact that it operates at a constant value unless the sensor is changed.

As said before, the maximum allowed error for V_{bias} is within a few millivolts, hence a value of 1 mV together with the V_{FS} are considered for the calculation of the number of bits of the converter. In this case

$$N_{bit} = \lceil \log_2\left(\frac{1 \text{ mV}}{V_{FS}}\right) \rceil = 12 \text{ bit} \quad (6.2.4)$$

where $V_{FS} = 2.5 \text{ V}$. Anyhow the maximum common denominator of the bias voltages of the considered sensors is 25 mV . This would permit to use a converter with less number of bits, calculated below

$$N_{bit} = \lceil \log_2\left(\frac{25 \text{ mV}}{V_{FS}}\right) \rceil = 7 \text{ bit} \quad (6.2.5)$$

It is fair to think that a converter with a fewer number of bits has a lower power dissipation, reason why it has been decided to set as project specification 7 instead of 12 *bit*.

The chosen component is the MAX5513 from Maxim Integrated, a dual channel 8-bit DA converter that additionally provides an output programmable reference voltage V_{refOUT} . The analog outputs are buffered, with the feedback terminal internally connected to the output, but is also available a version of this converted that exposes the feedback terminal, allowing the user to decide whether use it as buffer or insert a feedback factor. Its supply current during operation, of $8 \mu\text{A}$ at maximum, makes it suitable for the application. Its systematic and random sources of error of the outputs and output reference are analyzed below.

First of all it has to be cleared that the errors on V_{ref_2} does not affect the output error, because the position of this reference voltage does not affect the output voltage. The outputs of the converter that directly affect the accuracy of measurements in the system are the output designated to generate the V_{ref_1} voltage and the output reference voltage V_{refOUT} . For example, if V_{refOUT} is used as reference voltage for the analog-to-digital converter its error is directly added to the one of the ADC.

Output channels

The output systematic error is expressed by its static accuracy characteristics, as the integral and differential non linearity, offset and gain errors. Each contribute and the calculations are shown below.

The contributions shown in the 'Calculated value' column refers to a $V_{LSB} = 9.7 \text{ mV}$, retrieved from the equation

$$V_{LSB} = \frac{V_{FS}}{2^8} = \frac{2.5 \text{ V}}{256} = 9.7 \text{ mV} \quad (6.2.6)$$

Name	Datasheet value	Calculated value
Integral non linearity	0.25 <i>LSB</i>	2.4 <i>mV</i>
Differential non linearity	0.2 <i>LSB</i>	1.9 <i>mV</i>
Offset error	1 <i>mV</i>	1 <i>mV</i>
Gain error	0.5 <i>LSB</i>	4.8 <i>mV</i>
PSRR	85 <i>dB</i>	28 μV

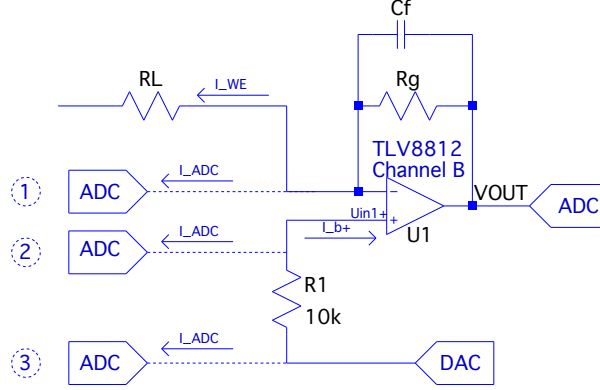


Figure 6.6

Therefore the error on each output channel is

$$\begin{aligned}\Delta V_{DAC_{out}} &= \Delta_{INL} + \Delta_{DNL} + \Delta_{off} + \Delta_{gain} + \Delta_{PSRR} \\ &= 2.4mV + 1.9mV + 1mV + 4.8mV + 28\mu V = 10.128mV\end{aligned}$$

that, in the case of the reference voltage V_{ref1} , the error $\Delta V_{DAC_{out}}$ is directly added to the output voltage error ΔV_o that should be maintained under $\Delta V_{o_{min}} \simeq 150 \mu V$. This happens because V_{ref1} is applied to the positive pin of the operational amplifier U_1 that constitutes the trans-impedance stage, as can be seen from the schematic shown in Figure 6.1. This raises the necessity to measure this quantity, reducing its error down to the resolution of the AD converter, in order to make a software compensation inside the measurement algorithm implemented in the Control-unit.

Using as reference the Figure 6.6, one idea could be of measuring, with the AD converter, the voltage of the negative pin of U_1 (position 1 in figure), in order to reduce both the error on V_o generated by the offset voltage of U_1 and by $\Delta V_{DAC_{out}}$ at once. Another option is to measure the voltage of the positive input pin of U_1 (position 2 and 3 in figure), permitting to compensate only the error on V_o caused by $\Delta V_{DAC_{out}}$. Though the first strategy could seem more effective, in reality is not. The reason is that every AD converter requires to sink a certain amount of current from its input channel, and a current absorbed by the analog input of the ADC, namely I_{ADC} , from the negative pin of U_1 would generate an offset error on V_o , equal to

$$\Delta V_o = I_{ADC} \cdot R_g \quad (6.2.7)$$

therefore in this case the advantage of compensating the error generated by the offset voltage of U_1 would be canceled by the introduction of another offset error.

Name	Symbol	Nominal value	Unit
Temperature coefficient	TC_{refout}	30	$ppm/^\circ C$
Line regulation	$LiReg$	200	$\mu V/V$
Load regulation	$LoReg$	2	$\mu V/\mu A$
Long term stability	LTS	200	$ppm/khrs$

Table 6.3: DAC output reference error contributions

Hence it has been preferred to place the positive pin of the input channel of the AD converter AD_{in+} on the positive input of the trans-impedance amplifier, because the current required from the analog input of the AD would be furnished by the output of the DAC. Another clarification is also needed on the exact point where the ADC input should be placed. If A_{in+} is placed directly between R_1 and U_{1in+} (position 2 in figure), the current I_{ADC} would generate an additional voltage drop on R_1 equal to

$$V_{R_1} = R_1 \cdot I_{ADC} \quad (6.2.8)$$

that again would be directly summed to V_o , increasing its error ΔV_o . This discussion has also to take into account the input bias current of U_{1in+} if it is bigger than I_{ADC} . In such a case could be useful to measure in that point because a compensation of V_{R_1} could also be needed. In this case the input bias current of U_1 is in the order of pico-ampere, as reported in the data-sheet of the TLV8812, making unnecessary and even wrong to measure across R_1 and U_{1in+} . Therefore the AD positive pin of the input channel is directly connected to the output channel of the DAC (position 3 in figure).

The AD7799 has three channels, therefore it has been decided to use the remaining spare channel to measure V_{ref2} , in order to retrieve precisely the two values of the reference voltages and therefore check that both the common mode voltage and the bias of the sensor are maintained to their nominal values. The same discussion made before can be applied to the precise position where to place the analog positive input of the last channel of the AD.

Output reference

The output reference of the DAC can be used as input reference for the ADC. In this case the absolute error that characterize V_{refout} is added to the ADC error. The static contribution to the V_{refout} absolute error is calculated below. All the contribution are listed in the Table 6.3 . The column "Nominal value" contains the data-sheet value at 25 °C while the "Calculated value" contains the values calculated at a temperature of 40 °C, for a $\Delta V_{PS} = 0.5 V$ and after one year.

$$\Delta_{refout} = (LiReg + LoReg \cdot I_{refin_{AD7799}}) \cdot (1 + LTS \cdot 8.76) \cdot (1 + 30 \cdot 15) = 102.86 \mu V \quad (6.2.9)$$

where 8.76 identify the number of kilo-hours after one year.

The random contribution at low frequencies to V_{refout} error is given by $V_{refout_{noise}} =$

$150 \mu V_{p-p}$, under $10 Hz$, that remains almost equal even when the LTD and TC_{refout} contributions considered. The sum of the two values is

$$\Delta_{TOT} = 102.86 + 150 = 252 \mu V \quad (6.2.10)$$

That is directly summed to the ADC error. In this case an ADC with a number of bit bigger than

$$N_{bit} = \lfloor \log_2 \left(\frac{V_{FS}}{252.86 \mu V} \right) \rfloor = \lfloor \log_2 \left(\frac{2.5 V}{252.86 \mu V} \right) \rfloor = 13 \text{ bit} \quad (6.2.11)$$

would be not useful because its resolution would be automatically lowered by the error on its input reference voltage.

ADC

The analog-to-digital converter that has to be used for this application needs a resolution under the minimum $\Delta V_{o_{min}} \simeq 150 \mu V$, that using a full scale voltage of $V_{FS} = 2.5 V$ yields

$$N_{bit} = \lceil \log_2 \left(\frac{V_{FS}}{150 \mu V} \right) \rceil = 15 \text{ bit} \quad (6.2.12)$$

Moreover a multi-channel ADC is needed because, as explained at the beginning of the chapter, is necessary to sense two different points of the circuit, the output voltage V_o and the reference voltage V_{ref1} . It has been chosen the AD7799 from Analog Devices, a 24-bit 3 channels $\Sigma\Delta$ converter. The principal reason for this choice is that it is a converter suitable for the application, actually overqualified, that was quickly available. However, further modifications of the system, such as the employment of sensors with a lower $\Delta V_{o_{min}}$, could fully exploit the characteristics of such converter, providing also a more precise reference voltage.

This converter has several positive aspects, outlined below, that are useful in this particular application.

- During a measurement operation it has a maximum current consumption of $500 \mu A$, it also supports a power down mode that reduces the current consumption to $1 \mu A$
- It offers the possibility of buffering the analog inputs, in order highly reduce their drawn current down to $\pm 1 nA$
- Its analog inputs can be filtered, up to a frequency of $4.17 Hz$, supporting the electronic filtering of the output voltage.

It also has a other features not used in this case as a programmable gain stage, a reference detection, an integrated power switch and the possibility to perform bipolar readings.

The configuration of the two used channels is listed in the table below

Gain	1
Buffered input	true
Filter update rate	4.17 Hz
Unipolar	true

In this case the calculation of the equivalent number of bit would be un-useful due to the extremely higher number of bit that this converter has respect to the ones that the actual project of the system requires. Anyway, a detailed analysis is present below, that could help for further system modifications. Using this configuration, the data.sheet of the component declares an equivalent number of bits equal to 20.5. However the output RMS noise for the same configuration is of 0.64 μV resulting in a peak-to-peak noise of $\simeq 4.22 \mu V$, that, for the reference voltage $V_{FS} = 2.5 V$ results in a resolution of $\simeq 19 bit$, as the application requires. Anyway some other sources of error has to be taken into account. The calculations are shown below and refers to the previous configuration. In the equations the subscript of Δ identify the source of the error. For example Δ_{offset} identify the offset error. For every thermal drift a temperature of 40 $^{\circ}C$ has been considered. Moreover a V_{PS} variation of 0.5 V has been considered for the calculation of the PSRR.

$$\Delta_{offset} = 1 \mu V + 10 nV/^{\circ}C \cdot (40 ^{\circ}C - 25 ^{\circ}C) = 1.015 \mu V \quad (6.2.13)$$

$$\Delta_{gain} = 10 \mu V \cdot [1 + 1 ppm/^{\circ}C \cdot (40 ^{\circ}C - 25 ^{\circ}C)] \simeq 10 \mu V \quad (6.2.14)$$

$$\Delta_{PSRR} = \frac{\Delta V_{PS}}{10^{\frac{100 dB}{20}}} \simeq 0 V \quad (6.2.15)$$

All this contributions, added to the output peak-to-peak noise, results in

$$\Delta_{TOT} = 4.22 + 1.015 + 10 = 15.235 \mu V \quad (6.2.16)$$

That lowers the resolution to

$$N_{bit} = \lfloor \log_2 \left(\frac{V_{FS}}{15.235 \mu V} \right) \rfloor = 17 bit \quad (6.2.17)$$

This converter also has the possibility to perform both an offset and a full scale calibration, that can be either internal or external. The external calibration requires that the positive input of the selected channel is externally connected either to the offset voltage, while the offset calibration is performed, and to the full-scale voltage while the full-scale calibration is done. The internal calibration does not require such operations because the component automatically make this connections internally while calibrating. During the circuit measurements both the internal calibration are performed prior to acquire the measurements from each channel. In this way both the gain and the offset error temperature dependence is reduced. The resolution with calibration is thus equal to

$$\Delta_{TOT} = 4.22 + 1 + 10 = 15.22 \mu V$$

Temperature

Parameter	Value [°C]
Resolution	0.01
Accuracy	0.3
Repeatability	0.1
Long term drift (one year)	0.04
Total ΔT	0.45

Table 6.4

Relative humidity

Parameter	Value [%RH]
Resolution	0.04
Accuracy	2
Repeatability	0.1
Long term drift (one year)	0.5
Hysteresys	1
Non Linearity	0.1
Total ΔRH	4.74

Table 6.5

Temperature and relative humidity sensor

The temperature and relative humidity sensor that has been decided to include in the measurement system is the SHT21 from [Sensirion](#). The SHT21 is a low-power sensor capable to communicate its measurements via I2C, thus employing only two wires. The tables 6.4 and 6.5 lists its measure characteristics and provides the total error calculation for the two quantities.

6.2.2 Output filtering

The image 6.7 shows the unfiltered output voltage for a SO_2 sensor. From the figure $V_{o_{p-p}} = 286 \text{ mV}$ and $\sigma_{V_o} = 51 \text{ mV}$. The noise contribution introduced by the conditioning circuit derives mostly from the superimposed noise of the output channels of the DA converter (MAX5513) because is used to generate V_{ref1} . The table 6.6 reports the noise specification for the MAX5513, that has an output noise of $620 \mu V_{p-p}$ at maximum. This prove that the noise observed in Figure 6.7 is mostly due to the amperometric gas sensor. Moreover it can be observed that is a low frequency noise, requiring a small low pass filtering frequency. Different filtering capacitors have been tested in order to choose the right one. When possible tantalum

NOISE	Frequency band	TYP	UNIT
Output noise voltage	$f = 0.1 \text{ to } 10 \text{ Hz}$	80	μV_{p-p}
Output noise voltage	$f = 10 \text{ to } 100 \text{ Hz}$	620	μV_{p-p}

Table 6.6: Noise specifications of the DAC output channels

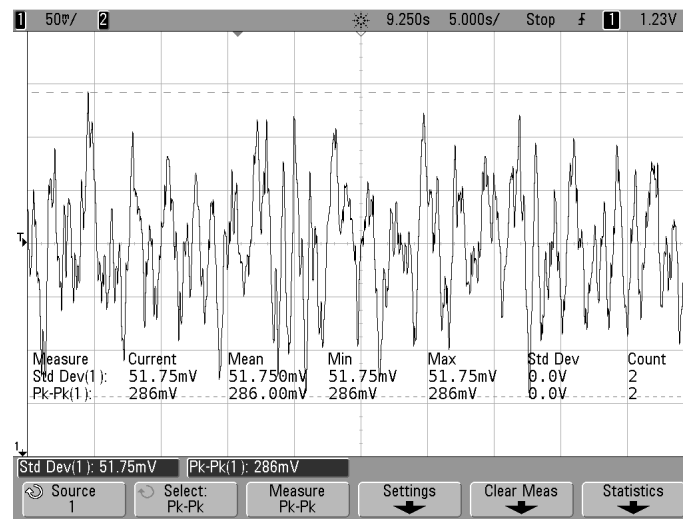


Figure 6.7: Agilent MSO6032A oscilloscope screen showing V_o without filtering capacitance

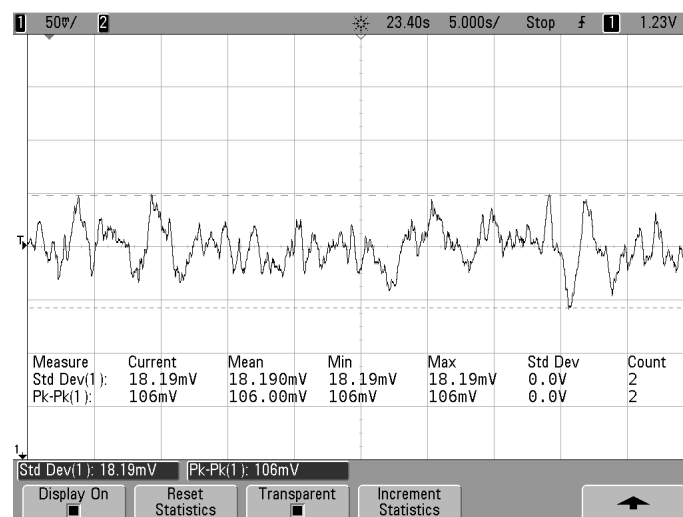


Figure 6.8: Agilent MSO6032A oscilloscope screen showing V_o with $C_f = 330 \text{ nF}$

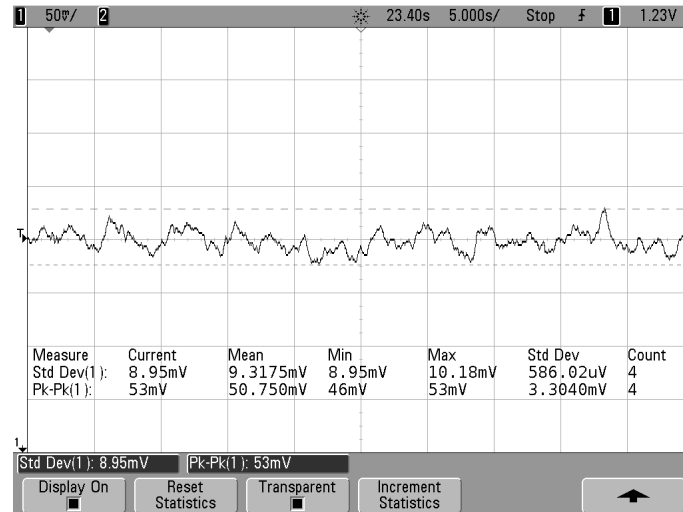


Figure 6.9: Agilent MSO6032A oscilloscope screen showing V_o with $C_f = 1 \mu F$

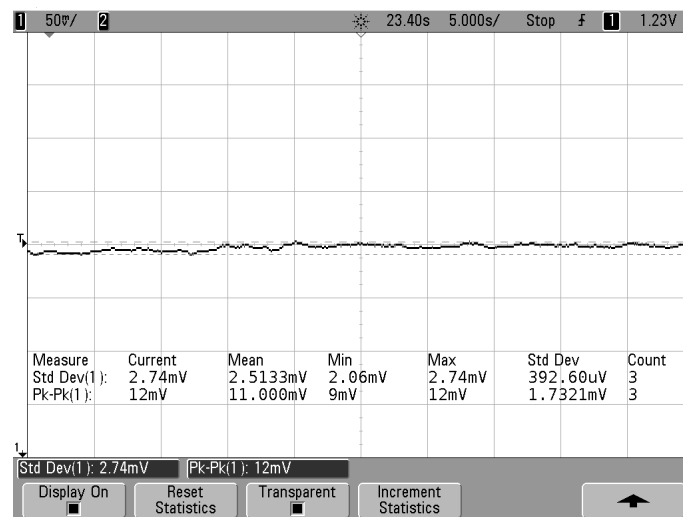


Figure 6.10: Agilent MSO6032A oscilloscope screen showing V_o with $C_f = 10 \mu F$

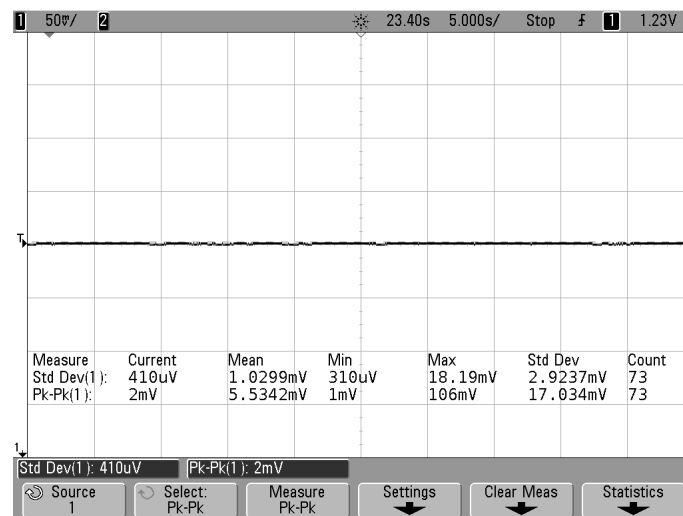


Figure 6.11: Agilent MSO6032A oscilloscope screen showing V_o with $C_f = 22 \mu F$

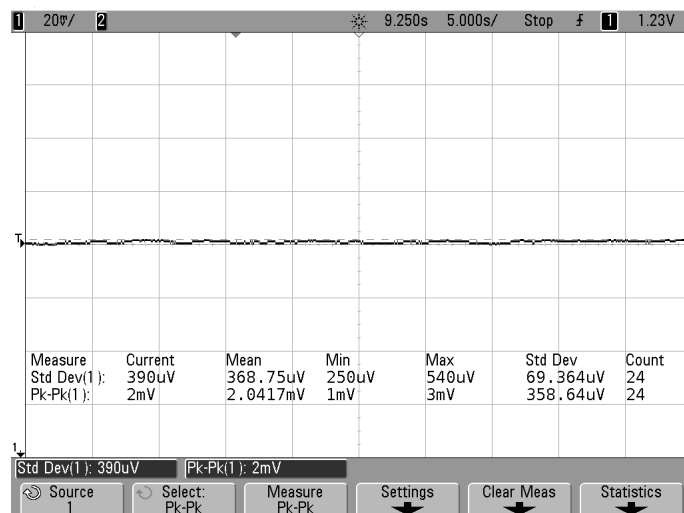


Figure 6.12: Agilent MSO6032A oscilloscope screen showing V_o with $C_f = 47 \mu F$

capacitors were used to further decrease any source of noise. In this case the SO_2 sensor have been used, that uses a gain resistance of $1.5 M\Omega$. This sensor has a sensitivity of $S_{calib} = 37.25 nA/ppm$ and a declared resolution of $20 ppb$. Leading to a minimum $\Delta V_o = 1.1 mV$ for $20 ppb$. Therefore σ_{V_o} should be lower than this value. The figures 6.8, 6.9, 6.10, 6.11 and 6.12 shows the output voltage for different values of C_f , where are also reported the values of σ_{V_o} and $V_{o_{p-p}}$. The choice of the filtering capacitance has to follow a trade of between required response time and output accuracy. If a promptly responsive system is needed, for example to identify a gas leakage the filtering capacitance has to be the set to the lower possible value, scarifying the final resolution. The response time of the SPEC sensors is $\sim 15 s$, therefore, in the SO_2 sensor case, the first order filter frequency is

$$f_p = \frac{1}{2\pi \cdot R_g \cdot C_f} \quad (6.2.18)$$

if is needed to maintain a reponse time of $15 s$ the maximum filtering frequency is $f_p = \frac{1}{15} = 66 mHz$ that results in $C_f = 279 nF$, therefore a $C_f = 330 nF$ should be used, for which $V_{o_{p-p}} = 106 mV$ and $\sigma_{V_o} = 18 mV$.

If the highest resolution is needed the $22 \mu F$ or $47 \mu F$ should be used that show $\sigma_{V_o} = 410 \mu V$ and $\sigma_{V_o} = 390 \mu V$ respectively, that are lower than $\Delta V_o = 1.1 mV$.

6.2.3 Complete circuit schematic

In Figure 6.13 is shown the complete conditioning circuit schematic where the name of the chosen components is indicated. The last component to include is the control unit, which will be addressed in the next chapter. A circuit schematic that shows the connections of each pin is also present in Figure 6.14. In this last schematic are also present the decoupling capacitors placed between the GND and VDD pins of the TLV8812, the MAX5513 and the AD7799. For the first two $100 nF$ ceramic capacitors are used, while for the AD7799 the decoupling capacitors are multiples. For this last component is important to separate the decoupling of its analog $AVDD$

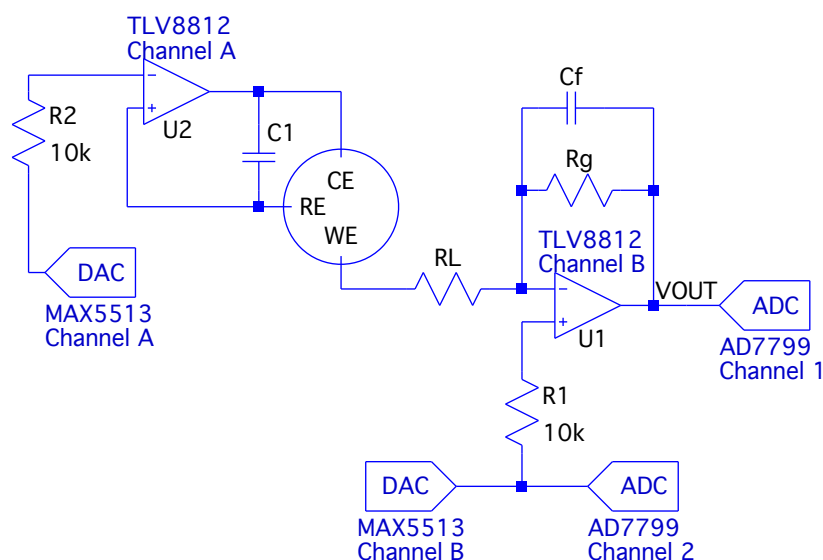


Figure 6.13: Circuit schematic evidencing the components used for the realization

pin from its digital $DVDD$ pin because the digital section of the component communicates with the Control-unit through SPI protocol generating noise on its $DVDD$ pin. A separate decoupling helps to avoid that the digital communications affect the conversion of the analog signals. As can be seen from Figure 6.14 two different capacitors are placed across each VDD pin, a $10\ \mu F$ tantalum capacitor in parallel with a $100\ nF$ ceramic capacitor.

The complete schematic also shows the digital pin designated for the SPI and I2C communications, that has to be connected to the respective modules of the Control-unit. The AD7799 has a complete 4-pin SPI interface. The MAX5513 uses only three of the four pins of the SPI bus because in this case the communication is unidirectional, from the Control-unit to the AD converter, due to the fact that this component needs only to receive the digital code to convert it into an analog signal.

This chapter marks the end of the design of the conditioning analog section of the measurement system. The following chapter discusses the choice and the programming of the Control-unit and of the wireless Bluetooth transmission.

6.2.4 Output equation with linear temperature compensation

Considering the circuit shown in Figure 6.1 the complete expression of the output voltage is

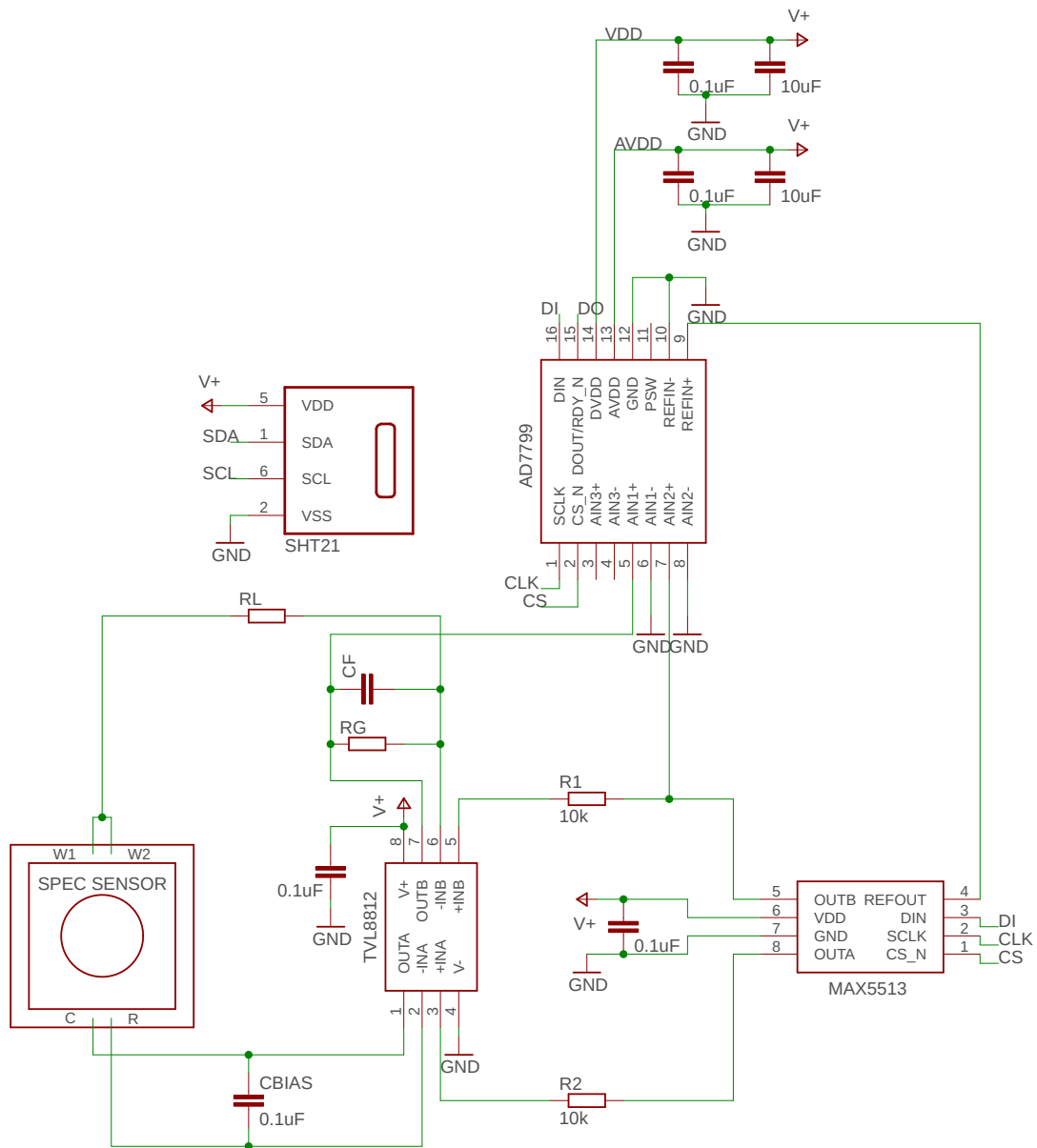


Figure 6.14: Circuit schematic evidencing each pin connection of the components

$$V_o = V_{ref1} + R_g \cdot i_{WE} \quad (6.2.19)$$

The dependence of i_{WE} from to gas concentration is

$$i_{WE} = G \cdot S \quad (6.2.20)$$

where

- G is the gas concentration expressed in *ppm*
- S is the sensitivity expressed in *nA/ppm*

This equation is not taking into account the effect of a temperature variation on the sensor current, leading to an error on the estimation of the gas concentration. Thus a compensation function is needed to improve the accuracy of the measurement system. In section 5.2.3 the temperature effect on this kind of sensors was already described and a compensation function suggested by the company was presented. That compensation function takes into account two distinct temperature effects on the sensor current, the baseline current dependence and the sensitivity dependence. Both are approximated assuming a linear temperature dependence. Both have a positive temperature coefficient, the first is expressed in *nA/°C* while the second is expressed as *%/°C*.

In the equations below an analogous compensation function is provided, but here both coefficients are expressed in $^{\circ}\text{C}^{-1}$. Thus, the equation expressing the WE current i_{WE} function of the gas concentration becomes

$$i_{WE} = G \cdot S_0(1 + TC_{sensitivity} \cdot \Delta T) + S_0 \cdot G_0(1 + TC_{baseline} \cdot \Delta T) \quad (6.2.21)$$

where the sensitivity dependence from the temperature is expressed by

$$S = S_0(1 + TC_{sensitivity} \cdot \Delta T) \quad (6.2.22)$$

where $\Delta T = T - T_0$ and S_0 indicates the sensitivity at T_0 .

The baseline current dependence is taken into account adding the term

$$S_0 \cdot G_0(1 + TC_{baseline} \cdot \Delta T) \quad (6.2.23)$$

to the equation. Here the value $S_0 \cdot G_0$ is the baseline current at temperature T_0 expressed as the product of two quantities

- G_0 that indicates a fictitious gas concentration in *ppm*. It is the value of gas concentration that would be read by the system, at temperature T_0 , if the baseline compensation would not be present.
- S_0 that permits to convert G_0 into a current. The value of S at temperature T_0 has been taken because because a multiplication for a temperature dependent sensitivity would have introduced a non present additional dependence of the baseline current from temperature.

Then, using equations 6.2.19 and 6.2.21 is possible to express the gas concentration G as

$$G = \frac{V_o - R_g \cdot S_0 \cdot G_0(1 + TC_{baseline}\Delta T) - V_{ref1}}{R_g \cdot S_0(1 + TC_{sensitivity}\Delta T)} \quad (6.2.24)$$

This kind of compensation function has to be applied only for a given temperature range, that usually goes from a few celsius degree to the maximum temperature that the sensor can withstand. The reason is that the baseline current is a phenomenon that is temperature dependent only above a certain temperature $T_{base-comp}$ that the company estimated to be around 20 °C. Below that temperature the baseline current assumes a constant value, therefore is sufficient to use the equation

$$G = \frac{V_o - R_g \cdot S_0 \cdot G_0 - V_{ref1}}{R_g \cdot S_0(1 - TC_{sensitivity}\Delta T)} \quad (6.2.25)$$

from which the temperature dependence of the baseline current has been eliminated. On the contrary the sensitivity temperature dependence is still present because its effect is always present across the whole temperature range of the sensor. The function expressing the gas concentration can therefore be completely written in this way

$$G = \begin{cases} \frac{V_o - R_g \cdot S_0 \cdot G_0(1 + TC_{baseline}\Delta T) - V_{ref1}}{R_g \cdot S_0(1 - TC_{sensitivity}\Delta T)} & \text{if } T_{base-comp} < T < T_{MAX} \\ \frac{V_o - R_g \cdot S_0 \cdot G_0 - V_{ref1}}{R_g \cdot S_0(1 - TC_{sensitivity}\Delta T)} & \text{if } T_{min} < T < T_{base-comp} \\ \text{undefined} & \text{elsewhere} \end{cases}$$

Chapter 7

Control unit

Every sensing node needs to be provided with a micro-controller that has to be capable of carrying out several operations that goes from the control of the components to the measurements gathering by mean of the external ADC. The components used inside the conditioning circuit communicates using two different protocols, I2C and SPI. The first is a 3-wire interface, plus an additional wire for each component, while the second works with 2 wires. In total are needed 7 wires to control the three components that directly communicates with the chip. Two of them are controlled via SPI and the third communicates via I2C. Hence a chip that disposes of this two kind of communication modules and enough digital lines is necessary. Moreover the micro-controller needs to be capable of wirelessly communicate via Bluetooth-LE with the central receiver, therefore such kind of wireless radio module needs to be either externally added to the circuit or already be present inside chip. All this requirements has to cope with an extremely low power capability, necessary for the application developed in this work.

All this aspect will be addressed in the next sections as with the description of the micro-controller and the component used to develop the firmware.

7.1 Micro-controller description

The selected system-on-chip is the nRF51 by Nordic Semiconductor. The motivations taht brought to choose it resides in its optimized architecture that permits to develop ultra low power wireless applications. In fact it disposes of a low power ARM®Cortex™-M0 processor and a 2.4 *GHz* transceiver that offers pin compatible device options for Bluetooth LE. In addition a 2 pin Serial Wire Debug Interface is provided that allows a non invasive program debug. All the detail on the architecture of this system-on-chip are described below [38].

7.2 Development environment

A fundamental role in the development phase is played by the development environment that can determine, firs of all, the velocity at which the firmware is developed and tested. A complete set of development tools include

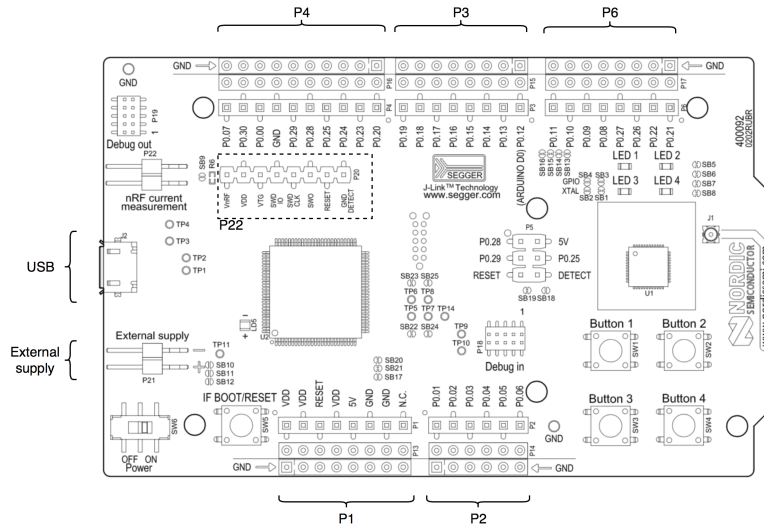


Figure 7.1

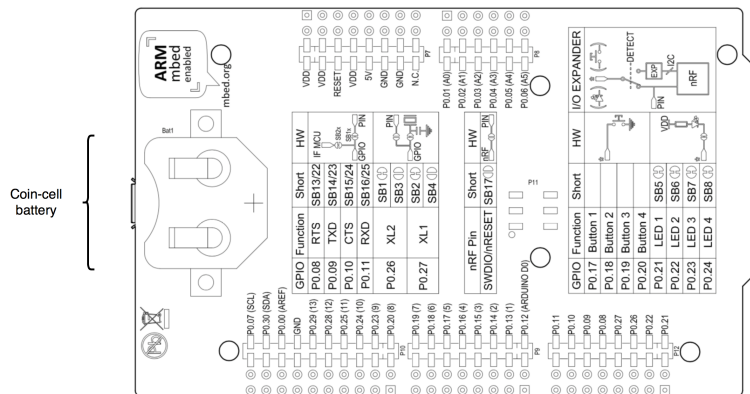


Figure 7.2

- a demo board on which the chip is mounted together with a chip programmer and enough ports that can be used during the prototyping phase
- a compiler
- a text editor sufficiently advanced capable to communicate with the development board through the COM port to flash and debug the code

The demo board used is the Development Kit Board for the nRF51, that will be described in the next sections. For the software part the Keil MDK-ARM Development Kit can be used, but is not a completely freeware solution. In this case full free-ware approach was preferred, without abandoning all the useful features listed above. A full description of each part of the development environment is provided in the next sections.

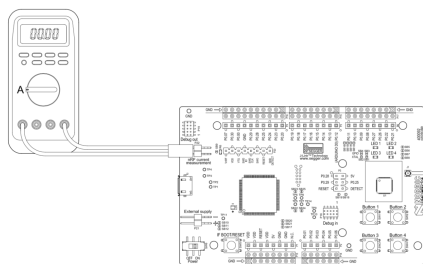


Figure 7.3: Current consumption measurement with multimeter

Demo board [2]

The developing board used in the prototyping phase, shown in Figure 7.1 and 7.2, is a PCA10028 specific for the nRF51 system-on-chip. It mounts a nRF51822 chip that is programmed via the interface MCU present on the board. In addition the development board offers several useful features

- buttons and LEDs for user interaction
- 21 pins organized in 5 ports that provide the access to the digital and analog chip pins and to the board LEDs and buttons
- a port in which are present a $VDD = 3.3 V$, two GND pins, a $5 V$ pin and a reset pin.
- 2.4 GHz radio compatible with the chip
- a SEGGER J-Link OB Debugger that for debug purposes
- a virtual COM Port interface via UART
- it supports Mass Storage Device programming

Moreover, also additional features particularly related with low power applications are present. In fact this board allows to use different kinds of power supplies besides the USB: an external power supply and a coin cell battery, both shown in Figure 7.1 and 7.2. Those can be used to make specific tests of consumption or emulate real situations. For example test the application sweeping the voltage of the power supply or experience the effect of a natural battery discharge. In addition the alternative power supply are used to make current consumption measurements as explained in the next paragraph.

This board allows to measure the chip power consumption, when is not USB alimented, using the *nRF current* pins (Port 22) indicated in Figure 7.1. Is possible to measure the current consumed by the chip either directly with a multimeter or indirectly by measuring the voltage drop on a 10 *Ohm* resistance that has to be soldered in a specific place on the board. The two configurations are shown in the Figures 7.3 and 7.4. The direct current consumption configuration is useful to estimate the average current consumption of the chip, but if a very accurate estimation of current in the unit of μA range is needed, other methods has to

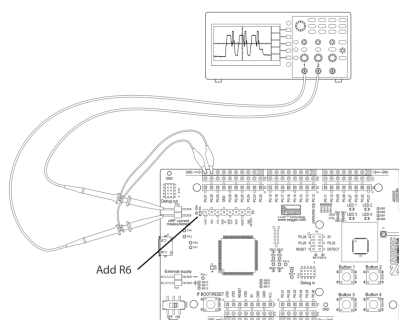


Figure 7.4: Current consumption measurement with oscilloscope

be employed. The indirect measurement through an oscilloscope is more useful to measure the instantaneous value of the current, but again, if a precise estimation is needed other methods need to be used. This is due to the fact that the oscilloscope measurements can have a superimposed offset value comparable or even bigger than the value measured across the resistance in series with the power supply. This can bring to bigger errors in the calculation of the value of a current in the μA range.

Software Tools

As anticipated before, the software tools used during the development can make the programming work more comfortable and fast. The presence of a debug interface to insert breakpoints and run the code step-by-step eases and fastens the debugging procedure.

There are not freeware programs that provide those functionalities, but if completely freeware software is needed other options are available. The first is a fast-to-set-up tool-chain that, on the contrary, does not provide debugging features. The second is a little more complex configuration but allows debugging, code completion, and program flashing in one solution.

First option The Nordic Libraries, and additional software written with them, can be compiled with the GNU Cross-Compiler (GCC) toolchain for ARM Cortex-M processors. The flashing phase can be made using a specific command-line tool provided by Nordic Semiconductor, the nRF5x-Command-Line-Tools, available for Linux, Windows, and MacOS.

Second option All the tools mentioned for the first alternative, plus the SEGGER J-Link debugger, can be used within Eclipse that is a freeware IDE that supports a wide variety of languages and third-party tools. The programming environment can be set up following the guide <https://devzone.nordicsemi.com/tutorials/b/getting-started/posts/development-with-gcc-and-eclipse>.

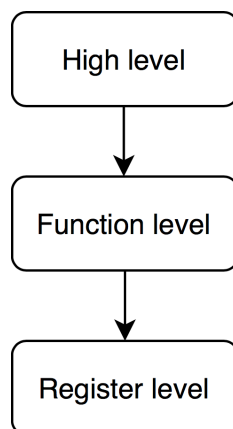


Figure 7.5

7.3 Developed libraries

The micro-controller needs to communicate with several external devices, using different kind of interfaces. Moreover every device works in a different way and provide a different set of functions. For example the temperature and humidity sensor communicates via I2C while the other components uses the SPI protocol. Thus is necessary to provide a way to easily communicate with each of this devices with both an high and low level of abstraction, in order to ease the steps of components test and final firmware writing. The solution adopted consist of several code modules for each components that represents the different levels of abstractions.

A representation of the general description of the code written for each component is provided in the Flow chart 7.5. As it can be seen from the graph the number of levels are three, the arrows represent the fact that a given module use the module indicated by the arrow. For example the function-level module uses inside it the register level-module.

- a register-level that include a virtual representation of the registers present in the device and all the values that they can assume.
- a function-level in which a set of function is provided that mirrors the functions that each component is capable to provide. This will be further explained with the aid of the written code.
- an high-level in which are present all the functions that are directly used inside the final firmware.

Another advantage of the provided solution is that the code is almost reusable in other projects. If the same micro-controller is employed both the register-level and the function-level can be used without modifications. If another kind of micro-controller is used the register-level can be re-used without modifications and the function-level needs only a few. Specifically has only to be substituted the functions of the chip-specific SDK, for example those used to communicate over SPI.

In the section below are described the code modules for the ADC AD7799.

7.3.1 AD7799 Library

As previously said there are three abstraction levels. The explanation will begin from the lower level to the highest.

Register level

This ADC has 9 register of different width (in bit). There are read-write register to access specific ADC functions or configure the component, and read-only registers in which the result of conversions and other data are stored. The code implementation of only the communication register is explained below. The other registers follows an analogous paradigm.

Communication Register Is the register used to communicate with the ADC. Every communication start with a writing of the specific value to this register that has the role to route the next part of the communication in the desired place. The register mask is shown below.

CR7	CR6	CR5	CR4	CR3	CR2	CR1	CR0
WEN(0)	R/W(0)	RS2(0)	RS1(0)	RS0(0)	CREAD(0)	0(0)	0(0)

The explanation of the function of each bit is not addressed because is not tightly related with the code paradigm adopted to write the library. Here the important point is that the register is composed by some fields and each of them has a specific function. As an example the field denoted by the letters *RS* identify the address of other registers inside the ADC.

In order to virtually mirror with a piece of code this register a `struct` is declared taking advantage of `bit fields` that permits to specify, for each variable that composes the `struct`, its length in bit. The code is reported below

```

1     typedef struct {
2         uint8_t write_enable_neg :    1;  //MSB
3         uint8_t read :                1;
4         uint8_t register_address :    3;
5         uint8_t continuous_read :    1;  //LSB
6         //two low bits
7     } communication_register;

```

This approach permits either to save memory and to avoid that a given register be loaded with a value that exceed its length when the code is written, because in that case the compiler will throw an error.

Every field of the register has a possible set of values that can assume. Those values can identify different things. For example, has already said, a specific value written in the *RS* identify a register. To avoid the memorization of each of this values by the programmer a set of constants are declared, which names describe each specific value of the register. The code listing below, showing the constants declared for the *RS* (register select) field, will better clear the concept.

```

1     #define ...
        AD7799_REG_SELECT_COMM_REG_DURING_WRITE_OR_STATUS_REG_DURING_READ...

```

```

0
2  #define AD7799_REG_SELECT_MODE_REG          ...
           1
3  #define AD7799_REG_SELECT_CONFIGURATION_REG ...
           2
4  #define AD7799_REG_SELECT_DATA_REG         ...
           3
5  #define AD7799_REG_SELECT_ID_REG           ...
           4
6  #define AD7799_REG_SELECT_IO_REG           ...
           5
7  #define AD7799_REG_SELECT_OFFSET_REG       ...
           6
8  #define AD7799_REG_SELECT_FS_REG           ...
           7

```

Other fields of the **struct** does not need additional if they represent a true/false value, in that case is only necessary to simply write the number 1 or 0 in the corresponding field. An example of utilization is shown below

```

1  communication_register comm = {
2      0,
3      0,
4      AD7799_REG_SELECT_CONFIGURATION_REG,
5      0
6  };

```

Now the **struct** has to be serialized into a sequence of bits to be transmitted. This is done by mean of a specific function that take each part of the **struct** and properly serialize it into a variable capable to contain it. In this case 8 bit register are serialized into **uint8_t** variables. For 16 bit registers the corresponding type is used. The code below shows the function

```

1  uint8_t convert_COMMUNICATION_register(communication_register ...
           register_struct)
2  {
3      uint8_t result = (register_struct.write_enable_neg << 7) ...
           +
4      (register_struct.read << 6) +
5      (register_struct.register_address << 3) ...
           +
6      (register_struct.continuous_read << 2);
7      return result;
8  }

```

Once a message containing the value of a register is received from the component could be useful to re-translate it to the corresponding **struct**, to easily manipulate it.

```

1  communication_register interpret_COMMUNICATION_register(uint8_t ...
           register_value)
2  {
3      communication_register result;

```

```

4     result.write_enable_neg = (register.value >> 7) & 1U;
5     result.read = (register.value >> 6) & 1U;
6     result.register_address = (register.value >> 3) & 7;
7     result.continuous_read = (register.value >> 2) & 1U;
8
9     return result;
10 }
    
```

The last step performs a not mandatory but useful function. Once a message containing the value of a register is received from the component could be useful to re-translate it to the corresponding `struct` and then print it.

```

1 {
2     void print_STATUS_register_struct(status_register ...
3         register_struct)
4         uint8_t rdy_neg = register_struct.rdy_neg;
5         uint8_t error = register_struct.error;
6         uint8_t no_ref = register_struct.no_ref;
7         uint8_t channel_selected = register_struct.channel_selected;
8
9         SEGGER_RTT_WriteString(0, "\nSTATUS register: ");
10        println_binary_8(convert_STATUS_register(register_struct));
11
12        SEGGER_RTT_printf(0, "Ready: %d\n", rdy_neg);
13        SEGGER_RTT_printf(0, "Error: %d\n", error);
14        SEGGER_RTT_printf(0, "Reference missing: %d (meaningful only ...
15            if reference detection is active)\n", no_ref);
16        SEGGER_RTT_WriteString(0, "Channel: ");
17        switch (channel_selected) {
18            case AD7799_CHANNEL_1:
19                SEGGER_RTT_WriteString(0, "AD7799_CHANNEL_1");
20                break;
21            case AD7799_CHANNEL_2:
22                SEGGER_RTT_WriteString(0, "AD7799_CHANNEL_2");
23                break;
24            case AD7799_CHANNEL_3:
25                SEGGER_RTT_WriteString(0, "AD7799_CHANNEL_3");
26                break;
27            default:
28                SEGGER_RTT_WriteString(0, "Code not present");
29                break;
30        }
31        SEGGER_RTT_WriteString(0, "\n");
32    }
    
```

The same work was done for all the registers present in the components.

Function level

This level includes the functions that, using the register-level code module, implement, by mean of the SPI protocol:

- the writing to specific on-chip registers using the `struct` representation provided by the register-level code module

- the reading from specific on chip-registers and translation to the corresponding **struct**

As an example the functions that permits to read and write the configuration register are reported below. In this case the value of the communication register is the same for both the functions, except for the bit that indicates the write or read operation.

- Write

The writing method accepts as input parameters both a pointer to the SPI driver and the **configuration_register struct** to be written

```

1         void AD7799_write_CONFIGURATION_register(...
           nrf_drv_spi_t const *const driver_instance_ptr,...
           configuration_register register_struct)
2     {
3         communication_register comm = {
4             0,
5             0,
6             AD7799_REG_SELECT_CONFIGURATION_REG,
7             0
8         };
9
10        uint8_t tx1 = convert_COMMUNICATION_register(...
           comm);
11
12        uint16_t tx_mode = ...
           convert_CONFIGURATION_register(...
           register_struct);
13        uint8_t tx[] = { (tx_mode >> 8) & 255 , tx_mode...
           & 255 };
14
15
16        nrf_drv_gpiote_out_clear(AD7799_CS);
17
18        uint32_t error_code;
19
20        error_code = spi_non_blocking_transfer( ...
           driver_instance_ptr,
21
22
23
24
25
26
27        #if ERROR_PRINT
           error_handler(error_code, "AD write comm");
28        #else
29        APP_ERROR_CHECK(error_code);
30        #endif
31
32        error_code = spi_non_blocking_transfer( ...
           driver_instance_ptr,
33
34
           tx,
           2,

```

```

35                                     NULL,
36                                     0);
37
38     #if ERROR_PRINT
39     error_handler(error_code, "AD write conf");
40     #else
41     APP_ERROR_CHECK(error_code);
42     #endif
43
44     nrf_drv_gpiote_out_set(AD7799_CS);
45 }

```

- Read

The reading method accept as input parameter the pointer to the SPI driver and return the `configuration_register` struct derived from the reading process

```

1     configuration_register ...
2     AD7799_read_CONFIGURATION_register(nrf_drv_spi_t ...
3     const *const driver_instance_ptr)
4     {
5         communication_register comm = {
6             0,
7             1,
8             AD7799_REG_SELECT_CONFIGURATION_REG,
9             0
10        };
11
12        uint8_t tx1 = convert_COMMUNICATION_register(comm);
13        uint8_t rx_buffer[2];
14        uint32_t error_code;
15
16        nrf_drv_gpiote_out_clear(AD7799_CS);
17        error_code = spi_non_blocking_transfer( ...
18            driver_instance_ptr,
19
20            &tx1,
21            1,
22            NULL,
23            0);
24
25        #if ERROR_PRINT
26        error_handler(error_code, "AD write comm");
27        #else
28        APP_ERROR_CHECK(error_code);
29        #endif
30
31        error_code = spi_non_blocking_transfer( ...
32            driver_instance_ptr,
33
34            NULL,
35            0,
36            rx_buffer,
37            2);
38
39        #if ERROR_PRINT

```

```

34         error_handler(error_code, "AD read conf");
35         #else
36         APP_ERROR_CHECK(error_code);
37         #endif
38
39         nrf_drv_gpiote_out_set(AD7799_CS);
40
41         return interpret_CONFIGURATION_register((rx_buffer...
42         [0] << 8) + rx_buffer[1]);
    }

```

High level

The high-level functions uses the other two levels to implement complete procedures that are used in the final firmware of the micro-controller. Below is reported the code that configures a given channel of the AD7799 and performs both the offset and the full-scale calibrations. The function returns 1 in case of error and 0 when the configuration is completed.

```

1  int AD7799_configure_channel(int channel_num)
2  {
3
4      configuration_register conf = {
5          0,
6          1,
7          AD7799_CONF_GAIN_1,
8          0,
9          1,
10         AD7799_CHANNEL_1
11     };
12
13     if (channel_num == 1)
14     {
15         conf.channel = AD7799_CHANNEL_1;
16     }
17     else if( channel_num == 2)
18     {
19         conf.channel = AD7799_CHANNEL_2;
20     }
21     else if(channel_num == 3)
22     {
23         conf.channel = AD7799_CHANNEL_3;
24     }
25     else
26     {
27         #if DEBUG_ENABLED
28         SEGGER_RTT_printf(0, "Parameter not valid\n");
29         #endif
30
31         return 1;
32     }
33
34     uint8_t write_conf_attempt = 0;

```

```

35
36 configuration_register_written_conf = ...
37     AD7799_read_CONFIGURATION_register(&driver_spi_0);
38 while ( written_conf.buffer           != conf.buffer ||
39         written_conf.burnout_current_enable != conf....
40         burnout_current_enable ||
41         written_conf.channel           != conf.channel ||
42         written_conf.gain              != conf.gain ||
43         written_conf.reference_detection != conf....
44         reference_detection ||
45         written_conf.unipolar          != conf.unipolar )
46 {
47     if (write_conf_attempt ≥ WRITE_CONF_MAX_ATTEMPT)
48     {
49         AD7799_reset(&driver_spi_0);
50     }
51     #if DEBUG_ENABLED
52     SEGGER_RTT_printf(0, "Configuration not right: writing conf\...
53         n");
54     #endif
55     AD7799_write_CONFIGURATION_register(&driver_spi_0, conf);
56     written_conf = AD7799_read_CONFIGURATION_register(&...
57         driver_spi_0);
58     write_conf_attempt++;
59 }
60
61 //OFFSET CALIBRATION
62 mode_register mode_off_calib = {
63     .filter_update_rate = AD7799_FILTER_UPDATE_RATE_10_HZ,
64     .mode = AD7799_MODE_INTERNAL_OFFSET_CALIB,
65     .power_switch = 0
66 };
67
68 AD7799_write_MODE_register_w_interrupt (&driver_spi_0, ...
69     mode_off_calib);
70
71 //FULL-SCALE CALIBRATION
72 mode_register mode_fs_calib = {
73     .filter_update_rate = AD7799_FILTER_UPDATE_RATE_10_HZ,
74     .mode = AD7799_MODE_INTERNAL_FS_CALIB,
75     .power_switch = 0
76 };
77
78 AD7799_write_MODE_register_w_interrupt (&driver_spi_0, ...
79     mode_fs_calib);
80
81 return 0;
82 }

```

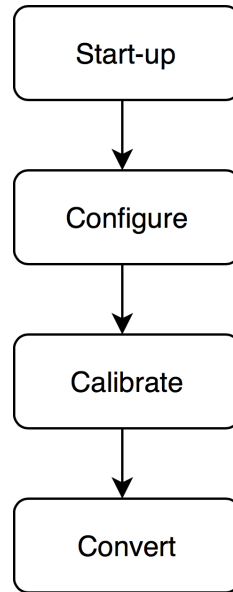


Figure 7.6

7.3.2 AD7799 Functioning

The AD converter, used to measure the voltage of different points of the circuit, needs to be used only in precise and as brief as possible moments, due to its consistent power consumption respect to the other components ($\sim 500 \mu A$ at maximum). Nevertheless precision and accuracy has to be maintained. Each decided measurement point needs to be sampled multiple times sequentially to subsequently operate an averaging of the measurements in order to lower the superimposed random noise. Hence the process that brings to obtain a single averaged measurement needs to follow several steps, shown in the Flow chart 7.6.

Start-up The AD7799 remains in power-down mode for long periods to preserve battery power. The possible consequence of this long sleep period is that the internal state of the registers can randomly change, bringing the ADC in an undetermined state. For this reason, when a measurement needs to be taken, the converter is first powered-up and resetted to its default state. This avoids that previous configurations influences the following operations, because if the state of the component is not well determinate the effect of the commands given to it cannot be determined. After this initial operation the component can be configured to perform the desired work.

Configuration Once the ADC is correctly powered up is necessary to configure it writing in the appropriate way its configuration register. A wrong configuration can bring to un-consistent readings that can influence the correctness of the data. For this reason, after a configuration is written, it is next read and compared to the desired one. If they result to be equal the reading process can continue. If not,

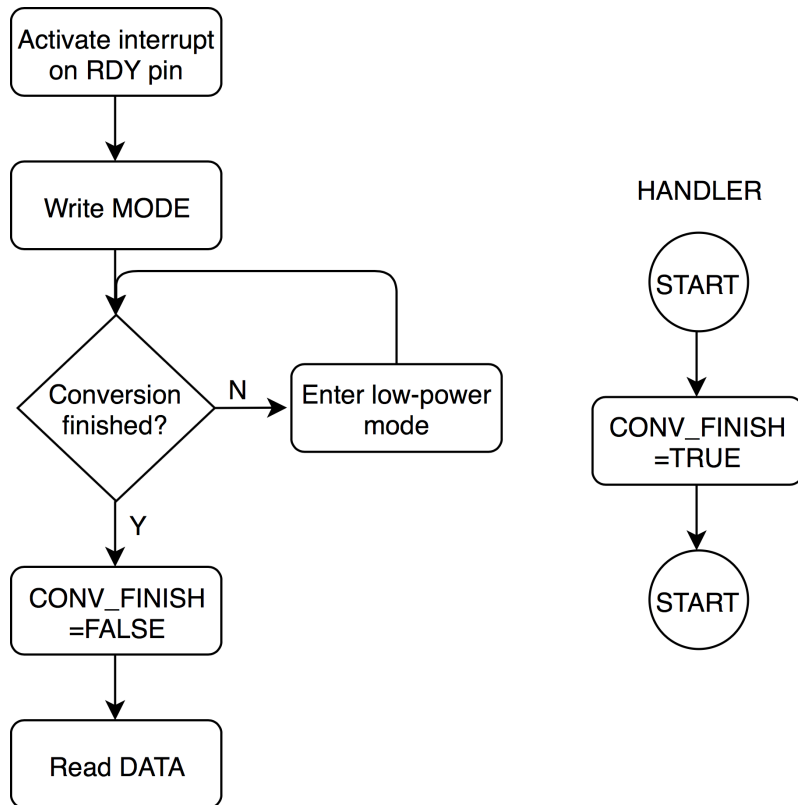


Figure 7.7

another writing attempt is performed and next the same check is executed. If the configuration writing fails a given number of times the reading process is re-started from the ADC reset.

Calibration The circuit operates in different temperature conditions, but is important to maintain its declared accuracy for the whole temperature range. The AD7799 offers the possibility reduce the temperature effect by calibrating the offset and the full-scale of each channel prior to take the readings. By the way these procedures require neither a negligible amount of time nor a small amount of power. In fact, each calibration take two conversion cycles to complete and consumes the same power of a measurement. Therefore the approach adopted consist of performing one offset and one full-scale calibration prior to make a set of measurements for a given point of the circuit, in order to diminish the time and the power that the converter needs.

Conversion After the calibration phase the real measurements can finally be taken. The points that needs to be sampled, especially the output voltage, carry a superimposed random noise, which RMS value vary from sensor to sensor. For example, in the case of the SO_2 sensor, is in the order of 30 *ppb*. Thanks to the fact that this source of error is random, it can be reduced with an averaging process.

Thus, each channel measurement consists of several readings that are subsequently averaged. The number of readings for each channel can be different depending on the RMS value of the noise, or can even be single.

Each reading begins with the writing of the *read* command to the *mode* register of the ADC. Then, each reading take some time to complete, depending on the selected filtering frequency. Due to the fact that this application do not require fast readings, the lower frequency filter has been selected, making the conversion to last more than 250 *ms*. On the contrary this enlarges the conversion time, making the busy wait of the conversion an extremely power consuming approach. Therefore an interrupt driven procedure has been implemented. This permits to drive the chip in low-power mode while the conversion is taking place and make it to be woken-up by the interrupt once the conversion is finished and the result can be read. The AD7799 allow such kind of implementation because, when it receives the conversion command, the \overline{RDY} pin remains high, indicating that the conversion is taking place. When the conversion finished the ADC drive this pin low, signaling the conversion is finished. Thus the described procedure can be implemented activating an interrupt on the trailing edge of the \overline{RDY} . The interrupt can be either activated before and after that the *read* command is sent the the ADC, but activating it just before the communication allow the chip to go to sleep as soon as possible and ensures that the event that would triggers the interrupt does not happen before interrupt activation. In this case, of long conversion time, due to the low frequency filter selection, it is difficult that such a thing would happen, but using higher filtering frequencies would bring the conversion time in the same order of magnitude of the activation time of the interrupt, making useful the employment of this technique. It is worth to mention that for fast conversions an interrupt driven approach cannot be crucial, but usually it permits to save some power. A representation of the phase is shown in the Flow chart 7.7.

Each step described above is detailed in the flow chart shown in Figure 7.8.

Low-power mode It can be noticed from the flow chart shown in Figure 7.8 that the low power mode is accessed inside a cycle. This method is employed because the execution of the function needs to continue, exiting the cycle, only when the specific interrupt that was set before is triggered. The reason is that when the low power mode is entered, the chip could be woken-up by any event. Therefore, if the low power command is not surrounded with a cycle, a different event from the one of interest can make the method execution to continue. In such a case the result would be a premature reading of the data register that would not contain the right information. Surrounding the instruction with a cycle ensure that, even if the chip wakes-up because another event needs to be executed, the low power mode is immediately re-entered. When the event of interest wakes-up the chip, it has to be guaranteed that the low-power instruction is no more executed. This behaviour can be provided setting properly the exit condition of the 'low power cycle'. If only one event determines the function resuming, the exit condition can be the control of a single *flag*, if multiple event needs to happen in a specified configuration the exit condition can be a Boolean expression that mirrors the configuration. When the condition is properly set is needed to provide a way to properly set the flag

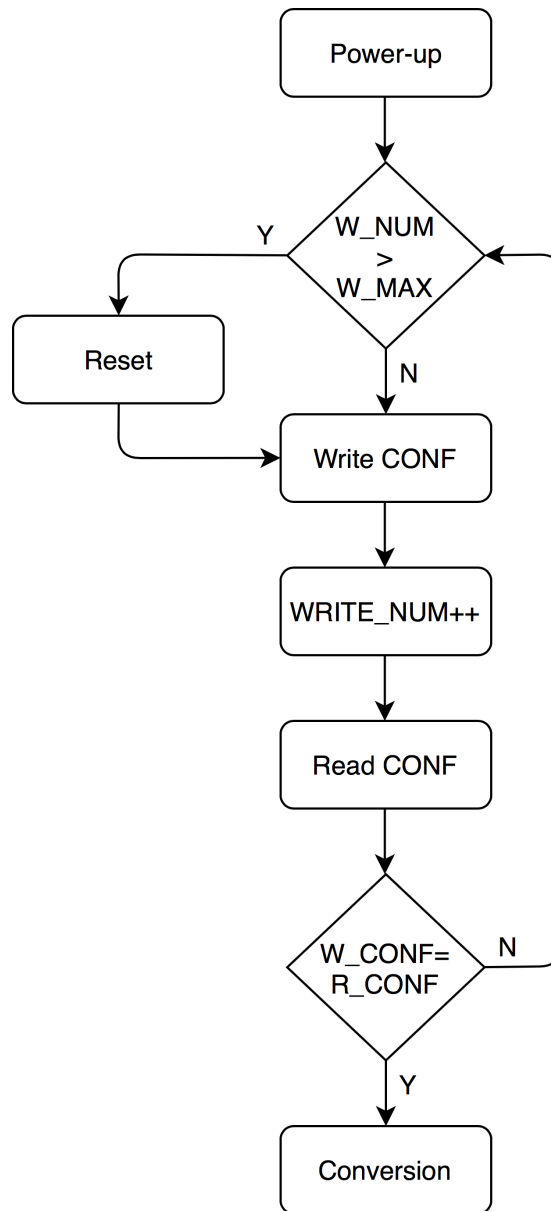


Figure 7.8

when the specific interrupt is triggered. This can be done inside the event handler, that, when called, has only to set the flag to the proper value. When such kind of approach is used is important to maintain the execution of the handler as brief as possible, this ensures that the corresponding flag is quickly set when the interrupt is triggered, because a long handler execution could prejudice the effective moment of wake-up. This can bring to an unwanted additional execution of the low-power method that can happen while the handler is executing.

7.4 Firmware

Every sensing node needs to be provided with a micro-controller that gathers and transmits the measurements together with the contextual alarms. The system-on-chip used for this application is the nRF51 from Nordic Semiconductor, already used in some of the working nodes. The principal motivation for this choice derives from the presence on the chip of a Bluetooth LE module. In addition its low power architecture permits an average current consumption in the order of unit of micro-ampere even when the wireless radio transmits at regular intervals.

The nRF51 is used both to control the conditioning circuit by mean of the DA converter, that sets the value of V_{ref1} and V_{ref2} and measure the quantity of interest by mean of the AD converter. Overall the chip has to be programmed to wake-up form sleep mode at regular intervals, perform the measurements and return to sleep for a long period. When it transmits the measurements, every few seconds, it wakes-up for a brief period of time. The whole operation procedure of the nRF51 will be addressed in the next sections, but first, for simplicity, the trigger conditions of alarms and warings will be described.

7.4.1 Alarms and warings

Identifying harmful conditions for humans caused by toxic gases imply the knowledge of the different illnesses caused by different exposition times to given quantities of toxic substance. This information can be expressed for example in terms of maximum exposure time to a given gas concentration. In this way the user, if a detected concentration of gas is potentially harmful, can be informed of the maximum time for which he/she can be exposed without reporting any damage. In order to employ this method is necessary to find an accountable source of information that has already performed several test with a wide variety of target analyses and therefore can provide reliable information on this field. Different organizations are employed on the environmental health in working areas. The American Conference of Governmental Industrial Hygienists (ACGIH) publish every year the Threshold Limit Value (TLV) for a wide variety of gases. The threshold values present in the annual publication of the TLV are

- Time Weighted Average (TWA)
Identify the maximum concentration to an 8 hour exposition time to which every worker can be exposed every day

- Short Term Exposure Limit (STEL)
Identify the maximum concentration for a 15 minutes exposition time
- CEILING
Identify the concentration to which every worker can be never exposed
- Immediately Dangerous to Life or Health (IDLH)
Identify the concentration that can immediately cause death or permanent damage

This threshold values can be used to inform the user of a potentially harmful situation. Furthermore the electrochemical amperometric sensors have a maximum temperature and humidity range that can potentially provide a permanent damage to the sensor. Thus, in addition to this kind of alarms is also necessary to implement a way to inform the user on the state of the gas sensor, in order to be sure that it is able to provide consistent and trustable readings.

Therefore the measurement system has to generate alarms either when the sensor is not correctly working or when a environmental harmful condition for humans is detected. Both are listed in the tables below, together with their triggering condition. For example, the alarm TWA is triggered when the gas concentration exceed a given value, specific for each type of gas.

Environment related alarms

Alarm	Triggering condition
TWA	$G > TWA_{th}$
STEL	$G > STEL_{th}$
CEILING	$G > CEILING_{th}$
IDLH	$G > IDLH_{th}$

where G identify the gas concentration measured in part-per-million.

Gas sensor alarms

Alarm	Triggering condition
Temp. out of range	$T[^\circ\text{C}] \notin [T_{GasSensor_{min}}, T_{GasSensor_{MAX}}]$
RH out of range	$RH[\%] \notin [RH_{GasSensor_{min}}, RH_{GasSensor_{MAX}}]$
V_{bias} out of range	$V_{bias} \notin [V_{bias_{sensor}} - \epsilon, V_{bias_{sensor}} + \epsilon]$

All this alarms, when generated, have to be transmitted to the receiver that has the role of informing the users.

7.4.2 Firmware description

The description of the firmware will begin with the presentation of some macro-blocks that will be further splitted in more elementary pieces that represents basic operations.

The flow chart 7.9 shows all the macro-operations. When the circuit is powered for the first time the reference voltages are set to their sensor specific values, determining V_{bias} and V_{comm} , that will remain constant for the whole sensor life.

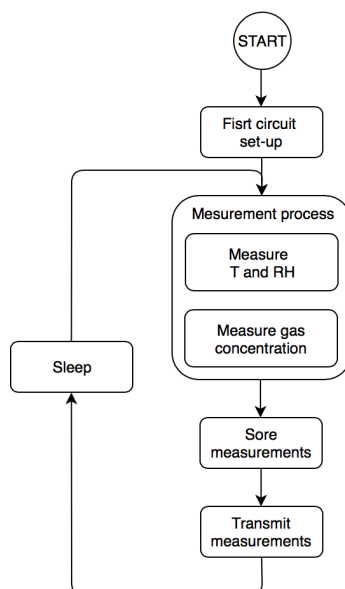


Figure 7.9: Flow chart representing a general overview of the firmware operations

After this initial procedure the chip is programmed to measure at regular intervals the environmental quantities of interest and go to sleep in the meanwhile. In each measuring phase, temperature, relative humidity and target gas concentration are retrieved from the specific sensors. After, a new transmission packet is built accordingly, containing both the measurements and, if necessary, the corresponding warnings.

Measurement phase

The flow chart 7.10 shows the measurement steps. First of all, the temperature and the relative humidity are measured, then, if those values are inside the a certain range, the gas measurement is performed. The reason is that every amperometric gas sensor is highly sensitive to variations of temperature and humidity and, in some conditions already described in the theoretical section, can be useless to read the gas concentration from the sensor. Thus is better to know in advance those values to avoid useless measurements that would represent a waste of battery power. The conditions that determine the sensor's readings invalidity are listed in Table 7.4.1, in which are also reported the corresponding warnings and alarms the are triggered in each case. Those conditions were also described in the theoretical section which explain the vulnerabilities of this kind of sensors.

If the environmental condition are appropriate, a final check of the sensor status is operated. The bias voltage V_{bias} is measured because it has to be equal to the nominal bias for the specific sensor, plus a tolerance ϵ . If also this test is passed the gas concentration measurement takes place, if not it is skipped and the corresponding warning is set.

Every gas measurement involves an averaging process, described below. In the circuit design phase it has been decided to measure both the output voltage V_o and V_{ref1} , which represents an offset for V_o . Due to the fact that each of this

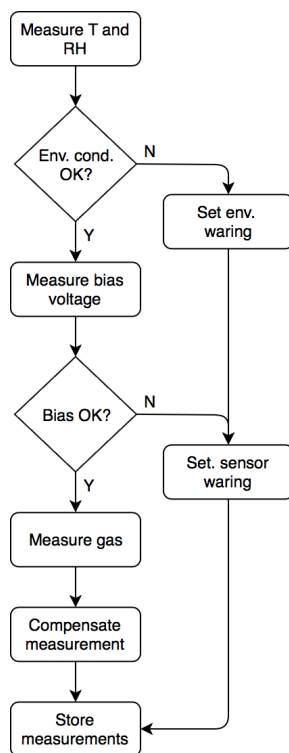


Figure 7.10: Flow chart representing the measurement process

measurements can not be taken in the very same moment, it has been decided to acquire a given number of measurements for each of this two points and then subtract the average values. The number of acquisitions taken for each of these two points can be modified in the chip programming phase.

Finally, the value retrieved from this procedure is compensated (as the flow chart 7.10 shows) to balance the effects of temperature. The compensation functions will be described in Chapter 8.

All the measurements performed in the measurement phase (Measurement phase block of Flow chart 7.9), are stored inside the flash memory of the nRF51 in order to be written in the transmission packet that is sent to the receiver.

Transmission packet building

During this phase the transmission packet has to be built with all the useful information retrieved during the measurement phase. After that the packet needs to be passed to the Bluetooth stack in order to be transmitted.

Size of the data

Data transmission over Bluetooth LE can be operated in different ways, depending on the throughput required. To precisely estimate this value is necessary to make detailed list of the information size that every sensing node has to provide and the frequency at which it is produced. For example, every numerical measured value can

occupy a different number of bit depending on its type. In this case the standard data types of C programming language are used, for which the size, in bit, is listed below

Data type	Size [bit]
<code>bool</code>	1
<code>uint8_t</code>	8
<code>uint16_t</code>	16
<code>int8_t</code>	8
<code>int16_t</code>	16
<code>float</code>	32

Transmission strategy

First of all a general distinction needs to be made about the state of a sensing node and the information that has to produce accordingly. A node can either correctly work or can be in a state in which its internal gas sensor is not able to produce consistent readings. If the sensor is correctly working, only the value of the environmental quantities has to be transmitted, together with the corresponding alarms. In the case of not working sensor is not necessary to transmit the gas concentration, because in that case would not be correct. Instead would be useful to transmit the other to environmental quantities together with an information that can help to identify the malfunction, as for example the values of the reference voltages, V_{ref1} and V_{ref2} , the output voltage V_o . Therefore the transmitted data in case of correct working are different from those sent when the internal amperometric sensor cannot provide correct readings, and this information needs to be included as first in the transmitted data. In addition these two transmission modes needs to both include also Sensor ID and a field that would permit to identify the type of target gas. In the Tables 7.1 and 7.2 are listed all the data, readings, warings and alarms, that needs to be sent in both cases together with the data type and the size in bit, useful to make an estimation of the throughput required by the transmission. The information that identify the type of the transmission, for correctly working node and for a sensor health waring, can be codified in a single bit, therefore a `bool` variable can be used in this case. For the variables representing environmental quantities, as gas concentration, temperature and relative humidity, it is necessary to use a representation that allows up to two decimal figures, that needs to be signed in the case of the temperature. In such a case the `uint16_t` and `int16_t` standard types have been used for the unsigned and signed quantities respectively that have been appropriately multiplied before transmission and divided after reception. For the variables representing voltage values it is preferable to represent quantity up to a 0.1 *mV* resolution. Inside the system the voltage signals ranges from 0 to 3.3 *V*, therefore with a `uint16_t` is possible to achieve both the range and the resolution required. It has been chosen to codify the information on the gas type in 3 bit, allowing eight type of different gasses and the sensor ID in 5 bit, in this way these two information can be stored in a single byte . Finally the variables representing warings can be represented in only 1 bit with the `bool` type.

Correctly working node

Data	Data type	Size [bit]
transmission type	bool	1
gas type	uint8_t : 3	3
Waring TWA	bool	1
Waring STEL	bool	1
Waring CEILING	bool	1
Waring IDLH	bool	1
sensor ID	uint8_t : 5	5
temperature	int16_t	16
relative humidity	uint16_t	16
gas concentration	uint16_t	16
Total		61

Table 7.1

Internal sensor problem

Data	Data type	Size [bit]
transmission type	bool	1
gas type	uint8_t : 3	3
Waring RH over range	bool	1
Waring Temp over range	bool	1
Waring bias out of range	bool	1
sensor ID	uint8_t : 5	5
temperature	int16_t	16
relative humidity	uint16_t	16
V_{ref1}	uint16_t	16
V_{ref2}	uint16_t	16
V_{out}	uint16_t	16
Total		92

Table 7.2

From the tables 7.1 and 7.2 it can be seen that the maximum number of bits by which every useful information can be represented is 104. This represent the minimum number of bit to be considered when the transmission method have to be decided. The reason is that the nature of the transmission can need some additional information some problems to arise, thus is better to always have in place some extra bit.

Data transmission

The Bluetooth stack send every information by mean of packets. Each packet is composed of four parts, shown in Table 7.3. The PDU identify the type of the packet that can be either a data packet or an advertising packet.

Every node part of a BLE network constantly identify itself, at regular intervals,

Name	size [byte]
Preamble	1
Protocol Data Unit - PDU	2 to 257
Cyclic Redundancy Check - CRC	3

Table 7.3: Bluetooth LE packet composition

sending an advertising packet. Thus the first information that every device send through BLE is contained inside this packet. If a connection is needed between two devices, after the advertising packet other data packets are exchanged. This imply that the least power consuming way to transmit data with this technology is through advertising mode, because it implies the transmission of a single packet.

The PDU of an advertising packet is formed by two parts, a 16 bit *header* and a variable size payload. The size of the payload depends on the *type* of advertising, and goes from 6 to 37 bytes. In order to transmit all the information within one packet at least $\lceil 163/8 \rceil = 21$ *byte* are required, that are available using the advertising mode. Hence it has been decided to take advantage of the advertising payload to transmit the data produced by the system. A further description of the advertising mode will follow, explaining all the implementation details.

The payload usually contains information about the device, specifically its Bluetooth related characteristics, such as the services offered via Bluetooth. According to the Bluetooth standards, each data present in the payload has to be preceded by two bytes that identifies the length of the data and its Advertising Data (AD) type. The standard AD types available are listed in the Bluetooth website. In the case of custom advertising data containing application specific information, like the data that are sent by the sensing nodes, the Manufacturer Specific Data AD type, $0xFF$, should be used.

The transmission packet composition used in this case is shown below

Byte number	0	1	2	...	31
Data	$0xFE$	$0xFF$	X	...	X
	Length	AD type	Tx data		

where the whole payload is used to transmit the data gathered at each measurement phase. In fact the byte at index 0 identify the length of the whole payload, equal to 31 (bytes) that in hexadecimal is $0xFE$. The next byte, at index 1, is set to the AD type corresponding to Manufacturer Specific Data. The remaining part will host the data to be transmitted.

Data reception

The data reception phase needs to guarantee that the data transmitted by alle the peripheral nodes is entirely received by the central node of the network. To comprehend all the critical aspects that characterize the reception a brief explanation of how the Bluetooth stack behaves in this phase is needed.

The packet transmission of a node in a Bluetooth network takes place in 40 channels in the $2.4000\text{ GHz} \div 2.4835\text{ GHz}$ frequency band. Every channel is spaced 2 MHz and the channel at lower frequency is the 37 at 2402 MHz . The advertising packets use three of these forty channels, the 37, 38 and 39 respectively at the frequencies 2402 MHz , 2426 MHz and 2480 MHz . Thus every Bluetooth device that transmits advertising packets transmits the same data in these three frequency bands.

A receiver needs to be set on the same channel in the same moment in order to gather the data and the big number of channels used by the Bluetooth physical layer can make the probability of this event very low in some conditions. Thus, if a reception probability near to 100 % has to be ensured by the communication, the number of times that the very same packet is sent by the transmitted N_{TX} has to be augmented by consequence.

In the specific use-case of peripheral node that is constantly advertising two solutions can be adopted, depending on the system constraints. If a minimum given advertising frequency is specified, for example for power dissipation constraints, is necessary to increase the time for which a packet containing the same information is transmitted to increase N_{TX} . On the contrary, if the constraint is the total advertising time, the advertising frequency needs to be incremented to increase N_{TX} . Considering the case of the gas sensor node advertising its data with a period of 3 seconds and a total advertising period of 1 minute, $N_{TX} = 60/3 = 30$, that is a number that guarantees the packet reception. Anyway a try and error procedure is needed in the specific operative condition of the whole network because other influencing factors not addressed here can be present.

Another possible requirement of the system is the portability of the reception software due to the fact that different receivers can use different operating systems. Different languages provide libraries to receive data over Bluetooth. One of the most portable and easy to implement approaches is provided by the Noble[39], a Node.js library, which was used in this case.

Data packet composition

It is necessary to find an efficient way of inserting all the necessary information into the available space. Two techniques can be adopted. The first consists of writing the data in ASCII format, in order to make a free-to-air transmission. The second consists of serializing the data in a byte array. The first transmission technique limits the information that can be transmitted with the same space, because it consists of ASCII characters, but has the advantage that it is immediately understandable. The second technique permits the transmission of much more information in the same space, but needs to be de-serialized when received. It is possible to alternate these two kinds of transmission techniques to take advantage of both.

The packet composition, in the two cases, is described below.

Free-to-air transmission

When using the free to air transmission is not possible to insert all the information listed in tables 7.1 and 7.2. If the gas sensor is working correctly the three funda-

mental measured quantities are printed in the advertising payload by mean of the function `sprintf`

```

1     uint8_t transmission_packet[29];
2     ...
3     char packet[] = "T=%u%3.0f C RH=%2.0f%% SO2=%2.2fppm";
4     sprintf( (char*) transmission_packet, packet, 0b00000001, ...
              current_temperature, current_RH, current_ppm_value);

```

Where in the first byte is codified the information that identify the type of transmission, a "1" in the first bit of the byte, resulting in the advertising packet:

1T=25°C RH=55% SO2=0.0ppm

in which can be noticed the presence of the transmission identification bit in the first character. In case of an activation of an alarm the free-to-air version of the advertising payload has to be changed to clearly represent the dangerous situation. For this reason, according to the alarm, the payload will be modified accordingly. Below is present one example for each situation.

In case of alarms regarding the value of the gas concentration

- Waring Time Weighted Average (TWA) in case of sulfur dioxide (SO_2) sensor
1WARING TWA 2.5 ppm of SO2
- Waring Short Term Exposure Limit (STEL) in case of sulfur dioxide (SO_2) sensor
1WARING STEL 5.2 ppm of SO2
- Alarm Ceiling in case of nitrogen dioxide (NO_2) sensor
1ALARM CEILING 6.0 ppm of NO2
- Alarm Immediately Dangerous to Life or Health (IDLH) in case of nitrogen dioxide (NO_2) sensor
1ALARM IDLH 21.1 ppm of NO2

In case of alarms that identify a sensor malfunction

- Waring for temperature outside range
1WARING SENSOR TEMP T=52°C
- Waring for humidity outside range
1WARING SENSOR HUMIDITY RH=80%
- Waring for bias voltage outside range
1WARING SENSOR BIAS

Serialized transmission

The serialization method allows the transmission of much more information at once. When this technique is employed the functions to serialize before sending and de-serialize after receiving the data need to be written.

Again the packet is built into two different ways depending on the situation of the

node. The information encoded into the payload mirrors the tables 7.1 and 7.2 to which is added one bit to distinguish the serialized transmission from the free-to-air. The composition of each data packet is described below. The first row of the tables indicates the information stored while the second indicates the byte index unless otherwise stated.

Correctly working node

9	0xFF	T_{TX} + W	ID + T_{gas}	Temp		RH		G	
0	1	2	3	4	5	6	7	8	9

The composition of the byte at position 2 is shown below

Byte 2 expansion

free-to-air	TX type	0	0	TWA	STEL	CEIL.	IDLH
0	1	2	3	4	5	6	7

bit number

The composition of the byte at position 3 is shown below

Byte 3 expansion

Sensor ID	gas type
0 to 4	5 to 7

bit number

Gas sensor health warning

13	0xFF	T_{TX} + W	ID+ T_{gas}	Temp		RH		V_{ref1}		V_{ref2}		V_o	
0	1	2	3	4	5	6	7	8	9	10	11	12	13

The composition of the byte at position 2 is shown below

Byte 2 expansion

free-to-air	TX type	0	0	0	RH warning	Temp. warning	Bias warning
0	1	2	3	4	5	6	7

bit number

The byte at position 2 is the same as before.

De-serialization

The reception of the packets is made using a Node.js script using the Noble module for the Bluetooth communication and methods

`readUInt16LE(byte_position)`

`readInt16LE(byte_position)`

`readUInt8(byte_position)` etc.

of the Buffer class for the de-serialization procedure.

Measurements storing

The measurements should be stored on a flash memory capable of containing all the information produced during the entire life of the system. Considering the tables 7.1 and 7.2 the system produces 13 *bytes* per reading at maximum. If the sampling rate is 1 *min*, $N_{measure} = 525600$ for one year. Therefore the minimum size of the memory should be of 7 *Mbyte*, hence a 8 *Mbyte* memory should be used. It is possible to reduce that amount of data considering that the useful information that the node should store are only the readings of temperature, humidity and gas concentration, requiring therefore 6 *bytes* per reading, that would bring the memory size to ~ 3.2 *Mbyte* permitting to use a 4 *Mbyte* memory.

The memory to be used in the measurement system is a serial NOR flash memory with SPI interface from Windbond that has different available sizes, from 512 *MByte* to 512 *kByte*. The programming part of the SPI communication with the memory is not addressed in this work because the required libraries were already available from the implementation of the other sensing nodes of the network.

Chapter 8

Experimental results

The system verification has to include several steps, from the verification of its accuracy in different conditions to its power consumption, that, above all, is the more stringent requirement. More in detail the system specifications compliance involves

- evaluation of the accuracy of the output voltage. During this is evaluated the uncertainty of the output voltage using methods of class A.
- robustness and accuracy preservation under variation of the power supply V_{PS} voltage, down to a minimum value of V_{PS} .
The functioning down to a minimum V_{PS} value requirement derives from the fact that the power source is a battery that naturally discharges. This brings to a constant decrease V_{PS} . Thus the circuit has to be capable of working when this happens.
- accuracy preservation under temperature variation, from 10 °C to 40 °C, with the employment of a software compensation algorithm.
- calculation of the average current consumption that needs to be in the order of tens of micro-ampere. This ensures a lifetime of at least one year if the system is powered with a battery of small volume.

All the tests that aims to evaluate the measurement system accuracy have been made using the SO_2 sensor, while for the power consumption test the H_2S sensor was used.

8.1 Power consumption

The measurement of the average current consumption is a critical step because it needs to be as accurate as possible, an error on its estimation directly translates in a wrong calculation of the battery duration time, that in this application is a crucial requirement. As explained in the previous sections the Nordic development kit is equipped with a port for this specific purpose, despite being an useful feature it does not permit accurate measurements in this case. The reason is that the nRF current

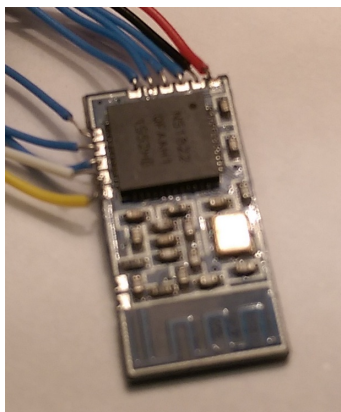


Figure 8.1: nRFBeacon

port measures only the system-on-chip power consumption, while here an accurate measurement of the whole system power consumption is needed.

Therefore is necessary to eliminate from the circuit all the exceeding parts that can fake the current consumption measurements, realizing a system that is as much as close as possible to the final product. The solution adopted consists of substituting the Nordic Development Kit with an nRFBeacon, shown in Figure 8.1. The beacon is a PCB on which are placed only the essential components useful for the application. The chosen beacon mounts the nRF51822 chip, a crystal oscillator, a 2.4 *GHz* transceiver and an printed antenna for Bluetooth transmission. Due to its minimal configuration the number of available pins for peripherals connection is limited, in fact the chosen beacon has only 11 pins, a V_{DD} pin and a GND pin. The number of interface pin with the chip required by the conditioning circuit are 7, thus the beacon is a valid option. The beacon is programmed via the Nordic Development Kit using the port 20, specific for programming shield mounted targets. Then is connected to the conditioning circuit to emulate a real system in the best possible way.

Different methods that uses different kind of instruments can be adopted, analogous to those of the Devopment Kit.

Current meter measurements Is possible to periodically sample the current consumed by the system putting a current meter in series with the power supply. This is a reliable method only if the current is almost constant, therefore can only be used to precisely measure the current consumption when the system is in some particular states, for example when the chip is in sleep-mode. But this approach neither permit to detect current consumption peaks nor the waveform of the current.

Indirect current measurements Another possibility consists of placing a small value resistor in series with the positive terminal of the power supply. The voltage drop across this resistor is then sampled with an oscilloscope. The acquired values then needs to be divided by the value of the resistance to calculate the current. This can be done making a differential measurement with two probe connected at the opposite sides of the resistance and then subtract the sampled values. This

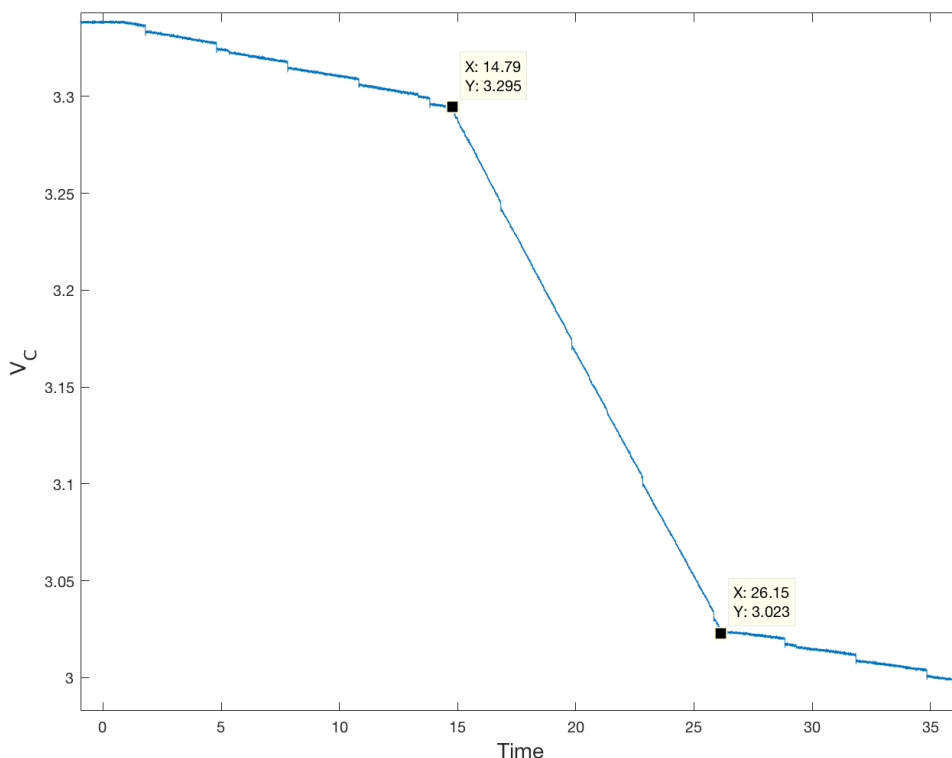


Figure 8.2: Voltage waveform vs. time of the discharge of the capacitance used to power the system. The two data-tips indicates the measurement phase, showing with X the corresponding time and with Y the corresponding voltage

method do not permit very accurate measurements that aim to calculate current consumption in the micro-ampere range because the sampled values are affected by an offset error, too big for this purpose.

To make a more precise calculation another method needs to be adopted, it is necessary to proceed with a hardware integration. A capacitor permits this physical integration process if used to power the system during a measurement phase, exploiting the fact that the charge needed for one measurement process is limited. Therefore observing the discharge of such capacitance the charge can be estimated using

$$Q_{meas} = C \cdot \Delta V \quad (8.1.1)$$

Considering a maximum raw estimation of 1 mA per reading $\sim 10 \text{ s}$, if the maximum wanted $\Delta V = 0.5 \text{ V}$ the needed capacitance would be

$$C = \frac{1 \text{ mA} \cdot 10 \text{ s}}{0.5 \text{ V}} = 5 \text{ mF} \quad (8.1.2)$$

Therefore three $2200 \mu\text{F}$ capacitors would permit to perform such kind of measurement. The measurement takes place putting in parallel those capacitors to the generator V_{PS} , that is alimenting the system, and measure the voltage across them.

Sleep period [<i>min</i>]	$\overline{I_{total}}$ [μA]	Battery capacity	Lifetime [<i>days</i>]
5	25	220 mAh	366
10	22.6	220 mAh	406
15	21.7	220 mAh	421

Table 8.1

Once that the capacitors are charged is possible to disconnect the generator and acquire the voltage waveform across them. The measurements taken are shown in Figure 8.2, where it can be noticed that when the system is measuring the voltage $V_C(t)$ has a steeper decrease respect to when the system is sleeping. Measuring the voltage drop resulting from a whole measurement process is possible to estimate precisely the total charge Q_{meas} needed by it. In Figure 8.2 are present two data-tips indicating the begin and the end of the measurement process. In this case the measurement phase can be observed to be from 3.29 V to 3.02 V, requiring a total charge of

$$Q_{meas} = C \cdot \Delta V = 6600 \mu F \cdot V = 6600 \mu F \cdot (3.295 V - 3.024 V) = 1.8 mC \quad (8.1.3)$$

Which results in an average current consumption calculated considering only the duration of the measurement phase, that is $\simeq 11.3 s$.

$$\overline{I_{measurement}} = \frac{1.8 mC}{11.3 s} = 160 \mu A \quad (8.1.4)$$

With the same method the sleep current is calculated.

$$\overline{I_{sleep}} = 6600 \mu F \frac{(3.338 V - 3.304 V)}{11.3} = 20 \mu A \quad (8.1.5)$$

The difference in the calculated values is that for the measurement phase, to calculate the final duration of the battery, is meaningful only the quantity of charge necessary, because it has a fixed duration in time. While for the sleep phase is better to calculate the average current because is a variable time-lasting state. Depending on the sleep period the average total current will be different. The calculations are reported in table 8.1, where $\overline{I_{total}}$ identify the total average current of the measurement and where the lifetime the estimated duration of the battery.

From this measurements is also possible to identify the charge needed by the system to send one advertising packet on each of the three designated radio channels. The Figure 8.3 shows the ΔV_C generated by the advertising, that yields

$$Q_{adv} = 26.4 \mu C \quad (8.1.6)$$

8.2 Output noise

During this test the output noise voltage is experimentally measured. A large number of measurements has been taken to evaluate the standard deviation of the output

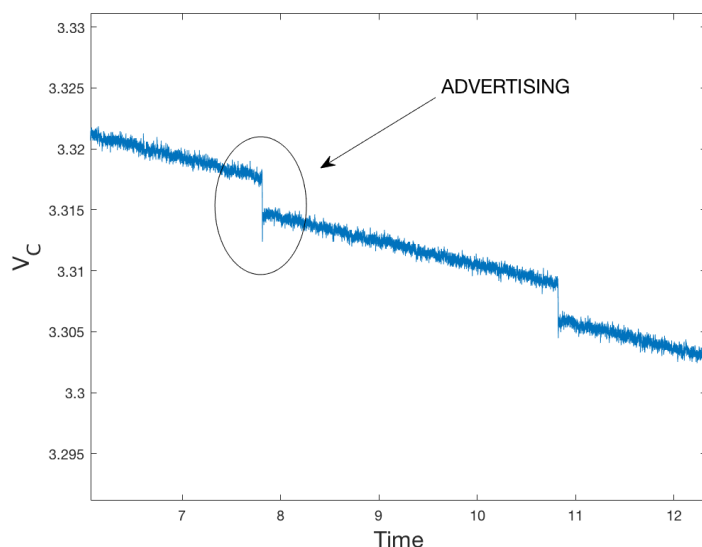


Figure 8.3: V_C step generated by the advertising process

voltage σ_{out} .

In order to verify the output noise is necessary that the output current of the sensor is maintained at a constant value during the whole test. As already said in the Sensors Comparison sections 5.2.3 and 5.2.2 the output current of this kind of sensors is affected by the ambient temperature and humidity. The temperature variation causes a change of the baseline current and sensitivity, while the humidity variation effect is transient, causing current spikes that lasts some seconds. Their effect on the output voltage is amplified in amplitude by the gain resistance R_g and in time by the filtering capacitor C_f . Depending on the sensor, the values of R_g and C_f can be different. As an example, for the SO_2 sensor $R_g = 1.5 \text{ MOhm}$ and $C_f = 47 \mu F$, leading to a zero-frequency amplification of $1.5 \cdot 10^6$ and a first order filtering frequency of 2.2 mHz , that brings the response time to $\simeq 7.5 \text{ min}$. Those values imply that any temperature and humidity variation of even small values or percentage can false the measurements, because in this case the only the measurement system needs to be tested. This brings the necessity to insert the system into a controlled temperature and humidity environment. To this purpose a climatic chamber has been used to perform the measurements.

The test needs also to be performed in a condition as close as possible to the real system, in order to make a complete test of the whole circuit, thus the implementation that includes the nRFBeacon was used in this case. The measurements are transmitted via Bluetooth by the beacon and gathered by a PC outside the chamber.

In this case the sampling rate, intended as the rate at which every measurement phase is performed, has to be increased to its maximum, thus avoiding that the nRF51 goes to sleep, in order to perform as much measurements as possible in a given period of time. Anyway the 7 min response time of the system allows to have a sampling period in the order of seconds. Moreover the compensation phase has to be skipped in this case because is necessary to gather the raw measurements to

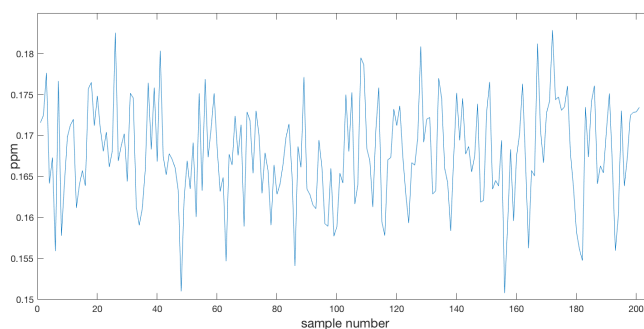


Figure 8.4: 200 samples taken with the SO_2 sensor at zero gas concentration, $25\text{ }^\circ\text{C}$ and 50 \%RH

precisely know how the system behaves under the test conditions. To achieve this requirements the firmware have been modified to continuously measure each channel and send the measurements through the advertising payload.

200 samples of the output voltage at zero gas concentration, at a temperature of $20\text{ }^\circ\text{C}$ and at a relative humidity of 50 \% have been taken. The SO_2 sensor was mounted in this case. The graph in Figure 8.4 shows all the samples x_i . It has to be notices that the gas concentration indicated is not null, even if no SO_2 is present inside the chamber. This is due to the effect of the baseline current of the sensor that is not null even if no gas is present. Though in this case the average value of the output vottage does not influence the test beacuse the standard deviation has to be caluclated in this case.

From the salmples x_i of Figure 8.4 it has been caluclated a standad deviation of

$$s_{out} = \sqrt{\frac{1}{N-1} \sum_{i=1}^N (x_i - \bar{x})^2} = 6.2\text{ ppb} \quad (8.2.1)$$

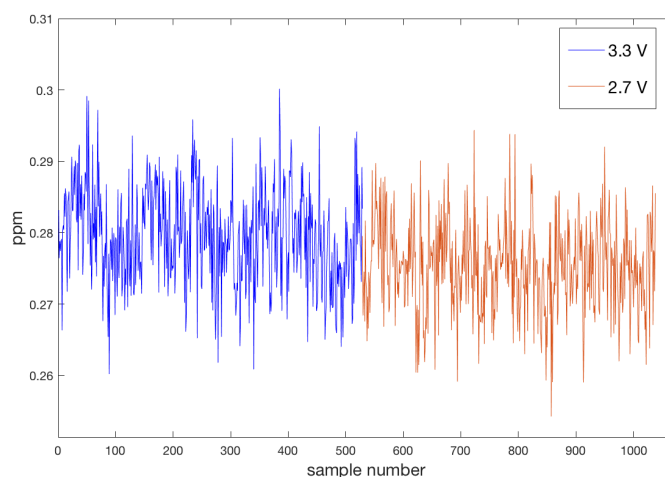
where $N = 200$ (samples) and \bar{x} indicates the average of the considered samples. In Volt is equal to

$$s_{out} = 345\text{ }\mu\text{V} \quad (8.2.2)$$

The resolution of the SO_2 sensor is 20 ppb , giving

$$\Delta V_o = 0.02\text{ ppm} \cdot 37.25 \frac{\text{nA}}{\text{ppm}} \cdot R_g = 0.02\text{ ppm} \cdot 37.25 \frac{\text{nA}}{\text{ppm}} \cdot 1.5\text{ M}\Omega = 1.1\text{ mV} \quad (8.2.3)$$

that is lower than s_{out} . Thus this test verify that the output noise is lower than the sensor resolution.

Figure 8.5: V_{PS} rejection reference measurements

8.3 Power supply rejection

The system is battery powered, therefore is necessary to cope with the fact that the value of V_{PS} will not remain constant during the whole battery life but will constantly decrease as the battery discharges. This imply that both the conditioning circuit and the system-on-chip have to function in this condition, down to a minimum value of V_{PS} . The conditioning circuit has to maintain its accuracy characteristics being capable of maintaining the sensor at a constant bias and preserving the output accuracy. As for the output uncertainty measurements also in this case is necessary to eliminate any effect on the output voltage caused by the sensor current dependence on variations of temperature and relative humidity. Therefore the measurements have been taken using a climatic chamber also in this case.

The system was tested at a temperature of 20 °C. The value of the relative humidity is stabilized to 50 % because its effect on the sensor is transient, therefore by principle does not influence the sensor steady-state response. The results of the measurements are shown in Figure 8.5. The V_{PS} sweep goes from 3.3 V to 2.7 V. From the image can be seen that a V_{PS} variation of 0.5 V produces a variation in the output voltage that is lower than 5 *ppb* in average. In fact, the average values of the two displayed samples yields $\overline{ppm_{3.3\text{ V}}} = 0.279$ and $\overline{ppm_{2.7\text{ V}}} = 0.275$.

8.4 Temperature effect

As already explained in the Section 5.2.3, every gas sensor's baseline current and sensitivity is affected by the temperature variation. The temperature coefficients of these two quantities vary from sensor to sensor, meaning that each purchased sensor, even if it is specific for a certain type of gas, shows different values of sensitivity and temperature dependence coefficient. Moreover those values are not given by the company, making necessary to perform this calibration step. The values measured would permit to correctly apply a calibration function to get rid of the temperature

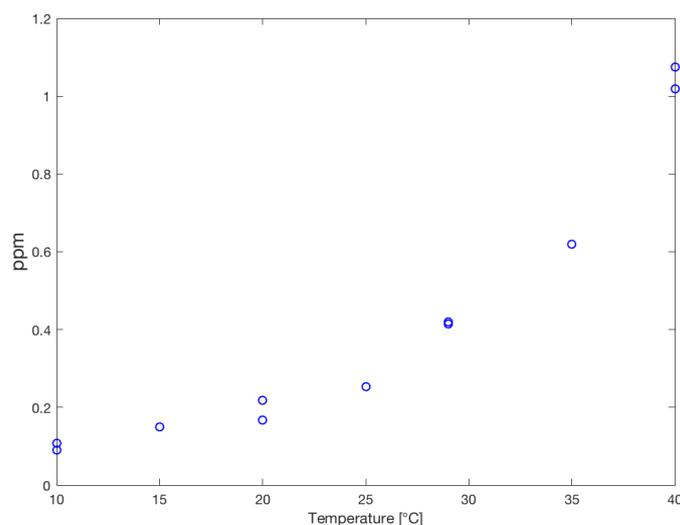


Figure 8.6: Baseline current temperature dependence

dependence. The other important purpose of this test is to compare the repeatability specifications of the datasheet, which declares it to be under the 3 % of the reading, with the measurements taken during the test. Lastly, the temperature characterization has not only the purpose of recording the sensor's behaviour but also to prove that the conditioning circuit does not introduces thermal drifts that can reduce the output voltage accuracy.

The thermal characterizations of the sensor and the conditioning circuit have not been performed separately because three terminal amperometric sensors needs to be biased in the correct way to function properly, therefore a feed-back circuit is needed, as explained in the section 6.1.1. Moreover the trans-impedance stage, due to the fact that it has to amplify a current in the order of micro-ampere, has a very high gain and to avoid the output saturation a current generator of the same order of magnitude (e.g. in the micro-ampere range) would be needed. Hence, being that this two parts, the sensor and the conditioning circuit, works tightly in conjunction, is much more simple to test them together rather than separately.

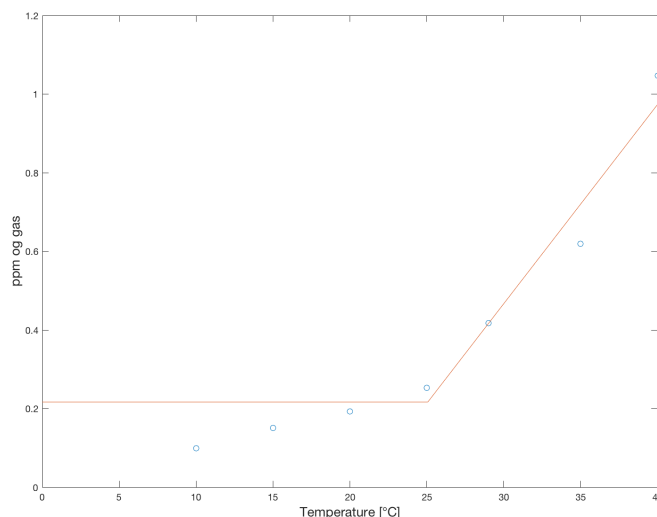
The test has been operated in the same way of the power supply rejection. The difference is that now the swept variable is the temperature rather than the power supply voltage. As before, every step of the calibration has to be performed at a constant relative humidity, due to its transient effect on the sensor output current. The application of a given temperature has been performed multiple times in order to test the repeatability characteristic of the system. Finally the temperature dependence of the sensor was studied to determine a proper calibration function.

The tests were performed from 10 °C to 40 °C with the SO_2 sensor. The temperature step is around 5 °C, implying that for every steep temperature change some time has to pass before taking correct measurements because the sensor needs some time to stabilize.

The graph shown in Figure 8.6 shows the temperature dependence of the baseline current of the SO_2 sensor. Every point is the result of an averaging process of

Temperature	Δ_{MAX} [ppb of gas]
10 °C	17.1
20 °C	49.7
29 °C	6.9
40 °C	56.6

Table 8.2


 Figure 8.7: Linear fit of the baseline current dependence for the SO_2 sensor

200 consecutive measurements. Different points at the same temperature shows the repeatability of the sensor. In particular the repeatability was tested for the temperatures 10 °C, 20 °C, 29 °C and 40 °C. For each of those points the difference of the average values Δ_{MAX} in *ppb* of gas is shown in table 8.2.

From the sample points of Figure 8.6 a compensation function of the baseline current can be retrieved. The company, inside the Application Notes related to this kind of sensors, suggests a linear compensation of this effect, already described in section 5.2.3 and considered in the equation 6.2.19 to calculate the gas concentration G with the conditioning circuit used in the implemented measurement system. That kind of compensation is applicable above a certain temperature, therefore it has been chosen fit the sample points starting from 25 °C, below that temperature the compensation value is constant and equal to the value of the fitting function at 25 °C. Implementing such kind of linear compensation would result in the fitting curve shown in Figure 8.7 applicable only above 25 °C and described by the equation

$$G_0(1 + TC_{baseline}\Delta T) \quad (8.4.1)$$

where

- $\Delta = T - T_0$ with $T_0 = 25$ °C
- $G_0 = 0.217$ ppm

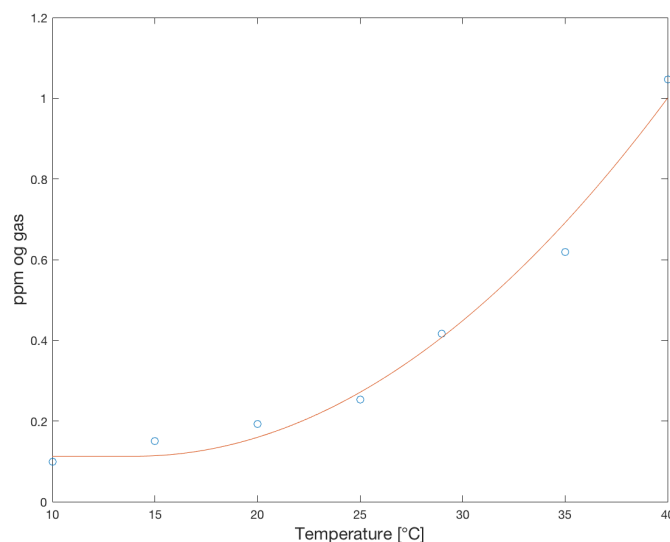


Figure 8.8: Quadratic fit of the baseline current dependence for the SO_2 sensor

- $TC_{baseline} = \frac{0.05}{0.217} = 230 \cdot 10^{-6} \text{ } ^\circ\text{C}^{-1}$

G_0 is the constant value assumed by the compensation function below 25 °C. This kind of baseline compensation would result in a maximum error, expressed as the maximum distance (in *ppm* of gas) of the sample points from the fitting curve, of $\Delta ppm_{MAX} \simeq 0.12 ppm$. Therefore it has been preferred to operate a quadratic compensation starting from 10 °C, that seemed to better fit to the sampled points.

The fitting function, retrieved using the `polyfit` function of Matlab, is shown in Figure 8.8, together with the sample points. To calculate the fitting function, the samples taken is different moments, were averaged, as for example the two points at 40 °C of Figure 8.6. The fitting function retrieved, calculated in *ppm* of gas, is

$$G_0(1 + TC_a\Delta T + TC_b\Delta T^2) \quad (8.4.2)$$

where

- $G_0 = 0.113 \text{ ppm}$
- $TC_a = -0.094 \text{ } ^\circ\text{C}^{-1}$
- $TC_b = 0.0115 \text{ } ^\circ\text{C}^{-2}$

G_0 is the constant value assumed by the compensation function below 14 °C. Using this kind of compensation the maximum error would be $\Delta ppm_{MAX} = 0.07 ppm$, determining the major effectiveness of this method respect to linear compensation. The two complete expressions for the calculation of the gas concentration G are shown below, together with the numerical values.

Using the **linear** compensation

$$G = \begin{cases} \frac{V_o - R_g \cdot S_0 \cdot 0.217[1 + 230 \cdot 10^{-6}(T - 25)] - V_{ref1}}{R_g \cdot S_0(1 - TC_{sensitivity}\Delta T)} & \text{if } 25^\circ\text{C} < T < 40^\circ\text{C} \\ \frac{V_o - R_g \cdot S_0 \cdot 0.217 - V_{ref1}}{R_g \cdot S_0(1 - TC_{sensitivity}\Delta T)} & \text{if } 10^\circ\text{C} < T < 25^\circ\text{C} \\ \text{undefined} & \text{elsewhere} \end{cases}$$

that provides a

$$\Delta ppm_{MAX} \simeq 0.12 ppm$$

where the minimum temperature is set to 10°C because the system has not been tested below that temperature.

Using the **quadratic** compensation

$$G = \begin{cases} \frac{V_o - R_g \cdot S_0 \cdot 0.113[1 - 0.094(T - 10) + 0.0115(T - 10)^2] - V_{ref1}}{R_g \cdot S_0(1 - TC_{sensitivity}\Delta T)} & \text{if } 14^\circ\text{C} < T < 40^\circ\text{C} \\ \frac{V_o - R_g \cdot S_0 \cdot 0.113 - V_{ref1}}{R_g \cdot S_0(1 - TC_{sensitivity}\Delta T)} & \text{if } 10^\circ\text{C} < T < 14^\circ\text{C} \\ \text{undefined} & \text{elsewhere} \end{cases}$$

that provides a

$$\Delta ppm_{MAX} = 0.07 ppm$$

A more accurate estimation of the uncertainty has been made that considers both the sources of uncertainty deriving from the conditioning circuit and those that derives from the sensor temperature and humidity dependence.

For the calculations it has been considered the expression of G that uses a quadratic compensation of the baseline current, to which it has been added the dependence on the offset voltage of the transimpedance stage V_{off} . The equation is shown below

$$G = \begin{cases} \frac{V_o - R_g \cdot S_0 \cdot 0.113[1 - 0.094(T - 10) + 0.0115(T - 10)^2] - V_{ref1} - V_{off}}{R_g \cdot S_0(1 - TC_{sensitivity}\Delta T)} & \text{if } 14^\circ\text{C} < T < 40^\circ\text{C} \\ \frac{V_o - R_g \cdot S_0 \cdot 0.113 - V_{ref1}}{R_g \cdot S_0(1 - TC_{sensitivity}\Delta T)} & \text{if } 10^\circ\text{C} < T < 14^\circ\text{C} \\ \text{undefined} & \text{elsewhere} \end{cases}$$

To evaluate the uncertainty it has been used the expression

$$u_G^2 = \sum_{i=1}^N \left(\frac{\partial G}{\partial x_i} \right)^2 \cdot \left(\frac{\Delta x_i}{\sqrt{3}} \right)^2 \quad (8.4.3)$$

where x_i identify every term present in that function apart from the sensitivity temperature coefficient TCS , that will be discusses later.

Now the contribution of every term will be analyzed in order to distinguish the measurements system contributions from the sources of uncertainty that derives from the temperature and humidity dependence of the sensor. Every term of uncertainty u_{x_i} is presented below as the square root of the term inside the summation, equal to

$$\left(\frac{\partial G}{\partial x_i}\right) \cdot \left(\frac{\Delta x_i}{\sqrt{3}}\right) \quad (8.4.4)$$

in order to better represent its final contribution to the total uncertainty U_G . The nominal values of the parameters and their error used in the calculations are

- $V_o = 2.5 V$ equal to the full-scale voltage
 $\Delta V_o = 253 \mu V$ that is the ADC error
- $V_{ref1} = 1.2 V$ is the voltage reference value used for the SO_2 sensor
 Its error is the same of the V_o voltage because also this point of the circuit is measured
- $V_{off} = 0 V$ is the nominal value of the offset voltage of the amplifier
 $\Delta V_{off} = 600 \mu V$ is the maximum offset voltage calculated in the conditioning circuit section
- $R_g = 1.5 M\Omega$ the resistance used for the SO_2 sensor test
 $\Delta R_g = 40 m\Omega \cdot (1 + 200 ppm)$ error of the digital multimeter AGILENT 34401A
- $T = 40 \text{ }^\circ\text{C}$ is the maximum considered temperature
 $\Delta T = 0.5 \text{ }^\circ\text{C}$ is the maximum error with which we know the temperature from the SHT21 sensor ΔT
- $S_0 = 37.25 nA/ppm$ is the calibrated sensitivity of the SO_2 sensor
 $\Delta S_0 = 0.1 nA/ppm$ is the estimated error on the sensitivity value
- $G_0 = 0.113 ppm$ is the fictitious gas concentration at $14 \text{ }^\circ\text{C}$ when no gas in present
 ΔG_0 will be calculated later
- $TCB_a = -0.094 \text{ }^\circ\text{C}^{-1}$
 $TCB_b = 0.0115 \text{ }^\circ\text{C}^{-2}$
 The error on these two values is considered null because the term

$$u_{fitting}^2 = \left(\frac{\Delta ppm_{MAX}}{\sqrt{3}}\right)^2 = 40 ppb$$

is added in the final expression

Each term calculated using the formula 8.4.4 is reported below. First are considered the terms of uncertainty introduced by the conditioning circuit, that are

- The contributions of V_o and V_{ref1} , being that they are measured with the same ADC, in sequence and they have most of times two close values, can be considered to have a correlation factor $\rho \simeq 1$, therefore the part of the expression of U_G^2 function of V_o and V_{ref1} would be

$$\left(\frac{\partial G}{\partial V_o}\right)^2 \left(\frac{\Delta V_o}{\sqrt{3}}\right)^2 + \left(\frac{\partial G}{\partial V_{ref1}}\right)^2 \left(\frac{\Delta V_{ref1}}{\sqrt{3}}\right)^2 + 2\left(\frac{\partial G}{\partial V_o}\right) \left(\frac{\Delta V_o}{\sqrt{3}}\right) \left(\frac{\partial G}{\partial V_{ref1}}\right) \left(\frac{\Delta V_{ref1}}{\sqrt{3}}\right) = \quad (8.4.5)$$

$$= \left[\left(\frac{\partial G}{\partial V_o}\right) \left(\frac{\Delta V_o}{\sqrt{3}}\right) + \left(\frac{\partial G}{\partial V_{ref1}}\right) \left(\frac{\Delta V_{ref1}}{\sqrt{3}}\right) \right]^2 \quad (8.4.6)$$

where

$$\left(\frac{\partial G}{\partial V_o}\right) = \frac{1}{R_g \cdot S_0}, \quad \left(\frac{\partial G}{\partial V_{ref1}}\right) = -\frac{1}{R_g \cdot S_0} \quad (8.4.7)$$

moreover

$$\left(\frac{\Delta V_o}{\sqrt{3}}\right) = \left(\frac{\Delta V_{ref1}}{\sqrt{3}}\right) \quad (8.4.8)$$

Thus their contribution to u_G^2 is null

- V_{off} contribution

$$\left(\frac{\partial G}{\partial V_{off}}\right) \cdot \left(\frac{\Delta V_{off}}{\sqrt{3}}\right) = 6.2 \text{ ppb} \quad (8.4.9)$$

- R_g contribution

$$\left(\frac{\partial G}{\partial R_g}\right) \cdot \left(\frac{\Delta R_g}{\sqrt{3}}\right) \simeq 0 \quad (8.4.10)$$

Now the terms introduced by the sensor temperature dependence are listed, including the uncertainty introduced by the compensation algorithm

- T contribution

$$\left(\frac{\partial G}{\partial T}\right) \cdot \left(\frac{\Delta T}{\sqrt{3}}\right) = 19.5 \text{ ppb} \quad (8.4.11)$$

- S_0 contribution

$$\left(\frac{\partial G}{\partial S_0}\right) \cdot \left(\frac{\Delta S_0}{\sqrt{3}}\right) = 8.3 \text{ ppb} \quad (8.4.12)$$

- As previously said the terms TCB_a and TCB_b are considered with zero error and the term $u_{fitting} = 40 \text{ ppb}$ is properly added in the final equation

- The term G_0 , in this case is calculated using the equation for the quadratic compensation, placing

$$G(T = T_0) = 0 \quad (8.4.13)$$

that yields

$$G_0 = \frac{V_0 - V_{ref1} - V_{off}}{R_g \cdot S_0} \quad (8.4.14)$$

therefore its uncertainty can be calculated as

$$\begin{aligned} u_{G_0}^2 = & \left(\frac{\partial G_0}{\partial V_o} \right)^2 \left(\frac{\Delta V_o}{\sqrt{3}} \right)^2 + \left(\frac{\partial G_0}{\partial V_{ref1}} \right)^2 \left(\frac{\Delta V_{ref1}}{\sqrt{3}} \right)^2 + 2\rho \left(\frac{\partial G_0}{\partial V_o} \right) \left(\frac{\Delta V_o}{\sqrt{3}} \right) \left(\frac{\partial G_0}{\partial V_{ref1}} \right) \left(\frac{\Delta V_{ref1}}{\sqrt{3}} \right) + \\ & + \left(\frac{\partial G_0}{\partial V_{off}} \right)^2 \left(\frac{\Delta V_{off}}{\sqrt{3}} \right)^2 + \left(\frac{\partial G_0}{\partial R_g} \right)^2 \left(\frac{\Delta R_g}{\sqrt{3}} \right)^2 + \left(\frac{\partial G_0}{\partial T} \right)^2 \left(\frac{\Delta T}{\sqrt{3}} \right)^2 + \left(\frac{\partial G_0}{\partial S_0} \right)^2 \left(\frac{\Delta S_0}{\sqrt{3}} \right)^2 \end{aligned}$$

where, as before the term dependent to V_o and V_{ref1} can be eliminated, reducing the equation to the last four terms evaluated below

$$u_{G_0} = \sqrt{3.85 \cdot 10^{-5} + 4.1 \cdot 10^{-13} + 7.5 \cdot 10^{-5}} = 0.011 \text{ ppm} = 11 \text{ ppb} \quad (8.4.15)$$

- The term $TC_{sensitivity}$ expressing the temperature dependence of the sensitivity needs to be calculated by calibration using a controlled environment with a certain variable amount of gas concentration. In this case was not possible to perform this calibration. However it can be said, from the equation used to calculate the concentration of gas, that a given relative error on the calculation of $TC_{sensitivity}$ is directly reported on the relative error of G

The sum of all this contributions brings to the final equation

$$u_G^2 = \left(\frac{\partial G}{\partial V_{off}} \right)^2 \left(\frac{\Delta V_{off}}{\sqrt{3}} \right)^2 + \left(\frac{\partial G}{\partial T} \right)^2 \left(\frac{\Delta T}{\sqrt{3}} \right)^2 + \left(\frac{\partial G}{\partial S_0} \right)^2 \left(\frac{\Delta S_0}{\sqrt{3}} \right)^2 + u_{G_0}^2 + u_{G_{fitting}}^2 =$$

$$= (0.0062 \text{ ppm})^2 + (0.0195 \text{ ppm})^2 + (0.0083 \text{ ppm})^2 + (0.011 \text{ ppm})^2 + (0.04 \text{ ppm})^2 = 2.2 \cdot 10^{-3} \text{ ppm}^2$$

That leads to

$$u_G = 47 \text{ ppb} \quad (8.4.16)$$

Now the total uncertainty on G can be calculated summing the previous calculations made using methods of types A and B. The method of types B yields

$$u_{G_B} = 47 \text{ ppb}$$

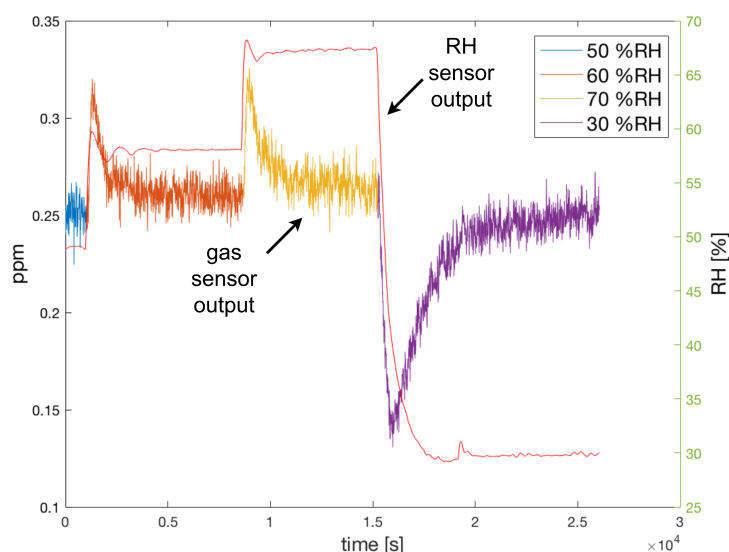


Figure 8.9: Relative humidity variation effect

while the result of the method of type A, used in the section 8.2, is reported here

$$u_{G_A} = 6.2 \text{ ppb}$$

Their quadratic sum results in the total uncertainty on G , that is

$$u_{G_{TOT}} = \sqrt{(47 \text{ ppb})^2 + (6.2 \text{ ppb})^2} = 47.4 \text{ ppb}$$

It is important to underline that this calculation does not take into account the sensitivity temperature dependence that require the characterization of the sensor in a climatic chamber with a given gas concentration. Any relative error on the estimated temperature coefficient of the sensitivity directly translates on an equivalent output relative error. Those calculations, supported by the test in climatic chamber, prove that the major source of uncertainty on G is due to the sensor.

8.5 Humidity effect

As already described in section 4.2.2, an ambient relative humidity variation generates current spikes of the WE current. The company declares that the value of the current, after the spike, returns to a level that has a difference from the previous (before the spike) under 10 *ppb*.

The Figure 8.9 shows the measurements performed with the SO_2 sensor at a controlled temperature of 25 °C and with zero gas concentration. The legend of the figure indicates the values of the relative humidity when the related measurements were taken and the transient variation of the humidity is also plotted referring to the right y-axes. The transient response is longer respect to that reported in SPEC Application Notes because in this case the variation of the humidity is not abrupt,

as the humidity samples shows. The averaged values taken once the response has been stabilized, listed in table 8.3, remains under a 16 *ppb* variation.

$RH[\%]$	$\overline{G}[ppm]$
50	0.253
60	0.261
70	0.265
30	0.249

Table 8.3: Averaged value of the measured gas concentration after humidity variations. The values in column $\overline{G}[ppm]$ are calculated averaging the measurements once the output has become stable

Chapter 9

Conclusions

The purpose of this work was to design a portable gas measurement system for indoor environmental monitoring of different gaseous analytes characterized by a long battery lifetime. This measurement system also acts as a node of an already designed sensors network for environmental monitoring. The system developed is composed by several parts, each playing a specific and fundamental role for its functioning. The sensing part of the system is constituted by a gas sensor and its conditioning circuit having the role of maintaining the sensor always operative and providing accurate readings. The control-unit permits to correctly control the conditioning circuit and read its output voltage in order to gather the ambient gas concentration. Furthermore it stores the readings inside the system flash memory and transmit them to the network receiver using the Bluetooth radio. The whole system is powered by a small 200 *mAh* battery that, with a 5 *min* sampling rate, can maintain the system operative for one year.

The design procedure followed several steps, from the sensing technology choice to the characterization of the electronics. The first step, as already mentioned, was the choice of a gas sensing technology feasible for the application, hence characterized by a low power consumption, wide variety of target gaseous analytes and low cost. The amperometric electrochemical gas sensing technology was the result of the study. Three amperometric sensors, of different target gases (H_2S , SO_2 and NO_2), were selected to test the whole system. Subsequently the condition circuit was designed with the aim of being able to host different amperometric sensor characterized by different bias voltages and current capabilities. The proposed solution can function with all the amperometric sensors used in this work, that have different bias voltages, and can also be used with other amperometric gas sensors. The designed circuit has then been realized using specific low power components chosen for the purpose. After these steps, the work proceeded with the choice of an appropriate low power control unit with the capability of make use of the Bluetooth stack. The nRF51 system-on-chip from Nordic Semiconductor was the result of the choice. The firmware of the chip has then been written addressing all the aspects described in the first paragraph, that comprise the communication with the AD and DA converters of the circuit, the Bluetooth transmission, the measurement post-processing and the management of the sleep and functioning phases. The whole system, realized on a prototyping board, has finally been tested. The first step of the test consisted of ver-

ifying its current consumption both during the measurement process and during the sleep mode, that resulted to be $150 \mu A$ and $20 \mu A$ respectively. This permitted to verify the one year system lifetime, that was one of the most stringent requirement of the system. After such verification the test phase proceeded with the temperature and humidity characterization performed to verify the stability of the measurement system and characterize the temperature dependence of the sensor without the presence of target gas. This last test permitted to extrapolate a quadratic compensation function that has been implemented inside the control-unit. All the performed tests verified the compliance of the developed measurement system with the initial proposed specifications.

Further developments should include both other system characterization steps in controlled environmental conditions and a bidirectional communication with the receiver.

The system characterization should be performed in presence of the target gas in order to calibrate the whole system, sensor plus electronics. Moreover it should be useful to expose each sensor to different gaseous analytes for cross-sensitivity verification. In addition long term drift tests should be performed to completely characterize the system.

The development of a bidirectional communication with the receiver would bring several advantages. First of all, it would permit a time synchronization of the sensing node, permitting to include a locally (i.e. inside the sensing node) a timestamp. Secondly, it would allow the employment of an acknowledge process with the receiver, avoiding additional transmissions of already received packets. Lastly, it would make possible a wireless re-configuration of the node parameters, as for example its sampling rate.

Bibliography

- [1] J. R. Stetter and J. Li, “Amperometric gas sensors a review,” *Chemical reviews*, vol. 108, no. 2, pp. 352–366, 2008.
- [2] N. Semiconductor, “nrf51 development kit user guide - v1.2.”
- [3] L. Lombardo, S. Corbellini, M. Parvis, A. Elsayed, E. Angelini, and S. Grassini, “Wireless sensor network for distributed environmental monitoring,” *IEEE Transactions on Instrumentation and Measurement*, 2017.
- [4] S. Corbellini, E. Di Francia, S. Grassini, L. Iannucci, L. Lombardo, and M. Parvis, “Cloud based sensor network for environmental monitoring,” *Measurement*, 2017.
- [5] Z. Yunusa, M. N. Hamidon, A. Kaiser, and Z. Awang, “Gas sensors: A review,” vol. 168, pp. 61–75, 04 2014.
- [6] E.-B. Lee, I.-S. Hwang, J.-H. Cha, H.-J. Lee, W.-B. Lee, J. J. Pak, J.-H. Lee, and B.-K. Ju, “Micromachined catalytic combustible hydrogen gas sensor,” *Sensors and Actuators B: Chemical*, vol. 153, no. 2, pp. 392–397, 2011.
- [7] L. Xu, T. Li, X. Gao, Y. Wang, R. Zheng, L. Xie, and L. Lee, “Behaviour of a catalytic combustion methane gas sensor working on pulse mode,” in *Sensors, 2010 IEEE*, pp. 391–394, IEEE, 2010.
- [8] M. A. Butler, “Optical fiber hydrogen sensor,” *Applied Physics Letters*, vol. 45, no. 10, pp. 1007–1009, 1984.
- [9] H. Manap, R. Muda, S. O’Keeffe, and E. Lewis, “Ammonia sensing and a cross sensitivity evaluation with atmosphere gases using optical fiber sensor,” *Procedia Chemistry*, vol. 1, no. 1, pp. 959–962, 2009.
- [10] S. Okazaki, H. Nakagawa, S. Asakura, Y. Tomiuchi, N. Tsuji, H. Murayama, and M. Washiya, “Sensing characteristics of an optical fiber sensor for hydrogen leak,” *Sensors and Actuators B: Chemical*, vol. 93, no. 1-3, pp. 142–147, 2003.
- [11] M. Girschikofsky, M. Rosenberger, S. Belle, M. Brutschy, S. R. Waldvogel, and R. Hellmann, “Optical planar bragg grating sensor for real-time detection of benzene, toluene and xylene in solvent vapour,” *Sensors and Actuators B: Chemical*, vol. 171, pp. 338–342, 2012.

- [12] H. Okajima, S. Kakuma, K. Uchida, Y. Wakimoto, and K. Noda, "Measurement of methane gas concentration using an infrared led," in *SICE-ICASE, 2006. International Joint Conference*, pp. 1652–1655, IEEE, 2006.
- [13] C. Massie, G. Stewart, G. McGregor, and J. R. Gilchrist, "Design of a portable optical sensor for methane gas detection," *Sensors and Actuators B: Chemical*, vol. 113, no. 2, pp. 830–836, 2006.
- [14] D. Garcia-Romeo, H. Fuentes, N. Medrano, B. Calvo, P. Martinez, and C. Azcona, "A ndir-based co2 monitor system for wireless sensor networks," in *Circuits and Systems (LASCAS), 2012 IEEE Third Latin American Symposium on*, pp. 1–4, IEEE, 2012.
- [15] G. Zhang, Y. Li, and Q. Li, "A miniaturized carbon dioxide gas sensor based on infrared absorption," *Optics and Lasers in Engineering*, vol. 48, no. 12, pp. 1206–1212, 2010.
- [16] L. Niedrach and H. Alford, "Novel fuel cell structure. us patent 3905832," in *Chem Abstr*, vol. 62, p. 11416c, 1965.
- [17] D. T. Sawyer, R. S. George, and R. C. Rhodes, "Polarography of gases. quantitative studies of oxygen and sulfur dioxide," *Analytical Chemistry*, vol. 31, no. 1, pp. 2–5, 1959.
- [18] M. Wienecke, M.-C. Bunescu, M. Pietrzak, K. Deistung, and P. Fedtke, "Ptfe membrane electrodes with increased sensitivity for gas sensor applications," *Synthetic Metals*, vol. 138, no. 1, pp. 165 – 171, 2003. Organic Materials for Device Applications. Proceedings of Symposium F, E-MRS Spring Meeting 2002, June 18-21, 2002, Strasbourg, France.
- [19] K. Blurton, P. Greenberg, H. Oswin, and D. Rutt, "The electrochemical activity of dispersed platinum," *Journal of The Electrochemical Society*, vol. 119, no. 5, pp. 559–564, 1972.
- [20] H. Bay, K. Blurton, H. Lieb, and H. Oswin, "Electrochemical measurements of blood alcohol levels," *Nature*, vol. 240, no. 5375, p. 52, 1972.
- [21] H. Bay, K. Blurton, J. Sedlak, and A. Valentine, "Electrochemical technique for the measurement of carbon monoxide," *Analytical chemistry*, vol. 46, no. 12, pp. 1837–1839, 1974.
- [22] K. F. Blurton and J. R. Stetter, "Sensitive electrochemical detector for gas chromatography," *Journal of Chromatography A*, vol. 155, no. 1, pp. 35–45, 1978.
- [23] K.-C. Ho, C.-M. Chen, and J.-Y. Liao, "Enhancing chemiresistor-type no gas-sensing properties using ethanol-treated lead phthalocyanine thin films," *Sensors and Actuators B: Chemical*, vol. 108, no. 1-2, pp. 418–426, 2005.

- [24] L. R. Jordan, P. C. Hauser, and G. A. Dawson, "Humidity and temperature effects on the response to ethylene of an amperometric sensor utilizing a gold-nafion electrode," *Electroanalysis*, vol. 9, no. 15, pp. 1159–1162, 1997.
- [25] T. Kappes and P. C. Hauser, "Simplified amperometric detector for capillary electrophoresis," *Analyst*, vol. 124, no. 7, pp. 1035–1039, 1999.
- [26] G. A. Dawson, P. C. Hauser, P. A. Kilmartin, and G. A. Wright, "Co₂ gas sensing at microelectrodes in nonaqueous solvents," *Electroanalysis: An International Journal Devoted to Fundamental and Practical Aspects of Electroanalysis*, vol. 12, no. 2, pp. 105–110, 2000.
- [27] H. Imaya, T. Ishiji, and K. Takahashi *Sens. Actuators, B*, vol. 108, p. 803, 2005.
- [28] G. J. Maclay, D. Keyvani, and S. B. Lee, "Electrochemical sensors for gas detection," Feb. 10 1998. US Patent 5,716,506.
- [29] G. Alberti and M. Casicola *Solid State Ionics*, p. 61, 1993.
- [30] D. N. Campbell, R. C. Davis Jr, and J. C. Schmidt, "Amperometric gas sensor containing a solid electrolyte," May 17 1988. US Patent 4,744,954.
- [31] A. B. LaConti *Chem. Abstr.*, vol. 90, p. 60474a, 1979.
- [32] H. V. Venkatesetty, "Electrochemical sensing of carbon monoxide," June 11 1985. US Patent 4,522,690.
- [33] T. Otagawa, S. Zaromb, and J. R. Stetter *J. Electrochem. Soc.*, p. 132, 1985.
- [34] J. C. Schmidt, D. N. Campbell, and S. B. Clay, "Electrochemical gas sensor," June 17 1986. US Patent 4,595,486.
- [35] H. Tataria, A. A. Schneider, W. A. Travers Jr, and L. E. Martin, "Electrochemical cell for the detection of chlorine," Jan. 22 1980. US Patent 4,184,937.
- [36] W. J. Albery, "Carbon dioxide measurement," Mar. 22 1983. US Patent 4,377,446.
- [37] D. M. Morgan and S. G. Weber, "Noise and signal-to-noise ratio in electrochemical detectors," *Analytical chemistry*, vol. 56, no. 13, pp. 2560–2567, 1984.
- [38] N. Semiconductor, "nrf51 series reference manual - nordic infocenter."
- [39] S. M. sandeep.mistry@gmail.com, "Noble."
- [40] C. S.-W. C. W. G. P. F. B. O'hayre, Ryan. John Wiley Sons, 2016.
- [41] A. J. Bard, L. R. Faulkner, *et al.*, "Fundamentals and applications," *Electrochemical Methods*, vol. 2, p. 482, 2001.
- [42] P. Kissinger and R. William, "Techniques in electroanalytical chemistry," 1996.

Appendix A

Electrochemical amperometric gas sensor theory

Electrochemical gas sensors chemically reacts with the target gas producing an electric current proportional to the concentration of the target gas. They can be divided into three main classes depending on their operating principle: potentiometric, conductometric and amperometric [1].

Potentiometric sensors measure the potential of a given reaction, occurring into the sensor, with the target analyte. Conductometric gas sensor incorporates a resistance that varies its conductance in function of the analyte concentration, chemically reacting with it in specific conditions. Amperometric gas sensors measures generates a current proportional to the concentration of the analyte at a fixed or variable potential that has to be provided externally by mean of a so called *potentiostatic circuit*.

In the following section **amperometric gas sensors** are described, that from now on will be referred as **electrochemical** sensors. Respectively, their working principle and practical aspects concerning their realization will be described.

A.0.1 Working Principle

The electrochemical gas sensors working principle is analogous to a *fuel cell*; in fact, these type of sensor are often called *micro fuel cell*. According to this, in order to clearly explain the process that permits to this sensors to detect different gas concentrations, a brief explanation of the theory at the basis of fuel cells is presented below.

Fuel cells basic theory [40]

Fuel cells can be thought as devices that transform fuel into electrical energy, but in a completely different way with respect to combustion engines. In combustion engines the energy produced is both mechanical and thermal, while in a fuel cell, like previously said, it is electrical.

In combustion engines the fuel is *burned*; chemical reactions that take places inside the engine are fast, in the order of picoseconds, releasing instantly mechanical and thermal energy. The combustion of hydrogen can be taken as an example, where

hydrogen-hydrogen bonds and oxygen-oxygen bonds are broken, while hydrogen-oxygen bonds are formed:



Hydrogen molecules are oxidized, water and thermal energy is produced almost instantly. Of course the energy of the produced water bond is lower than the energy of the reactant bonds, H_2 and O_2 .

Fuel cells somehow seek to exploit chemical reactions to produce directly electrical energy. The basic idea to achieve that is to make use of the electrons involved in the reaction as they move from the reactants high-energy bonds to the low-energy product bonds. In order to implement this idea is necessary to split the chemical reaction into two spatially separated steps. The previously described hydrogen combustion can be engineered to be split-up. The first step is the process by which electrons are separated from the hydrogen molecule that becomes a positively charged hydrogen ion (i.e. a proton):



The two electrons $2e^-$ can now power an electrical circuit and then be used as bonding electrons for the second part of the reaction that involves oxygen and the hydrogen positive ions, in fact it is an **oxygen reduction**¹:



In this way the electrons can spend their energy before completing the reaction. The spatial separation of the reactions is accomplished using an electrolyte, a material where electrons cannot pass.

Based on this description a basic fuel cell can be represented as in Figure A.1 that consists of two platinum electrodes immersed into sulfuric acid, the electrolyte. The electrodes are connected to an electrical circuit providing a path for the free electrons. When hydrogen is injected below the left electrode it splits into electrons and hydrogen negative ions, like reaction described in Equation (A.0.2). H^+ ions reach the other electrode through the electrolyte, but electrons, stopped by it, passes through the electrical circuit, powering it. Near the right electrode, where oxygen is furnished to complete the reaction, when both electrons and H^+ ions reach it, water is produced following the Equation (A.0.3). Overall this process is constituted by an **oxidation**² at the **anodic electrode**³ that generates electrons and a **reduction reaction** at the **cathodic electrode**⁴ that recombines the electrons coming from the circuit to form the resulting element, that in the example above is H_2O . This implies that for the device correct operation both fuel, at the anode, and *oxidant*,

¹ *Reduction* of a given element is the process for which the given element gains electrons.

² *Oxidation* of a given element is the process for which the given element loses electrons reaction

³ An electrode of a given device is defined anodic if electrons flows **out** from it, going **from** the device **towards** the external circuit

⁴ An electrode of a given device is defined cathodic if electrons flows **into** it, going **from** the external circuit **into** the device

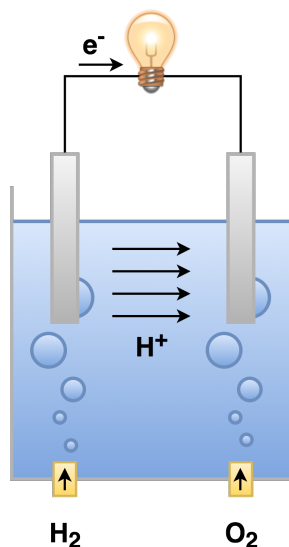


Figure A.1: Basic fuel cell



Figure A.2: A planar fuel cell

at the cathode, have to be provided. Most times the oxidant is oxygen.

In this way, a fuel cell continuously alimented with hydrogen and oxygen can produce electrical energy. The amount of energy is directly proportional to the number of reactions (equations (A.0.2) and (A.0.3)) that take place inside the system, therefore to the size of the *reaction area* of the cell and to the amount of fuel provided to it. In fact, doubling the area of the fuel cell, approximately doubles the current produced. Surface broadening is also accomplished by the employment of porous electrodes that permits to fuel molecules to diffuse inside them.

Another important limiting factor for performance is the reactions *speed* at both electrodes. For this reason are equally important either the local reaction rate at one electrode and the transport of elements between them. The local rate of reactions is increased by the adoption of *catalysts* while for the elements transport thin structure are used. The reason resides in the nature of electrons and ions transport inside the cell. Electrons moves easily towards the cathodic electrode through the conductive path provided to them, almost independently from its length, but the ions transport inside the electrolyte is much more difficult resulting to be the bottleneck of the process. Thin structures puts electrode as close as possible in order to reduce this path.

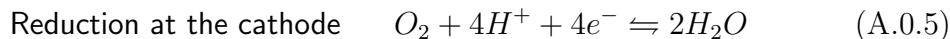
For this reason the geometry of this devices is usually designed to maximize the

surface-to-volume ratios, resulting in thin and planar structures, shown in Figure A.2.

As previously said, the whole chemical reaction has leftovers, that are usually water and carbon dioxide. This waste elements needs to be removed once produced to ensure the proper operation, or even the life, of the cell.

...back to electrochemical sensors

The same concept at the basis of fuel cell theory can be applied to make sensors. In this case the fuel, the H_2 atom before, is the gas to measure, and its presence or absence determines the magnitude of the electrical current flowing inside the circuit. In general the whole process once again consists in an oxidation reaction of the target gas at the anodic electrode and a reduction reaction at the other electrode, the cathodic. The electrode that comes in direct contact with the analyte is known as Working Electrode (WE) or Sensing Electrode and should be well exposed to it. The other electrode is known as Counter Electrode (CE). If the target gas is oxidized during the process the WE is the anodic terminal of the structure, while the CE is the cathodic, that needs an adequate supply of oxidant element to complete the reaction. A sulfuric acid (H_2S) sensor can be an example:



Where it is clear that oxygen, the oxidant element, is needed in the reduction process at the CE.

There are sensors that, differently from the example described above, involve a reduction reaction of the target gas, such as nitrogen dioxide (NO_2), chlorine (Cl_2), ozone (O_3). In this kind of devices the role of the electrodes is exchanged, the WE become the cathodic electrode and the CE become the anodic terminal. At the WE we have, for the three elements



Were it can be noticed that, differently from other sensors, oxygen supply is not needed.

Of course the purpose of electrochemical sensors is not to produce an electric current used as a source of power, but to generate a signal that contains an information. Therefore an electrochemical gas sensor can be significantly smaller than a classic fuel cell, actually a *micro fuel cell*, having an output current in the order of $X0 \text{ nA}$ or $X00 \text{ nA}$.

The relation that links the current with the target gas concentration depends on many factors and can have a complex mathematical expression.

There are two principal operating conditions for which this expression can be simplified becoming suitable for sensing purpose. They are two *current limiting conditions* [1]. The limitation factors are the rate of reactions that occurs at one electrode (r_r) and the rate of analyte transport, for diffusion, towards the electrode (r_d).

In the first case $r_r \ll r_d$. This means that the reactions of the analyte are much slower than the analyte diffusion inside the sensor. The limiting factor is the rate of reactions. In this case the concentration of the target gas inside the sensor is all the same, from the aperture in which the gas enters, to the WE. For this situation the relation between the current and the gas concentration is [41, 42]:

$$i = nFkACe^{\frac{\alpha nFE}{RT}} \quad (\text{A.0.9})$$

where

- k is the standard rate constant
- F is the Faraday constant
- R is the gas constant
- T is the temperature in Kelvin
- A is the area of the electrode
- C is the gas concentration
- n is the number of electrons per molecule reacting
- α is the transfer coefficient
- E is the overvoltage of the electrode reaction

This relation involves terms that has to be held constant in order to have a proportional relation between i and C with an exponential temperature dependence. This is hard to achieve in a system where electrodes can be consumed by reaction with the analyte and the electrolyte.

To overcome this issue the geometry and the composition of the sensor can be modified in order to force the rate of diffusion to be the limiting factor, $r_d \ll r_r$. This can be achieved, for example, reducing the size of the aperture of the sensor until it becomes a *capillary diffusion barrier* that would limit the analyte diffusion by the required amount. Under this limitation assumption the rate of reactions is fast enough to instantly consume every target gas molecule as soon as it comes in contact with the sensing part of the structure. Therefore the gas concentration inside the sensor is no longer constant but approaches to zero near the WE. This lead to a much more simple relation

$$i = kC \quad (\text{A.0.10})$$

that has a square root dependence from temperature. In electrochemical gas sensors this approximation is widely used.

Further important characteristics that define the performance of this kind of sensors, together with the relation linearity between gas concentration and current, are their selectivity to the target gas, their sensitivity - in order to have a sufficient large signal to read - and their operating life.

Selectivity to the target gas is achieved using specific materials for the electrodes, the sensor membrane and the electrolyte. In the previous fuel cell example, platinum was used for the electrodes and sulfuric acid for the electrolyte [40]. Instead, for an oxygen gas sensor lead or cadmium can be used for the electrodes and either an acid or basic electrolyte. This specific choice follows directly from the oxygen reactions required for the sensor to work, as shown in the following equations

For acidic electrolyte



In this case the *Pb* electrode acts as a *catalyst*. In other cases also different materials for each electrode are used. It is important to notice that a perfect choice of elements in terms of selectivity is not possible. In fact every sensor shows a certain cross-sensitivity to other kinds of gasses. For example a sulfur dioxide (SO_2) sensor responds to 20 *ppm* of *NO* as if they are 11 *ppm* of SO_2 or to 20*ppm* of Ethanol as if they are 11.6 *ppm* of SO_2 . Another aspect that characterizes the selectivity and the sensitivity of a sensor is the *bias voltage* applied between the two electrodes. In fact some sensors, at a given, and fixed bias potential shows an higher sensitivity, enhancing the sensor response. In general the nominal response to a specific gas sensor made with specific materials has a maximum value at a given and fixed bias potential. Any changes in it can result in an high modification of the sensor sensibility, needing a long stabilization time once the bias is brought back to its nominal value. While the sensor is working and furnishing current to the circuit from its WE, its bias potential, between WE and CE, tends naturally to change. The sensor is un-biasing itself. This is due to the charges that flow inside and outside the cathodic and anodic terminals. In order to solve this important aspect some sensors are provided with a third terminal, the Reference Electrode (RE), at which a stable reference voltage is applied. Inside this additional terminal no current has to flow. It is placed between the WE and CE, completely inside the electrolyte and very close to the sensing electrode WE. The RE has the function to stabilize the potential at the WE, thus stabilizing the whole sensor reactions and by consequence its sensitivity. Large sensitivity is usually achieved, similarly to fuel cells, by using porous electrodes that maximize the reaction surface with the gas molecules.

Operating life of the sensor most of times is limited by the evaporation process of the electrolyte, that is combated using membranes that let target gas molecules to enter and avoid as much as possible the electrolyte evaporation. Moreover, in some cases, waste product of the chemical reactions, as H_2O , can be a problem if they are not correctly expelled from the device.